# Local structure and dynamics of dense colloidal systems : from patchy particles to hard spheres

Susana Marín Aguilar

université
PARIS-SACLAY

# Local structure and dynamics of dense colloidal systems: from patchy particles to hard spheres

**Thèse de doctorat de l'université Paris-Saclay**

École doctorale n° 564, physique de l'Ile-de-France (PIF)
Spécialité de doctorat: Physique
Unité de recherche: Université Paris-Saclay, CNRS, Laboratoire de Physique des Solides, 91405, Orsay, France.
Référent: Faculté des sciences d'Orsay

**Thèse présentée et soutenue en visioconférence totale, le 18 Décembre 2020, par**

**Susana MARÍN AGUILAR**

**Composition du jury:**

| | |
|---|---|
| **Emmanuel TRIZAC**<br>Professeur, Laboratoire de Physique Théorique et Modèles Statistiques, Université Paris-Saclay | Président du jury |
| **Luca CIPELLETTI**<br>Professeur, Laboratoire Charles Coulomb, Université Montpellier | Rapporteur & examinateur |
| **Daniele COSLOVICH**<br>Professeur, University of Trieste | Rapporteur & examinateur |
| **Marjolein DIJKSTRA**<br>Professeure, Institute for Nanomaterials Science, Utrecht University | Examinatrice |
| **Kirsten MARTENS**<br>Professeure, Laboratoire Interdisciplinaire de Physique, Université Grenoble Alpes | Examinatrice |
| **Giuseppe FOFFI**<br>Professeur, Laboratoire de Physique des Solides, Université Paris-Saclay | Directeur |
| **Frank SMALLENBURG**<br>Chargé de recherche CNRS, Laboratoire de Physique des Solides, Université Paris-Saclay | Coencadrant |
| **Rik WENSINK**<br>Chargé de recherche CNRS, Laboratoire de Physique des Solides, Université Paris-Saclay | Coencadrant |

Thèse de doctorat

NNT: 2020UPASP052

# Acknowledgments

*Pleasure in the job*
*puts perfection in the work.*
***Aristotle***

First of all, I would like to express my deepest gratitude to my three supervisors: Giuseppe, Frank and Rik. Each of them, with their own personality, has guided me with patience and wisdom in this PhD journey. I thank them for the many interesting discussions and for being always willing to listen to my ideas, answer my many questions and, to always work as a team. Also, thank you for encouraging me to attend and present the PhD research at conferences, seminars, and summer schools where I met a lot of interesting people with whom I had really nice discussions. Moving to another country and to start working in a new place is always a big unknown full of uncertainty and I could not be more happy and grateful for having chosen the Theo Soft Matter group of the LPS. Thanks to the three of you for making my PhD a very enriching experience that I really enjoyed and where I learned not only about glasses and soft matter but also that academia can be such a friendly environment.

I acknowledge the financial support given by the National Council of Science and Technology (CONACyT) (scholarship 340015/471710) for the scholarship granted to do the PhD and to the *Consejo Mexiquense de Ciencia y Tecnología* (COMECyT) for the economic support to start the PhD and the expenses of moving to France.

I would also like to thank the other members of the Theo Soft Matter group who were always willing to discuss the topics I was working on: Claudia, thank you very much for so many questions that you helped me solve, also for being the voice of experience always giving me very good advice. Saheli, it has been very pleasing to have someone to share the experience of the PhD and to discover together the glassy soft matter universe and for being my partner in all the summer schools, thank you for your friendship. To Etienne, with your analytically and critical way of seeing the scientific life, several times you have made me think out of the box and it has been very enriching to discuss with you. To the other members of the LPS theory group who were always very kind and with whom I had really interesting conversations.

But this journey would not have been so enjoyable without a good balance between life at the laboratory and the personal life. In the end, both of them are part

of a whole and this is why I would like to thank the people who have share time and experiences with me in these three years: to Christian and Assya Van Gyssel, who made me feel at home, make the yoga practice a part of my weekly life and thank you for teaching me that if my goals, desires, and intentions are all aligned I can achieve whatever I want. To Claudia and Raúl, my gastronomic guides in Paris, I enjoyed very much those relaxing weekends exploring the streets of Paris, thank you for being such good friends. To Markus, who cheers me up and invites me to explore new places and to go outside my comfort zone.

I must also thank all the people that are in Mexico, who from there give me their entire support and never let me give up. To Sofi, I have no words to thank you for everything you do for me: you cheer me up, you listen to me, you make me laugh and I know that I can always count on you. Thank you for all the times that I was stressed out and you told me that I could do it. To Claudia (Kngu), because you are always there for me, for listening to all my scientific traumas and always telling me the right words so I can see things in a better way, thanks for all the support when I was writing my thesis. To Dany, Miriam, Jovanna, Pili and, Ingram, the friendship you give me keeps me on going.

And I wouldn't be here without the truly and never-ending support of my family: Ani, Marthita, Ro, Pa, Raque, you have never stopped seeing all the potential I have, thank you for encouraging me to achieve all my dreams.

Thank you very much!

# Contents

# Résumé

Les verres sont des matériaux omniprésents dans notre vie quotidienne. Elles proviennent de l'arrêt dynamique d'un fluide. Si un fluide est refroidi ou comprimé suffisamment rapidement, il évite la cristallisation et sa dynamique est fortement ralentie. De ce fait, le temps de relaxation, qui est le temps nécessaire à un système pour perdre la mémoire de ses conditions initiales, augmente fortement. Si la température continue à baisser, en dessous d'une température $T_g$, le comportement dynamique est si lent que le temps de relaxation est supérieur à la durée typique d'une expérience : le fluide est devenu un verre. Le système tombe en déséquilibre, car il n'est pas capable d'explorer tout l'espace des phases dans le créneau temporel d'une expérience et ce qui est également connu sous le nom de phase non-ergodique.

En général, avant que le système ne soit complètement hors équilibre, ses caractéristiques dynamiques commencent à s'écarter de celles du liquide : le temps de relaxation augmente de plusieurs ordres de grandeur, il développe une relaxation en deux étapes et le système se divise en régions plus rapides et plus lentes. Ceci s'accompagne de petits changements dans la structure locale. Ce régime est appelé le régime vitreux [1]. Lorsqu'un liquide est amené vers la transition vitreuse en diminuant la température, le système arrive à une phase métastable par rapport à un cristal, c'est ce qu'on appelle un liquide surfondu [1, 2].

Même si la structure globale d'un verre est désordonnée comme dans un fluide, plusieurs études soulignent que certains changements de la structure locale apparaissent dans le fluide lorsqu'il se dirige vers la phase vitreuse. Ces structures sont des structures favorisées localement (LFS) qui minimisent l'énergie libre locales [3,4]. Lorsque les particules interagissent avec le potentiel de Lennard-Jones, les clusters icosaédriques minimisent l'énergie libre locale et sont donc un exemple de LFS. L'idée d'une augmentation du nombre des clusters icosaédriques lorsque un fluide s'approche du régime vitreux a été proposée pour la première fois par Sir Charles Frank en 1952 [5]. Plus récemment, il a été démontré que ces structures sont présentes dans une grande variété de substances qui forment des verres [6–9]. Ces éléments ouvrent la porte à plusieurs questions : est-il possible de contrôler la dynamique d'un système vitreux en changeant sa structure locale ? Peut-on prédire le comportement dynamique à partir des seules informations structurelles ? Cette thèse cherchera à répondre à ces questions par une étude détaillée de simulation de dynamique moléculaire de certains modèles de verres colloïdaux.

Nous divisons cette thèse en deux parties principales : dans la première, nous utilisons des particules à patchs (patchy particles) comme moyen de contrôler la structure locale d'un fluide vitreux. Dans la deuxième partie, nous nous concentrons sur l'étude de mélanges de sphères dures pour répondre s'il est possible d'extraire des informations sur la dynamique à partie de la structure locale.

## Les particules à patch : un moyen de contrôler la dynamique vitreuse.

Une façon de modifier la structure locale d'un fluide est d'utiliser des interactions directionnelles. Pour cela, nous utilisons des particules à patchs. Afin de modéliser ces interactions, nous utilisons le modèle de Kern-Frenkel [10]. Ces particules sont des sphères dures avec $n$ régions attractives (patchs) sur leur surface. Deux particules interagissent de manière attractive lorsque le vecteur qui relie leurs centres passe par un patch de chacune des particules, comme le montre la figure 1 où la ligne rouge représente ce vecteur. L'interaction attractive est modélisée comme un potentiel de puits carré directionnel. Les particules interagissent de manière répulsive lorsque la distance entre les particules est égale au diamètre de la particule.

Le potentiel d'interaction de Kern-Frenkel est donc le suivant :

$$U_{ij}(\mathbf{r}_{ij}) = U_{ij}^{\mathrm{HS}}(r_{ij}) + U_{ij}^{\mathrm{SW}}(r_{ij}) f(\mathbf{r}_{ij}, \hat{\mathbf{n}}_\alpha, \hat{\mathbf{n}}_\beta), \tag{1}$$

où $r_{ij}$ est la distance de centre à centre entre les particules $i$ et $j$, $U_{ij}^{\mathrm{HS}}$ est le potentiel de la sphère dure, $U_{ij}^{\mathrm{SW}}$ est le potentiel de puits carré avec une portée d'interaction donnée par $r_c$ et $f(\mathbf{r}_{ij}$ précise la direction des interactions.

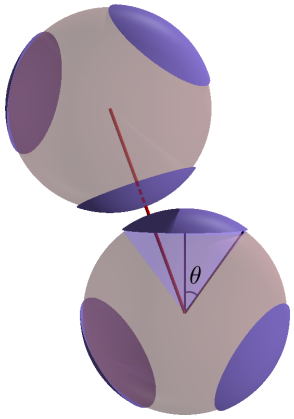


Figure 1: Représentation des particules à patch. La ligne rouge correspond au vecteur qui relie le centre de masse des deux particules. L'angle $\theta$ contrôle la taille du patch.

Les paramètres à contrôler sont les caractéristiques des patchs : leur nombre $n$, leur position et leur taille. La taille du patch est contrôlée par l'angle $\theta$ entre les vecteurs pointant du centre de la particule au centre du patch et à son bord, comme le montre la figure 1. On peut définir le pourcentage de surface couverte par les patchs $\chi$ comme $\chi = n(1 - \cos\theta)/2$. Il convient de noter que cette expression fonctionne tant que les patchs ne se superposent pas. Ici, nous utilisons un modèle de Kern-Frenkel modifié où chaque paire de particules ne peut former qu'une seule liaison. Cette condition nous permet d'interpoler entre deux cas extrêmes : lorsque la particule est complètement recouverte par les patchs, c'est-à-dire $\chi = 100\%$, l'interaction se

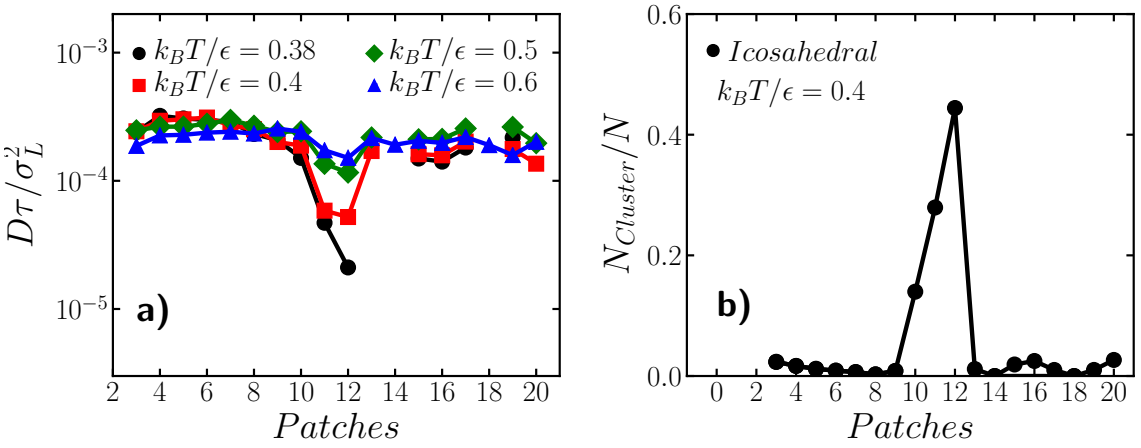


Figure 2: a) Coefficient de diffusion en fonction du nombre de patchs, à différentes températures, pour des particules à patch avec fraction de couverture fixe $\chi = 40\%$. Les points manquants correspondent à des systèmes cristallisés. b) Fraction des particules faisant partie de structures icosaédriques pour un nombre différent de patchs à température fixe $k_BT/\epsilon = 0.4$.

traduira directement par un puits carré et l'interaction correspondra à un potentiel de sphère dure lorsque $\chi = 0$.

## Dynamique translationnelle

Afin d'explorer en détail l'effet de la géométrie des patchs, nous explorons des systèmes de 3 à 20 patchs uniformément répartis sur la surface. Pour ce faire, nous localisons les patchs de manière à ce que la distance minimale entre deux patchs quelconques de la surface soit maximisée. Le cas à 12 patchs correspond à l'icosaèdre qui permet d'obtenir celui à 11 patchs en omettant un sommet. Afin d'empêcher la cristallisation, nous simulons un mélange binaire de particules de Kern-Frenkel de deux tailles, avec le rapport des tailles donné par $q = \sigma_S/\sigma_L = 0.833$, où $\sigma_{L(S)}$ désigne la taille des grandes (petites) sphères. Nous fixons la limite d'interaction $r_c = 1.031\sigma_{ij}$ , où $\sigma_{ij}$ est la distance de contact entre les particules $i$ et $j$. Pour simuler les particules à patch, nous utilisons des simulations de dynamique moléculaire conduite par événements (EDMD) avec des conditions aux limites périodiques.

On commence notre étude en explorant l'interaction entre la dynamique translationnelle et la structure. Afin de comparer les différentes géométries, nous comparons les systèmes de même fraction de couverture $\chi = 40\%$, ce qui correspond à comparer des systèmes qui ont le même second coefficient du viriel. Afin de caractériser la dynamique, nous mesurons le coefficient de diffusion $D\tau/\sigma_L^2$ où $\tau = \sqrt{m\sigma_L^2/k_BT}$ est notre unité de temps. Sur la figure 2 a), nous reportons la constante de diffusion en fonction de du nombres de patchs pour différentes températures. De façon surprenante, on constate que le coefficient de diffusion est largement indépendant de la position des patchs, sauf lorsque celle-ci correspond à l'ordre icosaédrique (c'est-à-dire $10_{ico}$, 11 ou 12 patchs). Dans ce dernier cas, on observe un ralentissement extrême à basse température.

Les résultats précédents ont montré des preuves irréfutables que l'ordre icosaédrique influence la dynamique. Afin de caractériser en détail la structure locale de ces systèmes, nous utilisons l'algorithme de classification topologique des clusters (TCC) [11]. Cet algorithme caractérise la structure locale en capturant différents motifs structurels du clusters de $3$ particules à cluster plus complexes composés de $13$ particules. Sur la figure 2 b), nous montrons la fraction de particules qui font partie d'au moins un cluster icosaédrique pour une température fixe $k_BT = 0.4$ et pour toutes le nombre de patchs. L'ordre icosaédrique n'est observé en quantité significative que pour les systèmes à $10_{ico}$, $11$ et $12$ patchs. De plus, lorsque la température diminue, le nombre de clusters icosaédriques pour ces géométries augmente fortement, ce qui prouve que la localisation des patchs renforce l'ordre icosaédrique lié à un ralentissement extrême de la dynamique.

On peut donc conclure que les particules à patch sont un bon moyen de contrôler la dynamique en renforçant les clusters icosaédriques. Et, fait remarquable, les locations de patchs qui ne correspondent pas à l'ordre icosaédrique local n'ont pas d'impact notable sur la dynamique.

## Dynamique rotationnelle

L'ajout d'interactions directionnelles par l'utilisation de particules à patch fait qu'il est intéressant de suivre la dynamique de rotation. Dans cette section, afin d'explorer l'effet des patchs sur la dynamique rotationnelle, nous simulons des mélanges binaires de particules à 6 et 12 patchs. Nous modifions la taille des patchs en entre les deux cas extrêmes : les sphères dures et les interactions à puits carré. L'emplacement des patchs est tel que la distance entre eux est maximisée.

Afin de caractériser la dynamique de rotation, nous calculons la fonction de corrélation de rotation [12]:

$$C_l(t) = \frac{1}{N} \sum_j^N P_l \left( \hat{\mathbf{u}}_j(t) \cdot \hat{\mathbf{u}}_j(0) \right) \tag{2}$$

où $P_l$ est le polynôme de Legendre du $l$-ième degré et $\mathbf{u}$ est un vecteur unitaire fixe qui tourne avec la particule. La façon dont $C_2$ décroît fournit des informations sur le mécanisme de la relaxation rotationnelle. De plus, nous pouvons extraire le temps de relaxation rotationnelle de la longue décroissance temporelle de $C_2$ [13]. En particulier, on a constaté que les particules avec des patchs relativement petits ont tendance à tourner autour du même axe pendant une longue période, ce type de mouvement est appelé 'free spinner' et il se traduit par une augmentation soudaine du $C_2$ après sa décorrélation, comme le montre la figure 3 a). Cela se produit lorsque le système forme très peu de liaisons, de sorte que les collisions sont rares et que les particules continuent à tourner autour du même axe. De plus, dans le cas des $12$ patchs, on constate qu'il y a un plateau dans la décroissance de $C_2$ (Voir figure 3 b)) qui signale le ralentissement de la dynamique de rotation dû aux liaisons avec les particules voisines, cela se produit principalement lorsque la taille des patchs est relativement grande et que les particules forment plus de

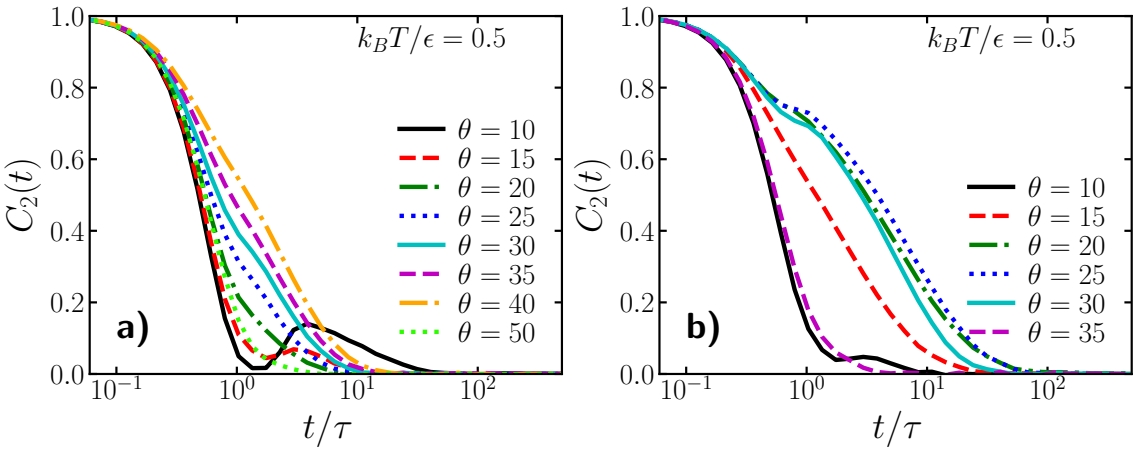


Figure 3: Fonction de corrélation de rotation pour a) le système à 6 patchs et b) le système à 12 patchs.

liaisons. Par conséquent, afin de décorréler complètement à partir de l'orientation initiale, plusieurs liens doivent se rompre, ce qui entraîne un ralentissement de la dynamique de rotation.

Pour finir, nous avons comparé les échelles de temps de relaxation rotationnelle et translationnelle. La première est considérablement plus petite que la seconde. Cela indique un mécanisme de relaxation plutôt local. Nous confirmons cette hypothèse en utilisant un modèle simple pour approximer la relaxation rotationnelle de chaque particule dans sa cage locale. Pour ce faire, nous utilisons des simulations de type "Monte Carlo Dynamique", où on fixe les positions de toutes les particules sauf une, puis on échantillonne les rotations de cette particule à l'intérieur de sa cage locale. Nous avons constaté que ce modèle simple est capable de reproduire le même comportement de relaxation rotationnelle que la dynamique moléculaire complète. Enfin, on peut conclure que la relaxation rotationnelle dans les systèmes de particules à patch est essentiellement régie par des réarrangements locaux. La dynamique est une conséquence de l'interaction entre la géométrie de la structure locale et le nombre de liaisons dans lesquelles la particule est impliquée.

## Particules à patchs monodisperses

Dans le régime vitreux, les systèmes ont évité la cristallisation. Il existe différentes façons d'éviter la cristallisation, comme l'utilisation de mélanges de différentes tailles et compositions. Cependant, cela peut enchevêtrer la dynamique des différentes espèces, et un verre monodisperse pourrait aider à simplifier l'étude de ses propriétés dynamiques. Nous proposons ici l'utilisation de particules à patch comme voie vers le développement d'une substance de verre monodisperse. Cette idée est basée sur l'observation que les systèmes binaires de particules à patch se sont montrés être un excellent outil pour explorer et contrôler l'interaction entre la structure et la dynamique des liquides, et que les change-

ments qui induits sur la structure locale peuvent suffire à éviter la cristallisation.

Dans cette étude, on a exploré deux systèmes de patchs monodispersés : l'un avec $n = 12$ patchs et l'autre avec $n = 8$ patchs. Le premier renforce les clusters icosaédriques et le second n'est lié à aucun cluster spécifique. Afin de déterminer s'ils sont de bons précurseurs dynamique. Nous avons montré que les deux géométries sont capables d'éviter la cristallisation. Cependant, le $n = 12$ favorise de forts changements structurels, qui s'écartent fortement de la structure d'un 'liquide simple'. Au contraire, le système à $8$ patchs montre à la fois la capacité d'éviter la cristallisation à basse température et de préserver la structure globale du liquide à différentes fractions de remplissage.

Cette section nous permet de conclure que les particules à patch sont d'excellents outils pour explorer la relation entre la dynamique et la structure. Les particules à patchs représentent une voie pour contrôler la dynamique de rotation et de translation en renforçant l'ordre icosaédrique dans le système.

## Sphères dures : Prédiction du comportement dynamique à partir d'informations structurelles

Dans la deuxième partie de la thèse, on se concentre sur la possibilité d'extraire des informations sur le comportement dynamique à partir des seules informations structurales. Pour cela, on se tourne vers l'un des modèles les plus simples de formation du verre : les sphères dures.

Les sphères dures sont sans doute le modèle le plus fondamental de la science colloïdale, tant pour la théorie que pour la simulation et les expériences. Leur interaction n'est infiniment répulsive que lorsque les particules se trouvent à une distance égale à leur diamètre $\sigma_{ij}$. À haute densité, les mélanges de sphères dures présentent une dynamique vitreuse. Ici, nous explorons la relation entre la dynamique et la structure dans une grande variété de mélanges de sphères dures. Pour cela, on simule des mélanges binaires de sphères dures avec des rapports de taille $q = \sigma_S/\sigma_L$ allant de $0.6$ à $0.85$ par incréments de $0.05$. En outre, on fait varier la composition du système $x_L = N_L/N$, où $N_L$ est le nombre de grosses particules et $N$ le nombre de particules, de $x_L = 0.2$ à $0.65$ tous les $0.05$. La combinaison de ces deux paramètres nous donne au moins $60$ systèmes différents. De plus, nous simulons des systèmes polydisperses avec une polydispersité comprise entre $1\%$ et $20\%$.

Nous commençons par caractériser leur comportement dynamique en calculant le temps de diffusion comme : $\tau_D = \sigma_L^2/D\tau$ où $D$ est le coefficient de diffusion. Nous démontrons que le comportement dynamique des mélanges binaires est fortement dépendant de la composition des systèmes et, en général, il présente un comportement complexe et non-monotone en fonction de la composition. De plus, chaque rapport de taille montre des comportements qualitativement différents. Sur la figure 4 a) nous reportons le temps de diffusion $\tau_D$ en fonction de

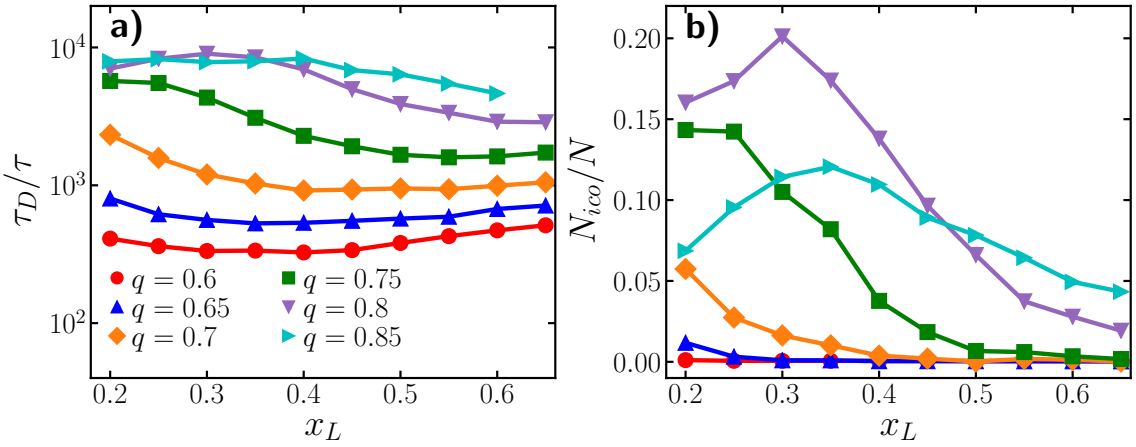


Figure 4: a) Temps de diffusion $\tau_D$ en fonction de la composition $x_L$ pour les mélanges binaires de sphères dures avec différents rapports de taille $q$ comme indiqué. b) Fraction de particules à l'intérieur d'un cluster icosaédrique pour les mêmes systèmes.

la composition $x_L$ pour chacun des rapports de taille $q$.

Sur la base de ces informations, nous nous tournons ensuite vers la structure locale. En premier lieu, nous examinons les changements de l'icosaédralité (nombre de particules impliquées dans des clusters icosaédriques). Afin de savoir si l'icosaédralité est capable de saisir tous les changements dans la dynamique nous utilisons l'algorithme TCC [11] pour quantifier le nombre de particules impliquées dans les clusters icosaédriques. Sur la figure 4 b) nous montrons cette quantité en fonction de la composition pour chaque $q$. Les résultats montrent qu'en effet, le nombre de clusters icosaédriques et donc la structure locale dépendent fortement de la composition. De plus, d'autres structures apparaissent également avec les clusters icosaédriques. Néanmoins, les changements de l'icosaédralité et des autres structures ne sont pas capables de capturer tous les changements sur la dynamique.

La solution à ce problème semble résider dans la prise en compte d'une structure plus simple : les clusters tétraédriques. En fonction de la morphologie de la structure locale, chaque particule peut faire partie de plusieurs clusters tétraédriques. Nous proposons donc de caractériser la structure locale par un nouveau paramètre d'ordre appelé Tétraèdre de la Structure Locale (TLS), qui consiste à compter de le nombre de tétraèdres auxquels chaque particule participe $n_{\text{tet}}$. Nous avons constaté que ce paramètre d'ordre est capable de saisir les changements de dynamique de la plupart de nos systèmes de sphères dures. De plus, le TLS fonctionne bien pour différentes fractions volumique, ce qui se reflète dans toutes nos données par fraction volumique qui convergent sur la même ligne. Cet effondrement nous permet de prouver que, pour chaque fraction d'emballage, $n_{\text{tet}}$ fournit un excellent prédicteur du temps de diffusion, révélant une relation approximativement exponentielle entre $n_{\text{tet}}$ et $\tau_D$, comme le montre la figure 4.

Un aspect important de la dynamique vitreuse, est l'apparition d'une hétérogénéité dynamique,c'est-à-dire qu'il existe des régions qui ont une dynamique plus rapide que d'autres. Afin de vérifier dans quelle mesure la tétrahédralité réussit à capturer les caractéristiques dynamiques, nous quantifions le déplacement local de

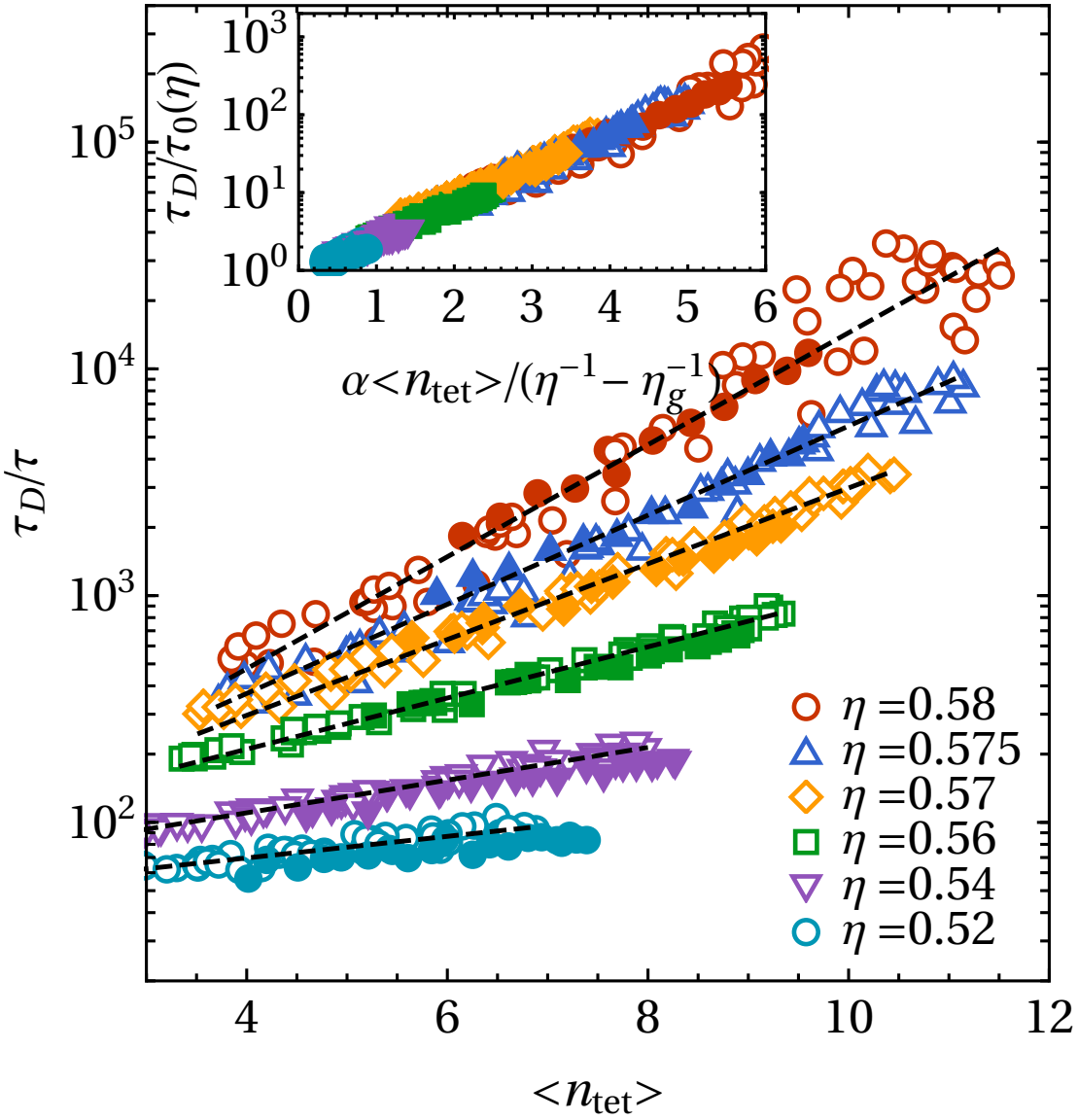


Figure 5: Temps de diffusion pour tous les mélanges de sphères dures étudiés en fonction de la tétrahédralité. Les différentes couleurs indiquent les différentes fractions volumiques. Dans chaque fraction volumique, les symboles ouverts correspondent à des mélanges binaires ayant des rapports de taille et des compositions différents. Les symboles fermés sont des systèmes polydispersés avec différentes fractions d'emballage. Les lignes pointillées sont des ajustements exponentiels aux données binaires pour chaque fraction volumique.

l'un de nos systèmes les plus lents. Ensuite, nous corrélons le TLS et la dynamique locale. On a constaté que ces deux quantités sont bien corrélées et que le TLS fonctionne bien pour capturer la dynamique locale, car les régions à dynamique lente correspondent aux régions à des valeurs plus importantes de la tétrahédralité.

Pour finir, on a testé le TLS dans deux modèles de précurseur des verres, les modèles Wahnström et Kob-Andersen. Les deux modèles consistent en un mélange binaire de particules qui interagissent avec le potentiel de Lennard-Jones. Mais le premier ne retient que la partie répulsive du potentiel et le deuxième a des interactions non-additives. On montre que le TLS est bien corrélé avec la dynamique locale sur les mélanges Wahnström. Notons que, en tant que répulsif comme les sphères dures, on s'attend à ce que des structures similaires apparaissent en allant plus loin dans le régime vitreux. Contrairement au mélange Kob-Andersen, le TLS montre une faible corrélation entre le nombre de tétraèdres et la dynamique locale. Notons par ailleurs que la non-additivité de ce mélange favorise des structures locales plus complexes qui peuvent être incompatibles avec la tétrahédralité.

Pour faire face à ce type de mélanges, nous nous sommes tournés vers une élégante méthode qui n'a comme entrée que des informations structurelles : *'méthode d'apprentissage machine non supervisé'* (UML). L'objectif principal de cet UML est de regrouper des particules ayant des structures locales similaires. Il fournit des informations sur la structure locale de chaque particule par le biais d'un ensemble de paramètres d'ordre de liaison. En appliquant l'UML à les mélanges de Kob-Andersen et Wahnström, nous avons constaté que pour les deux systèmes, l'UML capture des structures qui sont bien corrélées aux dynamiques locales. En plus, les corrélations sont plus élevées que celles obtenues avec le TLS. Il est à noter que l'UML ne dispose pas d'informations a priori sur le type de cluster, ce qui lui permet de capturer des structures non-triviales qui peuvent être corrélées avec la dynamique locale. Ces résultats ouvrent la voie à la prédiction de le dynamique dans divers d'autres systèmes vitreux, avec différents degrés de refroidissement de manière simple.

Avec les résultats présentés dans cette thèse, nous proposons une voie pour contrôler la dynamique des systèmes vitreux par l'utilisation de particules à patch. De plus, nous fournissons un paramètre d'ordre structurel simple et élégant qui est capable de capturer les changements locaux et globaux de la dynamique d'une grande variété de mélanges de sphères dures. La simplicité du TLS permet une comparaison avec les expériences et il fournit une voie pour connaître a priori les caractéristiques dynamiques générales d'un des verres les plus utilisés.

# List of Figures

# Symbols

| | |
|---|---|
| $\bar{Q}_i$ | Averaged bond order parameter over second shell neighbors. |
| $\chi$ | Percentage of the surface covered by the patches. |
| $\epsilon$ | Interaction energy. |
| $\eta$ | Packing fraction. |
| $\eta_c$ | Coefficient of shear viscosity. |
| $\hat{W}_i$ | Bond order parameter. |
| $n_{\mathrm{tet}}(i)$ | Number of tetrahedra each particle is involved in. |
| $\sigma_i$ | Diameter of particle $i$. |
| $\tau$ | Time unit of the simulations $\tau = \sqrt{m\sigma^2/k_BT}$. |
| $\tau_\alpha$ | $\alpha$-relaxation time. |
| $\tau_D$ | Diffusion time. |
| $\tau_R$ | Rotational relaxation time. |
| $\tau_T$ | Translational relaxation time $\tau_T = \tau_{0.3}$. |
| $\tau_{0.3}$ | Structural relaxation time defined as the time where the intermediate scattering function has decay to a value of $0.3$. |
| $\tau_{DMC}$ | Rotational relaxation time taken from the Dynamical Monte Carlo simulations. |
| $\tau_{FR}$ | Rotational relaxation time of a free rotor from Dynamical Monte Carlo simulations. |
| $\theta$ | Angle between the vectors pointing from the center of the particle at the center of the patch and its edge. |
| $\theta_F$ | Angle where the complete surface is covered. |
| $\theta_O$ | Angle where the patches start overlapping. |
| $B_2$ | Second virial coefficient. |
| $C_l$ | Rotational correlation function. |
| $D\tau/\sigma_L^2$ | Dimensionless diffusion coefficient. |
| $D_i$ | Dynamical propensity. |
| $F$ | Intermediate scattering function. |
| $F(k,t)$ | Intermediate scattering function. |
| $f_k$ | Non-ergodicity parameter. |
| $G_\infty$ | Instantaneous shear modulus. |
| $k$ | Wavelength. |
| $k_B$ | Boltzmann's constant. |
| $N_b$ | Number of bonds. |
| $N_{Dico}$ | Fraction of particles involved in an defective icosahedral cluster. |

| | |
|---|---|
| $N_{ico}$ | Fraction of particles involved in an icosahedral cluster. |
| $P_l$ | Legendre polynomial. |
| $q$ | Size ratio. |
| $Q_i$ | Bond order parameter. |
| $r_c$ | Interaction range or cut-off radius. |
| $S(k)$ | Structure factor. |
| $S_C$ | Configurational entropy. |
| $T$ | Temperature. |
| $T_f$ | Freezing temperature. |
| $T_g$ | Glass transition temperature. |
| $T_{MCT}$ | Mode Coupling Theory temperature. |
| $x_L$ | Composition. |
| $Y_{lm}$ | Spherical harmonics. |

# List of publications

- **S. Marín-Aguilar**, H. H. Wensink, G. Foffi, and F. Smallenburg, "Slowing down supercooled liquids by manipulating their local structure", *Soft Matter*, vol. 15, no. 48, pp. 9886-9893, 2019. [14].
- **S. Marín-Aguilar**, H. H. Wensink, G. Foffi, and F. Smallenburg, "Rotational and translational dynamics in dense fluids of patchy particles", *The Journal of Chemical Physics*, vol. 152, no. 8, pp. 084501, 2020. [15]
- **S. Marín-Aguilar**, H. H. Wensink, G. Foffi, and F. Smallenburg, "Tetrahedrality dictates dynamics in hard sphere mixtures", *Phys. Rev. Lett.*, vol. 124, no. 24, pp. 208005, 2020. [16].
- E. Boattini, **S. Marín-Aguilar**, S. Mitra, G. Foffi, F. Smallenburg and L. Filion, "Autonomously revealing hidden local structures in supercooled liquids", *Nat. Commun.*, vol. 11, no. 5479, (2020). [17].

# Introduction

*Natural science,*
*does not simply describe and explain nature;*
*it is part of the interplay*
*between nature and ourselves.*
***Werner Heisenberg***

Glasses are ubiquitous materials present in our daily life. The broad definition of a glass comprises innumerable types of systems. In short, if a fluid is cooled down or compressed sufficiently rapidly, it avoids crystallization and its dynamics sharply slow down. If the temperature keeps decreasing, the fluid becomes a glass, in where its dynamical behavior resembles to a crystal, as it apparently does not flow but structurally is similar to a liquid, as it does not have order.

In our histoy as a civilization, we have been in constant interaction with glasses. From the very beginning, we started using natural glasses, such as, the obsidian which is a glass made from the abruptly cooling of melt rock. With time, we have learned how to manufacture glasses and empirically make use of their properties. Our knowledge and control over glasses has evolved enormously from the first synthetic glasses found in Egypt 50000 years ago [18, 19]. Nowadays we have developed very precise and controlled ways of creating them and we have expanded their use to almost everywhere we see [20–23] .

Despite these advances, key knowledge is still missing, as some of the fundamental physics in the fluid's path to become a glass are not fully understood. One of these unknowns is the role the structure plays in the changes in dynamics. Even though the global structure in a glass is disordered as in a fluid, several studies point out that some changes in the local structure appear in the fluid as it heads towards the glass phase [6–8, 24, 25]. This point opens the door to several questions: what are the structures related to the changes on dynamics? is it possible to control the dynamics of a glassy system by changing its structure? And, can we predict dynamical behavior from only structural information?

This thesis will try to answer the previous questions through a detailed study of molecular simulations of some models for colloidal glasses. We will show that there is a clear relation between local structural changes and glassy dynamics and, that it is possible to learn something about the dynamical behavior of a glassy system only from its structure.

The present thesis is organized as follows: in Chapter 1 we revise the state of art of glasses, we begin with the definition of a glass, the features that characterize a glassy system, the main theoretical approaches and the advances on identifying the role of the structure on dynamics. In Chapter 2 we introduce the main tool used in this thesis: molecular dynamics and in particular Event Driven Molecular Dynamics.

From there, we turn our attention to the results. In Chapter 3 we explore the effect of adding directional interactions on the local structure of a glassy system. To do so, we analyze the translational dynamics and structure of binary mixtures of patchy particles. In particular, we will show that patchy particles that enhance icosahedral local structure promote a deep slow-down in translational dynamics. The directionality of the patchy particles allows us to distinguish between rotational and translational dynamics, Chapter 4 will be devoted to the analysis of the rotational dynamics of glassy patchy particles. There, we will show that rotational and translational dynamics are essentially decoupled as the first is only driven by local motion.

In line with the previous chapters, the changes on the local structure provoked by the directionality of patchy particles make them a great candidate as a monodisperse glass-former. In Chapter 5 we explore the idea of having a glassy patchy-monodisperse system. In particular, we show that a monodisperse system of patchy particles with $8$ patches preserves the 'liquid-like' structure in the supercooled liquid regime, making it a perfect candidate.

After showing the importance of the local structure in glassy patchy particles, we turn our attention to one of the simplest models of colloidal glasses: hard spheres. In Chapter 6 we explore the glassy dynamics of mixtures of hard-spheres, focusing on the effect of size ratio and composition on the local structure and dynamics. Finally, we show that the global and the local changes in dynamics can be captured by a simple order parameter called: Tetrahedrality of the Local Structure. This order parameter captures a universal local structure of hard spheres and can be used to predict local and global dynamics of hard-sphere mixtures. In Chapter 7 we extend the idea of tetrahedrality to other glass-former models. In line with these results, we briefly show how machine learning techniques can be applied to have a more general way of characterizing regions with similar structure as in the tetrahedrality.

To finish this thesis, in Chapter 8 we provide the general remarks about the results found in each Chapter. Additionally, we introduce some of the remaining open questions and perspectives.

Chapter 1

# Review of glassy systems

Glasses are present everywhere we look. They originate from the dynamical arrest of a fluid. In the fluid's journey to become a glass its dynamics slow down sharply and its relaxation behavior deviates from that of a fluid without strong structural changes.

The physics and the origin of this slow-down is still a subject of debate [1, 26] and at the present time, there is no theoretical approach that can explain all the changes in dynamical behavior. One approach for understanding the dynamical behavior of glassy systems is to look at the link between local structure and dynamics. In particular, a number of studies have shown that before the fluid becomes completely arrested, some mild changes on the local structure appear.

In this Chapter we will give a brief overview of the main points to understand the glass problematic, starting from a proper definition of a glass. We will discuss some of the main characteristics that arise in the fluid before it falls out of equilibrium and some of the proposed theories to explain them. Then, we examine the role of the structure in the glassy regime. Finally, to close this Chapter we review the behavior of some colloidal glass models that are central to this thesis: hard spheres, short-attractive potentials and patchy particles.

## 1.1 What is a glass?

We can distinguish the classical states of matter according to their dynamical and structural characteristics, in particular crystal and liquid phases. Liquids are characterized by short-range order, they have rotational and translational invariance and their particles have free movement controlled by the interaction between them. Their main dynamical characteristic is their ability to flow, i.e. if any amount of stress is applied to a fluid, it will change and adapt to this stress over a relatively short amount of time. On the other hand, crystals have long-range order as they consist of a unit-cell repeated in all directions. The particles in a

solid tend to vibrate around their averaged positions, and so, they do not flow.

In general, below a temperature $T_f$ a liquid undergoes to a first order transition to a solid phase. However, if the system is compressed or cooled down sufficiently rapidly, it can avoid crystallization and arrive to a glass phase. In this state, the fluid's liquid-like structure will be preserved (without long-range order). We will find a glass either at low temperatures or high densities where the crystal phase would be. Under these conditions, the dynamics of the system become slow as the particles cannot freely move as in a diluted fluid. As a result, the relaxation time, which is the time needed by a system to lose memory of its initial conditions, sharply increases. We say that a system has become a glass when below a temperature $T_g$ the relaxation time is larger than the experimental window of time. Below $T_g$ the system will fall out of equilibrium as it is not capable of exploring all of phase space in the window of time. For this reason, it is also known as a non-ergodic phase.

The definition of $T_g$ is rather ambiguous and is dependent on the system, the preparation protocol and also the probing window of time [27]. For molecular systems, often $T_g$ is defined as the temperature where the shear viscosity is $10^{12} Pas$[1] [1, 29] or the temperature where the relaxation time takes more than $100s$ [30, 31]. However, glasses can be found in other length scales including a wide variety of materials [1] and so, $T_g$ has to be adapted to each system. Among them, we find granular systems [32–34], molecular systems [35–37] and colloidal systems [38, 39]. The fact that there are several ways of defining the glass transition temperature indicates us that a proper glass transition is unclear.

In general, before the system fully falls out of equilibrium its dynamical features start deviating from the liquid ones: the relaxation time increases several orders of magnitude, the system develops a two-step relaxation and the system gets divided into faster and slower regions. This regime is called the glassy regime [1]. Once more, this is a general definition that can be applied to a wide variety of materials with intrinsic different characteristics. When a liquid is driven towards the glass transition by decreasing the temperature, the system typically arrives to a metastable phase with respect to a crystal. This is known as a supercooled liquid [1, 2]. Throughout this thesis, we will use the terms glassy regime and supercooled-liquid regime interchangeably.

### 1.1.1 Main characteristics of supercooled liquids

Once a fluid enters to the glassy regime it develops characteristic dynamical behavior different from the liquids. In this section, we will focus on three of the glassy fingerprints: two-step relaxation, fragility and dynamical heterogeneity.

[1] As a reference point, the shear viscosity of water at room temperature is $8.8 \times 10^{-4} Pas$ [28]

**Relaxation behavior**

In order for a system to relax, the system must decorrelate from its initial configuration, i.e. the particles should move enough such that the system loses any memory of the fluctuations of its initial configuration. Depending on the conditions of the system, the process of relaxation can vary. One of the common techniques to characterize the relaxation behavior is the time dependent density-density correlation $F(k,t)$, also known as intermediate scattering function (ISF). It measures the correlation between density fluctuations as a function of time and wavelength $k$, and is defined as follows [40]:

$$F(\mathbf{k},t) = \frac{1}{N}\langle \rho(-\mathbf{k},0)\rho(\mathbf{k},t)\rangle \tag{1.1}$$

where $N$ is the number of particles and $\rho(\mathbf{k},t)$ is the Fourier transform of the density:

$$\begin{aligned}\rho(\mathbf{k},t) &= \int \rho(\mathbf{r},t)\exp(-i\mathbf{k}.\mathbf{r})d\mathbf{r} \\ &= \int \sum_j [\delta(\mathbf{r}-\mathbf{r}_j)]\exp(-i\mathbf{k}.\mathbf{r})d\mathbf{r}, \\ &= \sum_j \exp(-i\mathbf{k}.\mathbf{r}_j)\end{aligned} \tag{1.2}$$

where $\mathbf{r}_j$ is the position of particle $j$ at time $t$.

At time $t=0$ the ISF is equal to the structure factor $F(k,0)=S(k)$. We define the normalized dynamic correlation function as $\Phi(k)=F(k,t)/S(k)$, which at time $t=0$ is $1$ corresponding to the full correlated state. And, at $t\to\infty$ it goes to $0$ when the system has fully decorrelated from its initial configuration. If the fluctuations of all length scales are uncorrelated, i.e. $\Phi(k,t\to\infty)=0$ we can consider that the system has reached equilibrium. Additionally, the decay of the ISF provides information on the process of relaxation over time. Moreover, a relaxation time can be extracted from its long-time decay, as we will describe later in this section.

In general, the ISF can be obtained from molecular simulations as the position of the particles are known at all time. Alternatively, it can be obtained from experiments, where the ISF is measured from dynamic light-scattering, inelastic neutron scattering and x-ray scattering.

In the limit of high temperatures, the ISF decays exponentially as the system rapidly loses memory of its initial configuration, this can be seen in Fig. 1.1 a), where we show the ISF for different states. The picture changes in the glassy regime, the relaxation behavior becomes more complex as it deviates from the high temperature liquid. In particular, the ISF presents a two-step relaxation behavior, as shown in more detail in Fig. 1.1 c).

At short times the particles start diffusing and the system begins to decorrelate. This is reflected in a first decay in the ISF called $\beta$-relaxation. However, since

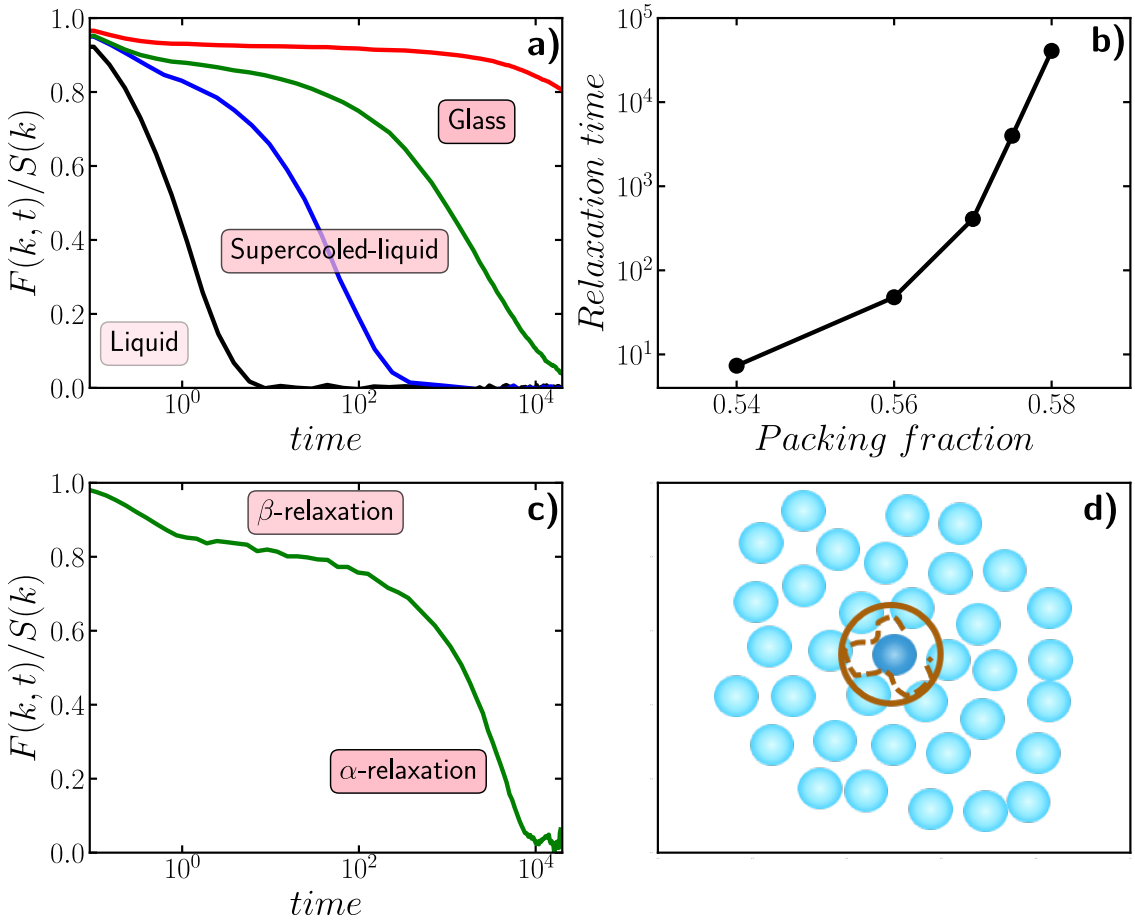


Figure 1.1: Two-step relaxation behavior of glassy systems. a) Shows the ISF at different states, in the liquid regime it decays exponentially. In the glassy regime the relaxation behavior presents a two-step relaxation. Once the system becomes a glass the ISF do not decay. b) As the system is cooled down or compress the relaxation time of a glassy system increases several orders of magnitude. c) Glassy systems have two step relaxation, the first relaxation corresponds to the $\beta$-relaxation. Once the particles encounter their neighbors they get arrested by the cage made by them. Finally, once the particles escape, the ISF continue relaxing. d) Illustration of the cage effect.

particles are typically quite close to each other in the glassy regime, a particle cannot move freely for long before its path is obstructed by a neighbor. Once the particles encounter their nearest neighbors, they get arrested inside a 'cage' formed by these neighbors. This is known as the 'cage effect', see Fig. 1.1 d). The particles spend time rattling inside the cage before breaking free. As a consequence, the density fluctuations decorrelate very slowly during that time and the ISF presents a plateau, which depends on the system conditions, i.e. the temperature or density. If the conditions of the system are not too tight, collective rearrangements eventually happen and the particles will escape their cages. Hence, the system undergoes a second relaxation, known as $\alpha$-relaxation. After this relaxation, the system finally fully decorrelates from its initial configuration.

In contrast, if the temperature of the system is $T < T_g$, the particles will get trapped permanently in their cages and the plateau will not decay over the entire window of time covered by the experiment or simulation, as shown in Fig. 1.1a).

In the glassy regime, the long-time relaxation ($\alpha$-relaxation) decays differently from an exponential function and it can be fitted with a Kohlrausch– Williams–Watts (KWW) relation, better known as stretched-exponential function. This expression takes the form: $A\exp(t/\tau_\alpha)^\gamma$ where $A$ and $\gamma$ are fitting parameters and $\tau_\alpha$ corresponds to the relaxation time. In particular, $\tau_\alpha$ will depend on the conditions of the system and it sharply increases as the system gets closer to the glass state, at larger densities or smaller temperatures. This behavior is shown in Fig. 1.1 b) where we show the relaxation time of a hard-sphere mixture as a function of its packing fraction. This non-exponential long time relaxation behavior [41, 42] has been found in a wide variety of glasses with different intrinsec natures: spin glasses [43], metallic glasses [44], molecular glasses [45] and colloidal glasses [46].

Another measurement that captures this anomalous relaxation behavior is the mean-squared displacement (MSD) which is a measure of the particle's displacement in time, calculated as:

$$\left\langle \mathbf{\Delta r}^2(t) \right\rangle = \left\langle \frac{1}{N}\sum_j^N |\mathbf{r}_j(t) - \mathbf{r}_j(0)|^2 \right\rangle, \tag{1.3}$$

At short times, before the particles collide they undergo ballistic motion, hence, the mean squared-displacement has a quadratic relation with time. As in the ISF, once the particles encounter their neighbors, the MSD develops a plateau as the particles cannot diffuse due to the cage effect. Finally, once the particles break free from the cages the system arrives to a diffusive regime, where the relation of the MSD with time becomes linear [2].

**Fragility**

As we have pointed out, there is a fast increase on relaxation time with temperature in the glassy regime. Depending on the nature of the relation between the relaxation time and the temperature we can distinguish between two types of glass-formers: fragile and strong. These different behaviors were first explored in terms of the fluid's viscosity. However, based on the Maxwell model that couples elastic and viscous behaviors (see Appendix A), the relaxation time and the viscosity can be linearly related as $\tau = \eta_c/G_\infty$, where $\eta_c$ is the viscosity and $G_\infty$ is the instantaneous shear modulus which does not vary in the supercooled liquid regime and thus, this relation is valid in the glassy regime [1].

The behavior of the strong and the fragile glass former can be seen from plotting the logarithm of the viscosity (or the relaxation time) versus $T_g/T$. This type of plot is known as an Angell plot [47]. In Fig. 1.2 we show a typical Angell plot for two of the typical strong and fragile glass formers.

[2] In real systems, such as colloidal systems, the ballistic motion is found at only extremely short times. Instead, at short time scales the particles undergo Brownian motion. This leads to distinguish in the MSD a short-time diffusive regime and a long-time diffusive regime. The ballistic motion is mainly found as an artifact in molecular simulations.

A system is considered a strong glass former when the relaxation time follows an Arrhenius behavior:

$$\tau_\alpha = \tau_0 \exp(E/k_B T), \tag{1.4}$$

where $\tau_\alpha$ is the relaxation time, $T$ the temperature, $k_B$ the Boltzmann's constant and $E$ an activation energy. This relation tells us that the relaxation is controlled by an energy barrier that activates the process [1]. In the Angell plot of Fig. 1.2 the strong glass regime can be seen in the upper part of the plot where the relaxation behavior tends to be a straight line. Some of the strong glass-formers are also known as networking glasses as they tend to have three-dimensional network structure with covalent bonds [48]. For example, they can have open tetrahedral networks [49], as found in e.g. pure silica $SiO_2$ and germanium dioxide $GeO_2$.

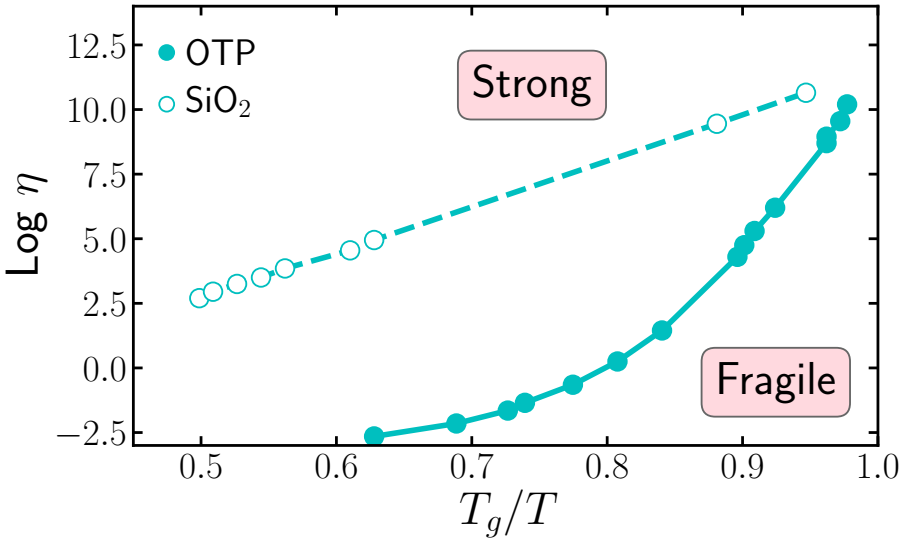


Figure 1.2: Angell plot of the prototypical strong glass former $SiO_2$ and fragile glass former $OTP$. Data reproduced from Ref. [50].

In contrast, the relaxation of fragile glass-formers follows a super Arrhenius behavior. One way of describing this relation is by fitting the relaxation time with a Vogel-Fulcher-Tamman (VFT) equation [41, 51]:

$$\tau_\alpha = \tau_0 \exp\left(\frac{DT_0}{T - T_0}\right), \tag{1.5}$$

where $\tau_0$, $T_0$ and $D$ are fitting constants and the value of $D$ will provide a measure of how fragile the system is. It is interesting to remark that the relaxation time diverges at a temperature $T_0$, which in general is lower than the glass transition temperature $T_g$. Among the fragile liquids the most used and well studied is the ortho-terphenyl (OTP). The fragile regime is easy to locate in the Angell plot as it corresponds to curved lines, as can be seen in Fig. 1.2.

### Dynamical Heterogeneity

In a simple fluid all the particles diffuse homogeneously without any particular restrictions. In contrast, in the glassy regime the particles are arrested by the cages

made by their neighbors, depending of collective rearrangements the particles will escape their cages. In this picture, some particles are going to start diffusing before others and as consequence, the system gets spatially divided by regions with faster and slower dynamics.

This behavior is known as dynamical heterogeneity (DH). DH has been found both in experiments [52–56] and simulations [53, 57, 58]. Different techniques have been applied to characterize DH, in particular in simulations the use of four-point correlation functions and the calculation of dynamical propensity have been of great use. The latter one allows us to color the particles depending on the effective displacement of each particle in a window of time. In Fig. 1.3 we show a glassy system of a Wahnström mixture [3] colored by their propensity where red regions correspond to fast dynamics.

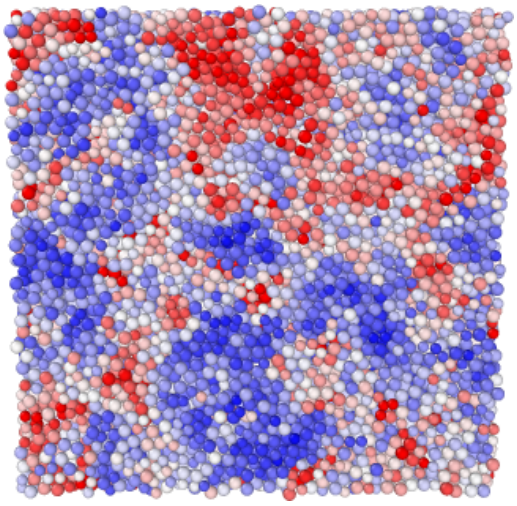

Figure 1.3: Example of dynamical heterogeneity of a Wahnström system at $k_BT/\epsilon = 0.7$. Particles colored by their dynamical propensity. Red regions have larger displacement than the blue regions.

It has been shown that as the system approaches the glass transition the correlation between this dynamical regions grows. This is translated in a growing dynamical correlation length similar to the growing correlation length in spin systems near to a transition [59]. In Chapter 6 we will talk in more detail about DH and the way of characterizing it.

### 1.1.2 Different length scales, similar glassy features

The transition between a fluid state to an arrested one is present in a wide variety of systems with different length scales. Examples of them are: molecular glasses, colloidal glasses, spin glasses and granular glasses. Most of them have in common the already mentioned glassy characteristics. However, one of the main difference between them lies in the different temporal and length scales at where things happen. Here, we will give a general description of these types of glasses making some emphasis on colloidal glasses.

One of the most common and studied glassy systems are molecular glasses. Their building blocks consist of small molecules. Depending on the molecules nature we can further classify them in: organic glasses, silicate glasses, phos-

[3] The Wahnström mixture consist of a binary mixture of particles interacting through Lennard-Jones potential with size ratio $q = 0.833$ and composition $x_L = 0.5$. The potential is truncated and shifted to the minimum of the potential, preserving only the repulsive part of the Lennard-Jones potential.

phate glasses, metallic glasses, etc. Each of them have their own physical and chemical particularities. Important to remark is that related to the small size of the molecules the time scale at where things happen is faster. As a consequence in experiments at low temperatures it is relatively easy to see the changes in the structural relaxation over many decades.

In contrast, granular systems are composed of macroscopic grains and thus the length scales are considerable larger. An example of granular systems is sand. The interaction between the particles is typically only repulsive and the gravity and friction both play important roles in their physical behavior. Moreover, the thermal fluctuations do not have any effect on granular systems [60]. If they are externally supplied with kinetic energy (e.g. by vibrating the system), granular systems can flow similarly to a fluid and at high packing fractions their relaxation time increases rapidly, similar to fluids in the glassy regime [26].

Finally, the length scales of colloidal glasses are in between the molecular and the granular ones. *"A colloidal dispersion is a system in which particles of size roughly between* $1nm$ *and* $1\mu m$ *of any nature (e.g. solid, liquid or gas) are dispersed in a continuous phase of different composition or state" [61].* Due to the size of the particles, thermal fluctuations are relevant in colloidal systems. Depending on the nature of the dispersed and the continuous phase the system takes different names: *suspension* (solid particles in a liquid) such as paint or milk, *emulsion* (liquid droplets in an immiscible liquid) such as salad dressing, *foam* (gas bubbles in a liquid or solid) like ice cream and *aerosol* (liquid droplets in a gas) such as fog [39]. Moreover, the dispersed particles can have different shapes, such as spherical particles, rods, polyhedral particles, etc. However, in this thesis we will focus on spherical particles.

In general, colloidal systems present several advantages that make them a perfect choice to study in detail the changes on structure and dynamics in the glassy regime. For example, colloidal suspensions present a glass transition similar as molecular glasses, their relative large sizes allows them to be followed in experiments using e.g. confocal microscopy, light scattering, among others [46]. However, a consequence of their large sizes is that their respective microscopic time scale is larger than the one of molecular glasses. As a result, dynamical slowdown in colloidal systems can only be observed over a few decades, before time scales become too long to probe in a reasonable amount of time. Thus, colloidal glasses can be only compared with molecular glasses at relatively high temperatures [1].

The scope of this thesis concerns mainly model systems inspired by colloidal glasses, and we will discuss in more detail some colloidal models in Section 1.4.

## 1.2 Theoretical approaches

Several approaches have been proposed to explain the peculiar dynamical characteristics of supercooled liquids. So far, there is not a full theory capable of

capturing at the same time all the features and changes towards the glass transition. However, each approach has their own victories on explaining parts of the dynamical changes towards the 'glass transition'.

Following the same trend of ideas as in Ref. [1] we divide the theories in two main families: the first one is related to mean-field approximations, in particular the Random-First Order Transition, the Mode Coupling Theory and the Adam-Gibbs Theory. The second family is related to the theories around Dynamical Facilitation. Here, we will briefly discuss each of these approaches and we refer the reader to dedicated reviews of each of them.

## Mean-Field Approximations

### Adam-Gibbs Theory

In 1965 Adam and Gibbs proposed a way of explaining the temperature dependence of the relaxation in the glassy regime [62]. It is mainly focused on the idea of cooperative rearranging regions and that the relaxation is controlled by its configurational entropy $S_C(T)$, which is obtained from subtracting the vibrational entropy from the total entropy $S_C(T) = S(T) - S_{Vib}(T)$ [63]. The rearrangements are thermally activated processes, and one of the main ideas of this theory is that the activation energy is inversely proportional to the configurational entropy:

$$\Delta E(T) \propto \frac{1}{S_C(T)}. \tag{1.6}$$

The increase of relaxation time is attributed to the growth of the cooperative rearranging regions [64].

Although these ideas are appealing for explaining part of the anomalous relaxation behavior, some gaps still remain to be filled, such as the nature of the rearranging regions [63].

### Mode Coupling Theory

In the 1980's the Mode Coupling Theory (MCT) was proposed as a mean field approximation [65]. Its main goal is to predict the peculiar relaxation behavior of a fluid in the glassy regime. In particular, it is focused on predicting the intermediate scattering function $F(k,t)$ by solving its equation of motion through some approximations. The most important part is that the only input is the structure factor $S(k) = F(k,0)$ which presumably contains all the structural information. We refer the reader to Refs. [65–67] for a full derivation of MCT equations.

In general, MCT performs incredibly well. It captures the changes in relaxation dynamics in the glassy regime by recovering the two-step relaxation and

the cage effect. Moreover, it has been applied to a wide variety of systems predicting interesting behaviors. Among them, it captures a reentrant behavior in the phase diagram of short-ranged potentials.

MCT seems to work less well deep in the glass regime. One of its predictions is a temperature $T_{MCT}$ where the system stops relaxing, which in general is larger than the experimental $T_g$. Nevertheless, in simulations and experiments the glassy systems keep on relaxing at $T < T_{MCT}$. This is because, at that regime the particles present 'hopping' motions that allow them to escape the cages and continuing relaxing [68]. MCT does not take into account this type of motion and fails on predicting the transition. Additionally, it lacks information on the dynamical heterogeneity present in the glassy regime and the explanation of the different fragilities. Some extensions have been done to the MCT to improve this failures, for example the incorporation of higher order correlations, the incorporation of external fields to the classical MCT equation, etc [65].

#### Random First Order Transition

Finally, the ideas of the Random First Order Transition Theory (RFOT) resonate with the previous ones, and in some limit cases the results of both can be recovered [69].

The RFOT is also based on the configurational entropy $S_C$ and in particular, it postulates that the liquid is divided into metastable regions with different sizes [64], called 'mosaic states'. Both the Adam-Gibbs theory and the RFOT predict a divergent length scale at low temperatures, however their main difference is the power of the divergence. In particular, RFOT predicts larger length scales compared to the ones predicted from Adam-Gibbs theory.

As explained in Ref. [1] and Ref. [30], RFOT can be considered in a more general sense as the union of the ideas of MCT, Adam-Gibbs theory and spin glass theory. These mean field theories can be rationalized in terms of the energy landscape of the supercooled-liquid. At low temperatures, the supercooled-liquid landscape presents many minima and saddle points, from here the definition of the configurational entropy is recovered as $S_C = 1/N \log N(f)$, where $N(f)$ is the number of free-energy minima. At temperatures $T > T_{MCT}$ there is just one minimum corresponding to the fluid equilibrium energy. At $T = T_{MCT}$ the landscape becomes fragmented in an exponential number of minima. At $T < T_{MCT}$ the relaxation is an activated process and the barriers between local energy-minimum grow as the temperature is decreased. The original RFOT mosaic idea applies in this last regime.

### Dynamic Facilitation

One of the most recent approaches to the glass problem is the idea of dynamic facilitation (DF). Differently from the previous approaches which were mainly

based on thermodynamic concepts, DF focuses on the dynamical aspects of the glassy regime, such as the dynamical heterogeneity [70]. DF is part of a series of models called kinetically constrained models, which formulate that the kinetical arrest is mainly driven by geometrical constraints [1].

The main idea of DF is that the relaxation of some few particle will facilitate the motion of the particles that surround them, as consequence a mobile region is created. In particular, the movement of those few particles is known as excitation lines. Once an immobile region is intersected by one of these excitation lines, the region will be able to move for a time $t$ until the excitation line leaves it.

In short, DF captures well the physical changes in the dynamical behavior of glassy systems, however their results can not been derived from microscopic calculations [1].

## 1.3 The role of the structure

None of the previous approaches make strong assumptions about the structure in the glassy regime. However, in principle each approach has room for the consideration of changes in structure of the fluid as it becomes more supercooled. This is clearer in the MCT approach where the dynamical behavior is characterized by only structural input and it is fair to ask what are the structural changes that lead to those extreme changes in dynamics?. In both RFOT and Adam-Gibbs theory, structural variations can be present between the inside and outside of cooperative regions and in between the 'mosaic' pieces that form the supercooled liquid. Finally, in the DF approach, one might think that the excitation lines or the immobile regions have a preferred structure.

The overall picture of glasses gets complicated near to the glass transition temperature where the role the structure plays is not clear [6]. In this thesis we will mainly focus in the changes on the structure and their relation with dynamics in the glassy regime. In the following section we will discuss in more detail the role of the structure in the glassy regime.

### 1.3.1 Geometrical Frustration (The role of five-fold symmetry)

A fluid can access the glassy regime only by avoiding crystallization. There a various mechanisms to avoid crystallization and we will address them in more detail in Chapter 5. However, one of the main ones is through geometrical frustration.

A crystal is characterized by long-range order, unit-cells with specific patterns are replicated in all directions to fill the space. However, some local structures cannot tile all of the space in a periodic manner as a consequence of the nature of their rotational symmetry. This symmetry is given by the value of the needed rotation around an axis that maps a lattice into itself. These rotations can be: $2\pi$,

$2\pi/2$, $2\pi/3$,..., $2\pi/7$, better known as one-, two-, three-, ..., seven-fold symmetry. Only two-, three-, four- and six-fold symmetry structures can be periodically replicated in all directions, the rest of them cannot [71]. The idea that some structures cannot tile periodically and that they would hinder the grow of a crystal structure is the heart of the geometrical frustration theory.

The importance of this frustration in supercooled liquids was first highlighted by Sir Charles Frank [5] in 1952. He analyzed the best ways of arranging 12 particles around a central one: thinking of crystal structures, the first arrangements that come to mind are a faced-centered cubic (FCC) lattice and an hexagonal close-packed (HCP)lattice. However, another option is to locate the particles on the vertices of an icosahedron. This last structure has five-fold symmetry and thus it cannot regularly fill space [72]. Moreover, if the particles are interacting through a Lennard-Jones potential the binding energy of the icosahedral order is lower than its crystal-like counterparts, making it energetically favoured. Hence, Frank suggested that it is likely that more particles would find themselves in an icosahedral environment by undercooling a fluid [5].

In Frank's ideas, icosahedral clusters represent a frustration in the system, as there is spontaneously formation of icosahedral clusters that do not fit with the crystal lattice, yet are energetically favored. In general, geometrical frustration is the incompatibility between the locally preferred structure and the global tiling [4]. Based on the previous ideas, in 1995 Kivelson et al. proposed a formal geometrical frustration theory for supercooled liquids [3,73]. The heart of theory is based on the following propositions:

- A liquid is characterized by locally favored structures (LFS) which are different from the crystal unit cells. This preferred structures minimize the local free energy.
- The LFS cannot tile the whole space.
- It is possible to build a reference system where the effect of the frustration can be turned off. This point is particularly interesting, because by changing the topology of the space some of the LFS can fill the space. This is the case of the perfect icosahedra, which can form a perfect phase on the surface of a four-dimensional hypersphere with radius $5/\pi$ times the interatomic geodesic distance [4,72].

From the ideas of the dynamical frustration theory, depending on the 'degree' of frustration, the size of the domains with LFS will grow upon undercooling the system, at weak frustration the domains will be larger than in strong frustration. Moreover, the 'degree' of frustration can be related to the fragility of a glass, large fragility is related to small frustrations [4]. If the frustration is removed, the system undergoes to a phase transition to an ordered phase [74, 75]. We refer the reader to Ref. [4] for a more detailed review of geometrical frustration.

The ideas of geometrical frustration have inspired a growing interest on the role of the structure on glassy dynamics [6–9]. Now the question is, what is the

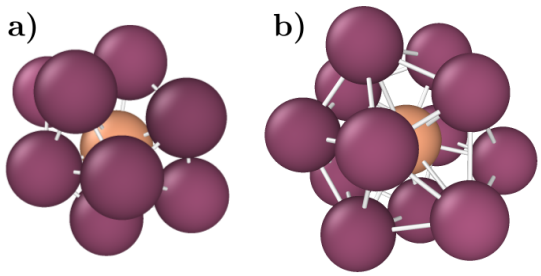


Figure 1.4: Defective Icosahedral Cluster and Icosahedral Cluster.

exact geometry of the LFS?

### 1.3.2 Local Favored Structures

In general, the nature of the LFS depends on the system and the interaction between the particles [76]. The now well known icosahedral cluster has been found in systems that interact additively, in particular in repulsive systems such as the Wahnström mixture. A closely related structure, the defective icosahedron cluster has been found as well in hard-sphere mixtures [8] (see Fig. 1.4 a) and b)). The number of these clusters increases sharply when cooling or compressing the fluid.

Conversely, in systems with non-additive interactions (used for modeling metallic glasses such as the Kob-Anderson mixture [4]). In this system, the icosahedral clusters are almost not present, however other types of LFS are found, among them are trigonal prismatic, capped trigonal prismatic and bicapped square antiprisms structures [7,74].

In general, the LFS possess long life times compared with other structures [7, 11,74,77]. As consequence of their life times, the LFS domains have been related to regions with slow dynamics, linking them with the concept of dynamical heterogeneity [77].

Finally, variations in fragility can be also related to the nature of the LFS and the degree of frustration. In particular, in additive systems which tend to be more fragile, there is a sharp increase of LFS at smaller temperatures. In return, the domains in non-additive mixtures are smaller in size and their increase with temperature is more modest, this translates to stronger frustration which is related to less fragile systems [4,7].

In order to characterize the nature of the LFS, different methodologies are proposed depending on the position of the particles. In Section 2.3 we will discuss in detail two techniques to identify the LFS: Voronoi Face Analysis [25] and Topo-

[4]The Kob-Andersen mixture consist of a binary mixture of particles with $q = 0.8$ and $x_L = 0.2$ interacting through a Lennard-Jones potential. This model is non-additive: the interaction depends on which species is interacting with which one: $\sigma_{AB} = 0.88\sigma_{AA}$, $\epsilon_{BB} = 0.5\epsilon_{AA}$ and $\epsilon_{AB} = 1.5\epsilon_{AA}$

logical Cluster Classification [11].

## 1.4 Colloidal Glass Models

To finish this Chapter we discuss some of the colloidal glass models used in this thesis. In general, colloidal systems are perfect candidates to explore the interplay between the structure and the dynamics on the glassy regime. They present numerous advantages: their relative big sizes allow a more detailed structural characterization in experimental realizations and their physical and chemical properties can be modified and controlled. Moreover, their interactions can be tuned by modifying the particle surfaces, by adding electrolytes or polymers, by changing the temperature or by changing the shape of the particles [78](from spherical, cubical and a wide variety of polyhedral shapes [79, 80]). This in turn has a strong effect on the local structure which can be used to explore the changes on glassy dynamics. Another important aspect from colloidal systems, is that due to their size, quantum effects can be neglected, and thus, the interaction between particles can be modeled in simple ways.

### 1.4.1 Hard-Sphere systems

The most simple way of modelling the interactions between colloidal particles is through a purely repulsive potential: the hard-sphere potential (HS). Two particles interact repulsively only when the distance between them is equal to the diameter of the particles. The phase behavior of HS is only controlled by the packing fraction $\eta$ which is the ratio between the volume occupied by the particles and the volume of the system. In 1957 Alder and Wainwright, with the use of molecular simulations, found that monodisperse hard-spheres exhibit a phase transition between a fluid phase and a crystal at high packing fractions [81]. This transition was later confirmed in experiments [82], where particles of polymethylmethacrylate (PMMA) grafted with a layer of a soft polymer were used as hard-spheres. Beside the crystal phase at high $\eta$ they found a glassy regime and a glass state. This glass state arose because their samples had some degree of polydispersity and one way to suppress crystallization is through mixtures of particles with different sizes. From more detailed simulations studies, we now know that for monodisperse systems below $\eta = 0.49$ the fluid is the stable phase. Then, between $0.49 < \eta < 0.545$ a coexistence region between crystal and liquid is found and finally at $\eta \geq 0.545$ the crystal becomes the stable phase [81, 83]. However, if crystallization is avoided, at high packing fractions $\eta > 0.49$ a supercooled liquid regime appears [39,84]. In this last region, hard-sphere systems present the glassy features mentioned in Section 1.1.1. Moreover, this is the region where we explore the interplay between structure and dynamics in Chapter 6. A schematic picture of the phase diagram as a function of the packing fraction is shown in Fig. 1.5.

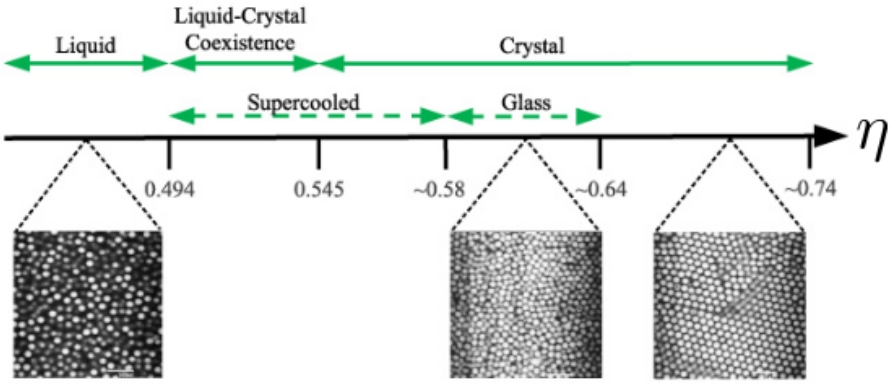


Figure 1.5: Schematic hard-spheres phase diagram. The top line shows the phases of the monodisperse phase diagram. Dashed arrows indicate the arise of the supercooled liquid regime and the glass phase once the system is polydisperse. Bottom images correspond to confocal micrographs of hard-sphere like colloidal particles with $5\%$ of polydispersity. Image reproduced from Ref. [39] G. L. Hunter and E. R. Weeks, *Reports on progress in physics*, vol. 75, no. 6, p. 066501, 2012 ©IOP Publishing. Reproduced with permission. All rights reserved.

### 1.4.2 Attractive colloids

In general, the interaction between colloidal particles can be also attractive due to e.g. van der Waals attractions or depletion interactions. For understanding this last interaction, we can imagine a system with $N$ colloidal particles mixed with $n$ smaller non-absorbing polymers, where the interaction of both is only repulsive as shown in Fig. 1.6. The configurational entropy of the polymer-chains will be maximized if the big colloidal particles get closer together, leaving more space for the small chains to move. This minimizes the free energy of the system, and it seems that the colloidal particles feel an 'attraction' in order to get close together even the colloidal-colloidal interaction is repulsive [78]. This 'effective attraction' is known as depletion interaction and it will depend on the size of the small particles, better known as depletants, and the solvent.

In experiments, one way of inducing attractions between colloidal particles is by attaching polymer chains to the surface of the particles. The range of the attraction depends on the solvent. A poor solvent will induce short-ranged interactions [78]. We can model this interaction through the addition of relatively short-ranged attractive interactions to hard-sphere-like particles. Which in turn, results in a richer phase diagram as now there is a gas-liquid coexistence.

In the glassy regime, an interesting phase behavior is found when the range of the attraction is smaller than approximately $0.1\sigma$, where $\sigma$ is the diameter of the particle. At high temperatures and high packing fractions, the particles behave like hard-spheres as the particles have enough kinetic energy to break the bonds between the particles. In that regime, the motion of the particles is hindered by the 'cage' made by their neighbors. Collective rearrangements are needed to free the particles from their cages. At lower temperatures, the short attractive interaction makes that some particles bond with their neighbors. Due to the really short interaction the bonded particles will get closer to each other, this as consequence

will free spaces where other particles can move, and the glass starts melting as the system regains mobility. Finally, if the temperature keeps decreasing, the bonding gets stronger and also last longer which result in a dynamical arrest.

This phase behavior is reflected in a reentrance in the phase diagram, at high temperatures the system is in a glass where the arrest is driven by the repulsion of the particles and so, is known as repulsive glass. At intermediate temperatures, the system melts and enters into a fluid phase. Finally at low temperatures, it gets into an arrested phase driven by the attractions of the particles, also known as 'attractive glass' [84–86].

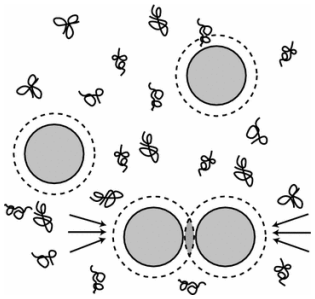

Figure 1.6: Depletion interaction. Reprinted by permission from: Springer Nature. Colloids and the Depletion Interaction by Henk N. W. Lekkerkerker and Remco Tuinier [78] ©2011.

This behavior was first predicted by MCT [87], later was confirmed through molecular simulations [84–86] and finally, it has been widely confirmed in colloidal experiments [46, 88]. In this thesis, we will focus in short-ranged attractions, however we are going to add some directionality to the interaction in order to explore the changes on the reentrant phase diagram and its effect on the local structure and dynamics.

### 1.4.3 Patchy colloids

The versatility of colloidal particles is reflected in the possibility of modifying and precisely controlling the interaction between the particles. One way of doing this is to modify the particle surface such that the interparticle interaction becomes anisotropic, these particles are known as patchy particles [89]. Although in principle, the shape of the particles can also be modified, in this thesis we will focus on spherical patchy particles. In short, a patchy particle can be a spherical particle decorated with $n$ attractive spots in its surface, such that the particles will only interact if their attractive regions are face to face. The directionality of the interactions results in particles with controlled valence and enables to craft materials with specific orientation constrains.

In experiments, spherical colloids can be coated with DNA strands which will bind only with the complementary strand, creating the desired directionality effect [89]. Other type of patchy particles is through particles with complementary shapes, called faceted patchy particles, DNA strands can be also used to deform liquid droplets to this end [90]. In simulations, we can model patchy particles as hard-sphere particles with $n$ attractive points modeled by square-wells as can be seen in Fig 1.7. The phase behavior of patchy-particle systems will depend on the size of the attractive regions, the number of them and their location [89, 91, 92]. Remarkably, the ability of controlling the valence of this type of

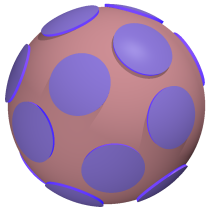

Figure 1.7: Patchy Particle.

particles that allow control over the phase diagram. For example, by decreasing the valence, the region of the gas-liquid coexistence is decreased [92]. The liquid phase gets more stable, as at low temperatures there can be patchy-particle systems that can form a fully-bonded fluid, which is more favorable than the crystal structure [91]. This in turn allows the system to access to arrested phases at low temperatures avoiding crystallization, making them perfect candidates to explore glassy dynamics.

We will discuss in more detail this type of colloidal particles in Chapter 3, 4 and 5 where we study in detail the interplay between structure and the different types of dynamics in glassy patchy particles.

Chapter 2

# Methodology

In this chapter we will introduce the main tool used in this thesis: molecular simulations and in particular Event-Driven Molecular Dynamics.

Since the first results obtained from molecular simulations that predicted a fluid-solid transition in a hard-sphere system [81], the use of molecular simulations has expanded into a wide variety of fields, and has become a vital tool in soft matter and colloidal science.

In general, we can divide molecular simulations into two different approaches: Monte Carlo (MC) simulations and Molecular Dynamics (MD). Typically, the goal of both methods is to obtain macroscopic observables from averages of microscopic quantities of the system, MC is based on ensemble averages and MD on temporal averages. In the thermodynamic limit these two averages are equivalent, according to the ergodic hypothesis.

## 2.1 Molecular Dynamics

The main idea of Molecular Dynamics (MD) is to obtain the trajectories of all particles by solving their equations of motion. The movement of the particles is controlled by their interaction potential.

Let us consider a system in the canonical ensemble where the number of particles $N$, the volume $V$ and the temperature $T$ are conserved. If the interaction potential is continuous and it is pair-wise i.e. $U = \sum_{ij}^{N} u_{ij}$, with $u_{ij}$ the interaction potential between particle $i$ and $j$. The forces between the particles are obtained from the gradient of the interaction potential $F = -\nabla U$. Once the forces are computed, the following step is to integrate Newton's equations of motion. To this end, different algorithms can be applied, which are based on Taylor expansions of the position and velocity of each particle in small time steps $\Delta t$. Examples of them are: the Verlet algorithm, the Leap-Frog algorithm and the Velocity-Verlet

algorithm. In order to have a fixed temperature, the system can be coupled to a thermostat. Repeating this process in time allows us to have access to the position and velocity of each particle at any moment in time. Finally, a macroscopic observable is obtained from the temporal averages derived from the trajectories of the particles. For more information about MD we refer the reader to Ref. [93] and Ref. [94].

The picture changes if the derivative of the interaction potential is discontinuous, since the forces cannot be obtained in the same way. Typical examples of such interactions are step potentials such as the hard-sphere and square-well potentials, that will be used in this thesis. For these type of systems, we require a different type of molecular dynamics, typically referred to as Event-Driven Molecular Dynamics (EDMD).

### 2.1.1 Event Driven Molecular Dynamics

The approach taken by EDMD is different from the continuous version: here the main idea is that the trajectories of the particles are obtained by solving collisions between pairs of particles. As its name suggest, EDMD is focused on resolving discrete events at specific times. The system is evolved based on the ordered timing of the events, which can be e.g. collision events, measurement events or cell events.

In general, the first step in the EDMD algorithm is to calculate all the event times for each particle. With these times a full time schedule is build, where all events are ordered by their scheduled time. Subsequently, the event with the earliest time is identified and the system is evolved to that time. If the event is a collision, the collision is resolved by updating the positions and velocities of the particles involved and new events for the two colliding particles are scheduled. Finally, the next event is identified and the process is repeated.

To better clarify the EDMD algorithm we will discuss in more detail its main points.

#### Collision Events

In the case of monodisperse hard spheres, the particles do not interact until the distance between two particles is equal to their diameter. In that precise moment they feel an infinite repulsion, resulting in an elastic collision. Outside of these collision events, the particles move with constant velocity. Thus, in order to obtain collision times we can consider two particles $i$ and $j$ with their initial positions at $\mathbf{r}_{i(j)}$ and velocities $\mathbf{v}_{i(j)}$. These particles collide when the distance between them is equal to their diameter $\sigma$:

$$|\mathbf{r}_{ij} - \mathbf{v}_{ij}\tau| = \sigma, \tag{2.1}$$

where $\mathbf{r}_{ij}$ is the distance between $i$ and $j$ at the original position and $\mathbf{v}_{ij}$ their relative velocity. At time $\tau$ the particles will collide, this time is obtained by solving Eq. 2.1:

$$\tau = \frac{-b_{ij} - \sqrt{b_{ij}^2 - \mathbf{v}_{ij}^2(\mathbf{r_{ij}^2} - \sigma^{\mathbf{2}})}}{\mathbf{v}_{ij}^2}, \tag{2.2}$$

where $b_{ij} = \mathbf{r}_{ij} \cdot \mathbf{v}_{ij}$. A collision will take place when $b_{ij} < 0$ and the discriminant of the root is positive. By imposing conservation of both momentum and energy, we can show that the velocities after the collision are:

$$\Delta\mathbf{v_i} = -\Delta\mathbf{v_j} = -\frac{b_{ij.}}{\sigma^2}\mathbf{r}_{ij}. \tag{2.3}$$

Once a collision is resolved, the velocities of the particles $i$ and $j$ are updated. Any future scheduled collisions of both particles are not longer valid and hence, must be deleted from the schedule. Additionally, new collision times for each particle are calculated and scheduled.

The picture gets more complex in the square-well case [1]. In this case, in addition to the repulsive interaction there is an attractive one. In particular, two particles interact attractively when the distance between the particles is $\sigma_a = \sigma + r_c$, where $r_c$ is the range of the potential. When two particles interact attractively we can consider this event as an 'attractive' collision. In other words, we again predict the associated collision time using Eq. 2.2, and update the particle velocities by considering conservation of energy and momentum. Depending on the conditions of $b_{ij}$ and the distance between the particles we can distinguish between attractive and repulsive collisions.

### Cell Events

In order to facilitate the search of the collision events, the system is divided into a grid of cells with an edge length slightly larger than the diameter of the particles. For each cell, we keep track of the particles that are currently inside it, and for each particle we keep track of the cell it is currently in. To have a record of the particles that belong to the same cell, linked lists are used. In these type of structures each element points to the next, for example if a cell contains the particles $23$ and $12$, a pointer from particle $23$ will point to the particle $12$ and vice versa. As the system evolves the particles can cross the cells, we define this as a cell event. The time when the particles will change cell is calculated and the cell event is also schedule. Once a cell event happens, the linked lists of the old and the new cell are updated and new collisions are schedule with the new neighbors.

[1] The square-well potential is:

$$U_{ij} = \begin{cases} \infty & r_{ij} = \sigma \\ -\epsilon & \sigma > r_{ij} \leq \sigma + r_c \\ 0 & r_{ij} > \sigma + r_c, \end{cases} \tag{2.4}$$

where $r_c$ is the interaction range and $\epsilon$ the strength of the attraction.

### Scheduling Events

The heart of EDMD resides in the method used for scheduling the events. In particular, it should be flexible and efficient for adding and deleting possible events, while ensuring that all events stay in chronological order. To this end, the future collisions are stored in a binary tree structure also known as "event tree". These type of structures are similar to linked lists however the main difference is that now each node can be connected to up to two nodes as we move down the tree. Each node contains information about the event: the particles involved, the type of event (collision, cell crossing or measuring event) and the time. The central node (parent node) points to a left node which corresponds to an event scheduled to occur before the parent node, and to a right node which is an event scheduled to occur after the parent. By adhering to this structure in the entire tree, the first event can always be found by starting at the top of the tree, and following the left nodes until encountering a node with no left child. An example of an event tree is shown in Fig. 2.1.

Once a collision between particle $i$ and $j$ happens or a cell crossing, the tree has to be modified. The future scheduled collisions involving $i$ and $j$ are not valid anymore and the nodes containing these collisions have to be deleted. When deleting these events, any child nodes of these events have to be linked back into the tree, maintaining the overall ordering. Additionally, the new calculated collisions must be added to the tree. To make easier to delete all events linked to a specific particle, each node is linked to two circular lists, one per particle ($i$ and $j$) if the event is a collision. The circular list of $i$ correspond to a list connecting all the nodes containing the events where particle $i$ is involved as the fist particle. Similarly, the circular list of $j$ links all events where $j$ is the second particle. In the case of a cell event of particle $j$, both circular lists are connected to $j$. Using this approach, any event involving a particle $j$ can be found by traversing two circular linked lists: one corresponding to the events where $j$ is the first particle involved in the collision and the other list where $j$ is the second particle. Both of these lists will be connected to the node corresponding to the cell event as shown in the bottom of Fig. 2.1.

### Algorithm

In general, EDMD follows the following steps:

1. Initialize the positions and velocities of the particles.
2. Assign to each particle a cell based on their position.
3. Calculate the next event times. As an advantage of the cell list, the possible collisions are only with the particles in the neighboring cells.
4. Find the next event in time.
5. If the event is a collision evolve the system to that time and calculate the new velocities after collision. If the event is a measuring event, update the positions of all particles to that time and perform any necessary calculations

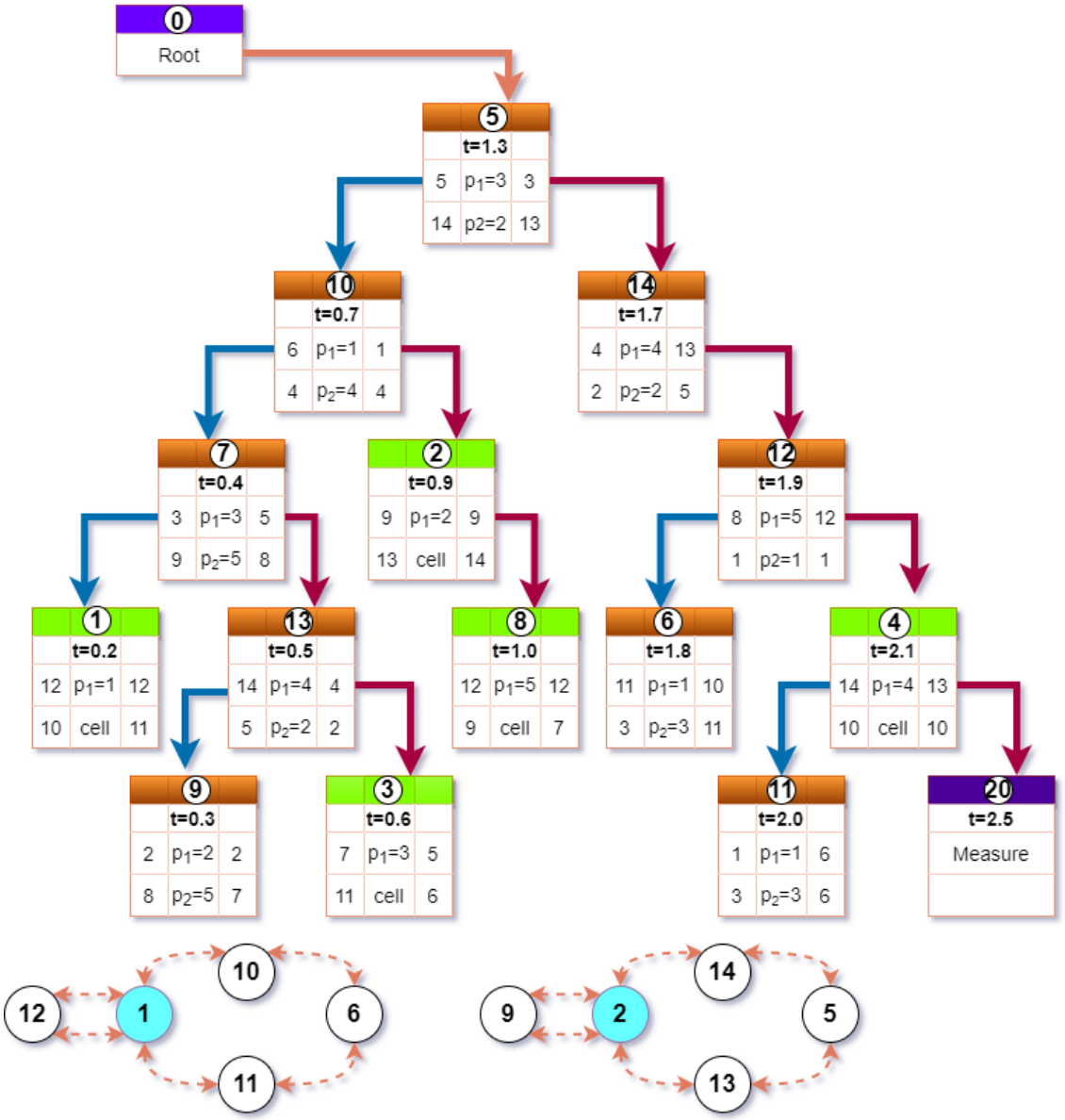


Figure 2.1: Example of an event tree. Each event contains the information of the event time, the particles involved and the information of the linked lists. The left child of each event (blue arrow) corresponds to an event in a previous time from the parent. Contrary, the right child (purple arrow) corresponds to an event on the future of the parent event. Orange events correspond to collision events, green events to cell events and purple events to thermostat events. In the bottom of the figure we show an example of the linked lists of each particle. The cell event connects the two linked lists, that correspond to the list where the particle is the first and the second particle involved in the collision respectively.

for the measurement.

6. Delete the nodes in the event tree of the particles involved in the event if it was a collision or a cell event and relink the remaining nodes.
7. Calculate the new events for the particles involved in the event, and link them into the event tree.
8. Go to step 4.

### Thermostat

As in continuous MD, in EDMD we can also control the temperature through a thermostat. Due to the nature of the algorithm, the most direct way of implementing a thermostat is through the Andersen thermostat. This approach corresponds to reassigning velocities according to the Maxwell-Boltzmann distribution of the desired temperature to a random selection of particles. This process is done every fixed amount of time, and thus, it can be scheduled in the event tree as another type of event.

### Initial Configurations

In this thesis we deal with systems at high packing fractions. In order to avoid overlaps between particles, the initial configuration must be constructed carefully.

In order to obtain random high-packing fraction configurations we use a hard-sphere EDMD in which the particles grow over time. In this type of EDMD, we start with $N$ small spheres of diameter $\sigma_o$ randomly located in a box of volume $V$. We then slowly increase the size of the particles until we arrive at the diameter we are interested in. As in the hard-sphere case two particles $i$ and $j$ will collide repulsively when the distance between them is equal to $\sigma_{ij} = (\sigma_i + \sigma_j)/2$, where $\sigma_{i(j)}$ corresponds to the diameter of particle $i(j)$. However for growing the particles now $\sigma_{i(j)}$ will depend on time as: $\sigma(t) = \sigma_o + \Delta\sigma t$, where $\sigma_o$ is the initial diameter and $\Delta\sigma$ the growing rate. By taking this growing into account the collision equations automatically include the particle growth when calculating the collision times.

With this method, we can ensure that the initial configurations will not overlap and we can achieve sufficiently high packing fractions for the purpose of the research in this thesis.

### Patchy Particles

As we mention in Chapter 1, patchy particles can be modeled as hard-sphere particles with $n$ attractive points on their surface, where the attractive interaction is through a square well. In this case, the particles interact attractively depending on the orientation between two particles. This fact significantly complicates the calculation, as it is no longer possible to predict collision times analytically.

To address this problem, we make use of numerical root-finding algorithms to predict collision times between patches. In order to clarify this point, lets revisit the hard-sphere case. One way of predicting a hard-sphere collision is by considering that a collision happens when a function $f_{ij}$ is $0$, where $f_{ij}$ corresponds to $f_{ij} = |\mathbf{r}_i - \mathbf{r}_j| - \sigma^2$. Hence, the roots of $f_{ij}$ will give us the collision times. In the patchy case, we have a function $f_{ij}(\mathbf{r_{ij}}, \Omega_i, \Omega_j, t)$ that depends of the orientations

and the positions of each particle. The collision times will be the roots of this function. To keep the simulation efficient, we numerically search for roots only when there is a suspected collision. In other words, first we can find analytically the time where the two particles will be within the interaction range, following the same procedure as in the hard-sphere and the square-well cases. Then, by means of root-finding algorithms we find the zeros of $f_{ij}$. More details on the process of dealing with anisotropic interactions can be found in Ref. [91, 95].

## 2.2 Monte Carlo

The Monte Carlo (MC) approach takes a different route from MD. Monte Carlo simulations are based on the notion of statistical ensembles and their goal is to sample configurations in phase space according to a probability distribution. An observable $A$ can be calculated as:

$$\langle A \rangle = \frac{\int d\mathbf{p}^N d\mathbf{r}^N A(\mathbf{r}^N, \mathbf{p}^N) \mathcal{P}(\mathbf{r}^N, \mathbf{p}^N)}{\int d\mathbf{p}^N d\mathbf{r}^N \mathcal{P}(\mathbf{r}^N, \mathbf{p}^N)}, \tag{2.5}$$

where $\mathcal{P}(\mathbf{r}^\mathcal{N}, \mathbf{p}^\mathcal{N})$ is the probability of a state with $\mathbf{r}^N$ positions and $\mathbf{p}^N$ velocities. In the canonical ensemble, the corresponding probability is the Boltzmann factor $\mathcal{P}(\mathbf{r}^N, \mathbf{p}^N) = \exp[-\beta \mathcal{U}]$, where $\mathcal{U}$ is the energy of the system and $\beta = 1/k_B T$ where $k_B$ is the Boltzmann constant. If the observable $A$ is independent of the momentum, we can integrate out the momentum integral and reduce Eq. 2.5 as:

$$\langle A \rangle = \frac{\int d\mathbf{r}^N A(\mathbf{r}^N) \exp(-\beta U)}{\int d\mathbf{r}^N \exp(-\beta U)}, \tag{2.6}$$

One way to evaluate Eq. 2.6 is through the Metropolis Monte Carlo algorithm. The main idea is to sample configurations according to the Boltzmann factor. In its most basic form, the Metropolis algorithm follows the next steps:

1. Start from an initial configuration.
2. Calculate the energy of the system $U_o$.
3. Choose a random particle $i$.
4. Move the particle $i$ a small distance $\Delta\mathbf{r}$.
5. Calculate the new energy $U_n$ after the movement.
6. Accept the movement if a random number $Ranf$ between $[0, 1]$ is $Ranf < \exp[-\beta(U_n - U_o)]$. If the movement is rejected the particle goes back to its initial position.
7. Go to step 3.

An important difference between MC and MD is that the former only has access to variables which depend only on the positions, i.e. static observables. In contrast, MD follows the trajectories of the particles over time, and hence also dynamical observables can be calculated, such as the mean squared displacement and the intermediate scattering function.

## 2.3 Characterizing LFS

In this thesis we will focus on the role of the structure in glassy dynamics. As we discussed in Section 1.3.2 some locally favored structures (LFS) arise once the system enters into the glassy regime. To finish this Chapter we will briefly discuss some of the techniques to characterize the nature of the LFS.

There are different ways of characterizing the order and symmetry of the local favored structures. The core of all the characterizations is to analyze the local environment of a particle, i.e. to find the geometrical arrangement of the first shell of neighbors around a particle. We will focus on two of the main techniques to characterize the LFS. Both of them are based on Voronoi constructions.

**Voronoi Face Analysis**

One of the first tools introduced to identify the geometry of the LFS is through the construction of Voronoi polyhedra [25]. Starting from a Euclidean plane with $p_n$ random points on it, we can divide the space into regions that surround each $p_n$, such that the distance between any $q$ point inside the region and the central $p_n$ is minimized. These will lead to divide the plane into polygons, where the shared edges of the polygons are all the points that are equidistant to two neighbor $p_n$ points and the vertex the equidistant point of three $p_n$ points [96]. In Fig. 2.2 we show an illustrative example of a Voronoi construction in two dimensions. This construction can be easily extended to polyhedra in 3 dimensions.

Each particle will represent the central point $p_n$ of a Voronoi polyhedron, and the structure of its local environment will be captured by the number of faces of the polyhedron and its geometry. The information of the polyhedron can be written as a vector $(n_3, n_4, n_5, n_6, \cdots, n_i)$ each $n_i$ entry corresponds to the number of facets with $i$ edges. Icosahedral clusters are then characterized by a vector (0,0,12,0) which means that is formed by 12 faces with 5 edges each (12 pentagonal faces), capped trigonal prism clusters corresponds to (0,3,6,0) and twisted bicapped square antiprims to (0,2,8,0), among others [25].

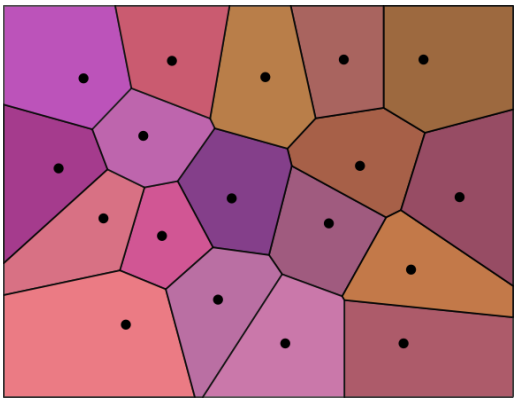

Figure 2.2: Schematic diagram of a Voronoi construction in 2 dimensions.

**Topological Cluster Classification**

The Topological Cluster Classification (TCC) allows us to have a detailed characterization of the exact nature of the LFS. It is based on a modified Voronoi construction. Its main goal is to detect minimum energy clusters, which correspond to the ones that minimize the potential energy of a certain number of particles,

taking into account different models and interaction potentials [11].

First of all, the algorithm identifies the neighbors of the particles through a modified Voronoi construction. In the original Voronoi Face Analysis two particles are considered neighbors if they share a face, however thermal fluctuations can lead to the inclusion of neighbors that would tipically be considered part of the second neighbor shell. To fix this problem, two particles are only considered neighbors if they share a face and if the line that joins the two particles passes through the shared face. Additionally, a parameter is introduced which controls the conditions under which four particles, located in a roughly planar geometries, are considered to be connected in a ring of four, rather than two rings of three. For example, in an unmodified Voronoi construction, if four particles are located on the vertices of a square, the pairs of particles on opposite corner are not bonded and they form a 4-member ring. However, if the square gets slightly distorted to a rhombus two of the opposite corners are considered bonded and two 3-member rings are created. The modified Voronoi construction used in the TCC uses a tuning parameter $f_c$ to allow a finite distortion of this ring before the additional bond is made. When $f_c = 1$ the neighbor definition of the unmodified Voronoi construction is recovered, and $f_c < 1$ allows a larger distortion. In particular, TCC with $f_c = 0.82$ performs well for capturing icosahedral clusters [11].

In general, the TCC algorithm is composed of the following steps:

- Identify the neighbors of each particles based on the modified Voronoi construction.
- Search for the shortest rings from 3 to 5 particles (called sp3, sp4 and sp5).
- Find 'basic clusters' which consist of adding one particle on top of one of the simple ring clusters or two particles, one on top and the other below the ring.
- Finally, more complex clusters are found as a combination of the basic ones, consisting of clusters between 5 to 13 particles. In particular, these complex clusters correspond to the minimum energy structure for one of the models (Morse potential[2], Wahnström model, Kob-Andersen model and Dzugutov potential[3]).

The complete list of the clusters identified by TCC can be found in Ref. [11]. In general, TCC performs well for capturing a wide variety of clusters. And in particular, in hard-sphere systems and the repulsive Wahnström it detects an increase of icosahedral clusters (named as 13A) and defective icosahedral cluster (named 10A) when these systems are undercooled [98].

[2]Morse potential is $U_M(r) = \epsilon_M \exp^{\rho_0(\sigma - r)}(\exp^{\rho_0(\sigma - r)} - 2)$, where $\epsilon_M$ is the depth of the potential, $\sigma$ the diameter of the particles and $\rho_0$ the range of the potentail.

[3]The Dzugutov potential of monodisperse particles is: $U_D = a_1(r^{m-1} - 1)\exp[b_1/(r - c_1)] + a_2 \exp[b_2/(r - c_2)$, where $a_1, b_1, c_1, a_2, b_2$ are fitting parameters so that the repulsive part of the potential coincides with the Lennard-Jones potential [97]

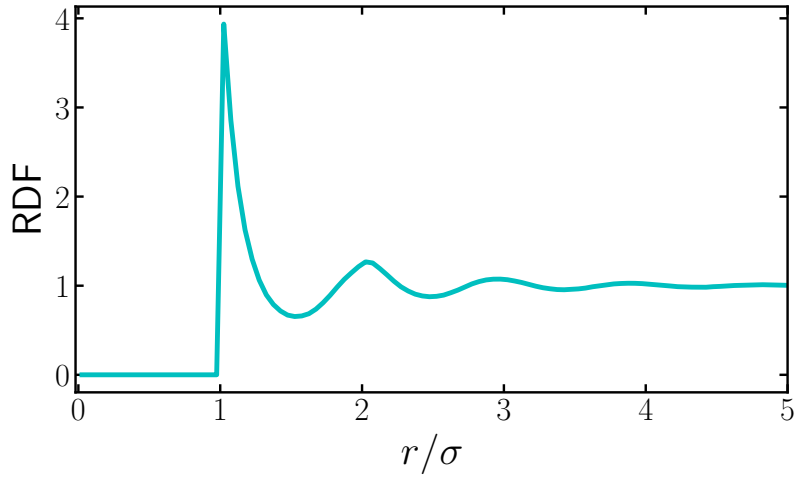


Figure 2.3: Typical radial distribution function of a diluted liquid.

### 2.3.1 Choosing the neighbors

In both of the previous techniques to characterize the LFS, it is of great importance the way the neighbors of each particle are obtained. Here, we will briefly discuss three different approaches that are used to define this neighbors.

#### Cutoff radius

The most straightforward way of obtaining the neighbors of a particle is by defining a cut-off radius $r_c$. A particle $j$ is then considered neighbor of particle $i$ when $|\mathbf{r}_i - \mathbf{r}_j| < r_c$, where $\mathbf{r}_{i(j)}$ is the position of particle $i(j)$. The choice of $r_c$ has to be adapted to the conditions of the system. The most commonly used way of choosing $r_c$ is through the calculation of the radial distribution function (RDF). In short, the RDF give us the probability of finding a particle at a distance $r$ from a given particle. A typical RDF of a liquid is shown in Fig. 2.3. Each peak in the RDF indicates a distance from a central particle where it is more likely to find a particle. The first peak of the RDF is found near $r \simeq \sigma$, where $\sigma$ is the diameter of the particle. In order to take into account only the particles in the first coordination shell, $r_c$ can be taken as the distance corresponding to the first minimum of the RDF. However, this can lead to an underestimation of neighbors, as the first peak in the RDF typically has not fully decayed to 0 at this point.

#### Voronoi Construction

One way of improving the choice of the neighbors is through the Voronoi construction (VC). As we mentioned before, in the VC we build a polyhedron for each of the particles, all the points inside the polyhedron are closer to the position of the particle than to the other particles. The faces of the polyhedron correspond

to the points where the distance between those points and two neighboring particles is equal (see Fig. 2.2 for a two-dimension example of VC). In the original VC two particles are considered neighbors when their polyhedra share one of their faces. The advantage of VC is that it does not need of a cut-off radius, however it is sensitive to thermal fluctuations that can lead to an overestimation of the neighbors [99]. Moreover, VC is a computationally expensive method. Modification to VC can be made in order to tune when particles are considered neighbors. For example, the Topological Cluster Classification algorithm [11], which adds conditions for two particles to be considered neighbors.

### Solid-angle based nearest-neighbor analysis

Finally, a method that avoids the need of defining a cutoff and that is computationally less expensive than VC is called solid-angle based nearest-neighbor analysis (SANN). In order to obtain the list of $m$ neighbors of a particle $i$ it determines a cutoff distance $R_i$ per particle. The heart of SANN lies in the way of obtaining $R_i$. It relies on an approximate Voronoi construction which uses solid angles to estimate the smallest $m$ such that the set of the $m$ nearest particles are sufficient to surround the particle [100]. The main advantage of SANN is that it is parameter-free and scale-free. Moreover, it is less computationally expensive compared to VF.

Chapter 3

# Patchy Particles: Translational dynamics and structure.

This chapter is based on the publication:

S. Marín-Aguilar, H. H. Wensink, G. Foffi, and F. Smallenburg, "Slowing down supercooled liquids by manipulating their local structure", *Soft Matter*, vol. 15, no. 48, pp. 9886-9893, 2019. [14].

## 3.1 Introduction

One of the points of debate in glasses is the role played by local structure in the slowing down of the dynamics. As we have discussed in section 1.3.1, from Frank's idea of icosahedral clusters [5] as a possible way to arrange 12 particles around a central one, to the actual quantification of specific clusters in various supercooled liquids, there is a growing body of evidence that points that glassy dynamics are accompanied by the emergence of long-lived locally favored structures [4, 6, 11, 101–106]. However, the exact role of these structures is still not completely clear, and these locally favored structures are mainly found a posteriori, i.e. there are characterized after the system is equilibrated without any initial control on them. Science in general must go one step further, and the logical question in here to answer is: how to control these local structures?. Moreover, being capable of controlling them, will approach us to a better understanding of their role in the dynamical arrest and ultimately this gives a way of controlling dynamics.

With the use of molecular simulations the systems can be biased towards the formation of specific structures [107]. This is useful to better understand the roles of specific symmetries. However, this biasing is mainly a mathematical tool that not necessarily is reproducible in experiments. Hence, the main challenge is to use a model that by tuning its interactions we can manipulate the local structure.

Based on the fact that exotic crystal and quasicrystal phases can be templated by using directional interactions [108], we can extend their use to supercooled liquids to disrupt and control the local structure. Imposing preferred directions give us a route to enhance clusters with preferred symmetries.

Directionality can be achieved in different ways, either by changing the shape of the particles or by changing their interaction. Colloidal particles with anisotropic shapes are a perfect example of the former case. This type of colloids has been extensively synthesized in experiments [80,109,110]. The latter case is implemented by using particles that by definition interact in a directional fashion. This is the case of patchy particles that have specific attractive regions in their surface (see Section 1.4.3). Hence, the way the particles interact is driven by the location of this directional regions. In this chapter and in the followings, we will focus on the use of patchy particles as building blocks for supercooled liquids.

The experimental availability of patchy colloidal particles has grown notably in recent years [79, 89, 111–115]. The directionality of these particles provides a precise control of the their valence, and as consequence they have been used to facilitate the self-assembly of open crystal structures [108, 116] and (at relatively low densities) as models for strong network-forming glasses [91, 114, 117]. Furthermore their directionality makes them a perfect candidate to control and manipulate the local structure of supercooled liquids.

Moreover, as the interaction of this model can be tuned to short range interactions, makes it a good candidate to explore the effect of directional interactions in the crossover between attractive and repulsive glass by changing the temperature. As it has been explained in Section 1.4.2, this crossover has been extensively studied in short range isotropic interactions, though directionality in this sense has not yet been explored.

Here, we make use of patchy particles to control the local structure of supercooled liquids and to characterize in detail the effect of changing the characteristics of the patches on the local environment and on the global dynamics. We confirm the close relation between the icosahedral clusters and the dynamical slowdown by reinforcing this type of cluster in our simulations.

In this chapter, we will first cover the general methodology of the patchy-particle simulations and the chosen model system. Next, we show in detail the tools we use for analyzing patchy particles. Finally, we show the dynamical and structural characterization of binary systems of patchy particles with different number of patches, location and sizes.

## 3.2 Model and Methodology

### 3.2.1 Kern-Frenkel Model

In order to model the patchy interactions we use the Kern-Frenkel model [10]. This model consists of hard-sphere particles decorated with $n$ attractive patches on their surface. The parameters to control are the characteristics of the patches: their number $n$, their location and their size.

In the Kern-Frenkel model, the particles interact attractively when the vector that joins the center of two particles passes through a patch in each of the particles as shown in Fig. 3.1 where the red line represents this vector. And repulsively when the distance between the particles is equal to the diameter of the particle $\sigma$. The attractive interaction is modeled as a directional square-well potential, hence the Kern-Frenkel interaction potential is as it follows:

$$U_{ij}(\mathbf{r}_{ij}) = U_{ij}^{\text{HS}}(r_{ij}) + U_{ij}^{\text{SW}}(r_{ij}) f(\mathbf{r}_{ij}, \hat{\mathbf{n}}_\alpha, \hat{\mathbf{n}}_\beta), \tag{3.1}$$

where $r_{ij} = |\mathbf{r}_{ij}|$ is the center-to-center distance between particles $i$ and $j$. Here, $U_{ij}^{\text{HS}}$ is the hard-sphere potential:

$$U_{ij}^{\text{HS}} = \begin{cases} \infty & r_{ij} = \sigma_{ij} \\ 0 & r_{ij} > \sigma_{ij}, \end{cases} \tag{3.2}$$

with $\sigma_{ij} = (\sigma_i + \sigma_j)/2$ the minimum distance between two particles, and $\sigma_i$ the diameter of particle $i$. Additionally, $U_{ij}^{\text{SW}}$ is a square-well potential, given by

$$U_{ij}^{\text{SW}} = \begin{cases} -\epsilon & r_{ij} \leq \sigma_{ij} + r_c \\ 0 & r_{ij} > \sigma_{ij} + r_c, \end{cases} \tag{3.3}$$

where $r_c$ is the interaction range and $\epsilon$ the strength of the attraction. Finally, $f(\hat{r}_{ij}, \hat{\mathbf{n}}_\alpha, \hat{\mathbf{n}}_\beta)$ specifies the directionality of the interactions:

$$f(\mathbf{r}_{ij}, \hat{\mathbf{n}}_\alpha, \hat{\mathbf{n}}_\beta) = \begin{cases} 1 & \begin{cases} \hat{\mathbf{n}}_\alpha \cdot \hat{\mathbf{r}}_{ij} < \cos\theta \text{ and } \hat{\mathbf{n}}_\beta \cdot \hat{\mathbf{r}}_{ji} < \cos\theta, \\ \text{for any two patches } \alpha \text{ and } \beta \end{cases} \\ 0 \end{cases} \tag{3.4}$$

where $\hat{\mathbf{n}}_\alpha$ corresponds to a unit vector that points to patch $\alpha$ on particle $i$, and $\hat{\mathbf{r}}_{ij} = \mathbf{r}_{ij}/r_{ij}$. The angle $\theta$ controls the size of the patches and is defined as the angle between the vectors pointing from the center of the particle at the center of the patch and at its edge, as it is shown in Fig. 3.1. Furthermore, we can define the surface percentage covered $\chi$ by the patches as: $\chi = n(1 - cos\theta)/2$. Note that this expression works as long as the patches do not overlap. Above that limit, numerical integration is required to calculate $\chi$.

Here, we use a modified Kern-Frenkel model where each pair of particles can form only one bond. This distinction is only important in the regime where the

patches overlap. In that case, even if two or more patches overlap the particles can only form strictly one bond. Hence the potential energy between those two particles will be $-\epsilon$. This condition lets us interpolate between two extreme cases: when the particle is completely covered by the patches, i.e. $\chi = 100\%$ the interaction will directly map into a square-well and the interaction will correspond to a hard-sphere potential when $\chi = 0\%$.

In order to explore the effect of the patch geometry in detail we explore systems with 3 to 20 patches. In principle, the patches can be located in any place of the particle's surface, so there is an infinite number of possibilities to arrange the patches in the surface. An intuitive way of arranging them is to locate the $n$ patches uniformly distributed over the surface. This is achieved by locating them such that the minimum distance between any two patches on the surface is maximized. The solution of this problem is sometimes referred as spherical codes [118]. Specific values of $n$ have trivial solutions corresponding to place the patches in the vertices of platonic solids ($n = 4$, $n = 6$, $n = 8$, $n = 12$ and $n = 20$).

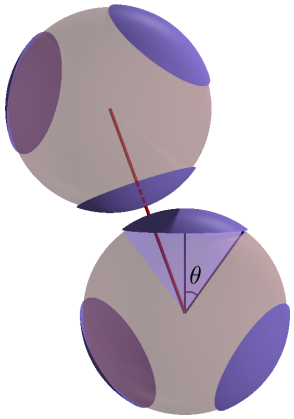


Figure 3.1: Patchy particles representation, the red line corresponds to the vector that joins the center of mass of both particles. The angle $\theta$ controls the size of the patch.

In Fig. 3.2 we show some of the cases we studied, we add the name of the corresponding platonic solid for the pertinent cases, the other ones have a numerical solution. Note that for 11 and 12 patches, this results in patches placed on the vertices of an icosahedron, where for 11 patches there is one vertex omitted. Although this selection of patch geometries is somehow arbitrary, it ensures an even coverage of the particle surface with patches, and makes sure patches only overlap when a very large fraction of the surface is covered. In addition this type of arrangement is likely easier to achieve in experiments [119,120]. To have a broader picture of the effect of icosahedral patch placement, we also simulate one alternative geometry for particles with 10 patches, where we follow the geometry of the 12-patch case, but omit two opposite vertices. We refer to this geometry as $10_{ico}$.

In order to suppress crystallization, a common practice is to simulate mixtures of particles with different sizes. Here, we simulate a binary mixture of Kern-Frenkel particles of two sizes, with the size ratio given by $q = \sigma_S/\sigma_L = 0.833$, where $\sigma_{L(S)}$ denotes the size of the large (small) spheres. We fix the interaction range $r_c = 1.031\sigma_{ij}$, where $\sigma_{ij}$ is the contact distance between particles $i$ and $j$. This interaction range was chosen to be consistent with the square-well interaction in Ref. [86], which provides us with a reference for the behavior of the system in the limit $\chi \to 100\%$. At high packing fractions, square-well systems with this

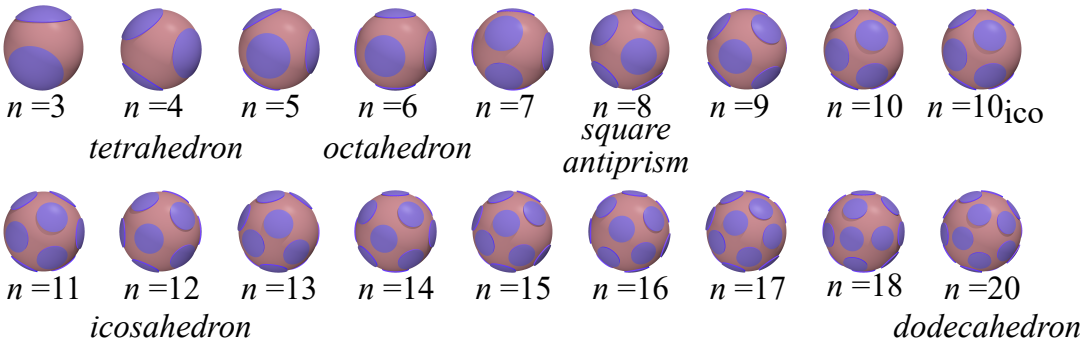


Figure 3.2: Illustration of the simulation model. The patch placements correspond to the positions that maximize the minimum distance between two patches. For some cases the patch placement corresponds to the vertices of platonic solids, as indicated. Note that the $10_{ico}$, 11, and 12-patch geometries correspond to icosahedra with two, one, and zero vertices missing.

size ratio and range interaction show a clear reentrant behavior in the phase diagram.

### 3.2.2 Simulation

To simulate the patchy particles, we use event-driven molecular dynamics (EDMD) simulations (as explained in Chapter 2) [91, 94, 95] with periodic boundary conditions. In each system, we fix the number of particles $N = 700$, the composition $x_L = 0.5$, and the packing fraction $\eta = 0.58$. At this packing fraction, the square-well limit of our system displays a clear reentrance in the dynamics as a function of temperature [86]. The systems were equilibrated at fixed temperature for at least $10^4\tau$, where $\tau = \sqrt{m\sigma_L^2/k_BT}$ is our time unit, $T$ is the temperature, $m$ is the mass of a particle and $k_B$ is Boltzmann's constant. The constant temperature is achieved by using a thermostat, which randomizes the velocities of a small percentage of particles with velocities corresponding to the Boltzmann distribution at the specific temperature $k_BT/\epsilon$ every $\Delta t$ time.

After equilibrating the system at constant temperature, we then analyze the structure and dynamics of the system in simulations at fixed energy. We simulate the systems with temperatures ranging from $k_BT/\epsilon = 0.3$ to $k_BT/\epsilon = 2.0$. In order to have a clear picture of the effect of the directionality we varied the covered percentage by the patches $\chi$ from $0\%$ to $100\%$ as shown in Fig. 3.3.

### 3.2.3 Analysis

Here, we will give a general description of some of the tools for the analysis of colloidal systems used in this Chapter and in the followings.

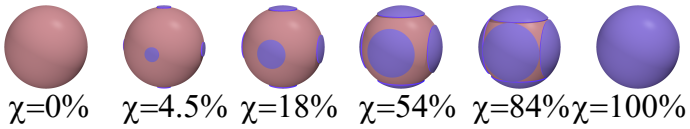


Figure 3.3: Illustration of the simulation model. The surface covered by the particles increases as the size of the patches.

#### 3.2.3.1 Dynamics

To explore dynamics, we measure the dimensionless diffusion coefficient $D\tau/\sigma_L^2$, which is related to the mean square displacement by Einstein diffusion equation as:

$$D\tau/\sigma_L^2 = \lim_{t\to\infty} \frac{1}{6N\tau} \left\langle \sum_{j=1}^{N} [r_j(t) - r_j(0)]^2 \right\rangle, \tag{3.5}$$

where $N$ is the number of particles and $r_j(t)$ is the position of particle $j$ at time $t$. Hence, in order to obtain $D$, we fit a linear function to the long-time behavior of the mean square displacement and obtain the diffusion coefficient with the previous expression.

In order to quantify the structural relaxation of the systems, we measure the time-dependent intermediate scattering function:

$$F(k,t) = \frac{\langle \rho(-\mathbf{k},t)\rho(\mathbf{k},0)\rangle}{\langle \rho(-\mathbf{k},0)\rho(\mathbf{k},0)\rangle}, \tag{3.6}$$

where $\rho(\mathbf{k},t)$ is the Fourier transform of the density. From $F(k,t)$, we extract the relaxation time $\tau_{0.3}$ by fitting its long-time behavior with a stretched exponential: $A\exp[-(t/\tau_\alpha)^\gamma]$, where $A$, $\tau_\alpha$ and $\gamma$ are fitting constants. We define the relaxation time $\tau_{0.3}$ as the time where the correlation decays to $0.3$. This last relaxation time is less sensitive to the fitting and here we used it instead of the most common $\alpha$-relaxation. In addition, these two relaxation times can be taken as equivalent.

#### 3.2.3.2 Local Structure

In order to characterize the local structure of the system we use two main tools: the local bond order parameters and the Topological Cluster Classification algorithm [11].

The local bond order parameters characterize the environment of each particle, based on its nearest neighbors. We assign to each particle $i$ a bond-order vector $Q_{lm}$, which contains the expansion of its local environment in terms of spherical harmonic functions of order $l$. The list of neighbors is built based on a cut-off radius $r_c = 1.2\sigma_L$, where all the particles $i$ within a radial distance $r_c$ are counted. We denote the number of neighbors for particle $i$ as $N_b(i)$. For each

| Geometry | $Q_4$ | $Q_6$ | $\hat{W}_4$ | $\hat{W}_6$ |
|---|---|---|---|---|
| FCC | 0.19094 | 0.57451 | -0.159317 | -0.013161 |
| HCP | 0.09722 | 0.48476 | 0.134097 | -0.012442 |
| Icosahedral | 0 | 0.66332 | 0 | -0.169754 |

Table 3.1: Values of the local bond order parameters for some of the common lattices.

particle $i$, $Q_{lm}(i)$ is then given by

$$Q_{l,m}(i) = \frac{1}{N_b(i)} \sum_{j=1}^{N_b(i)} Y_{lm}(\theta_{ij}, \phi_{ij}), \tag{3.7}$$

where $Y_{lm}(\theta, \phi)$ are the spherical harmonics, with $m \in [-l, l]$ and $\theta_{ij}$ and $\phi_{ij}$ are the polar and azimuthal angles of the center-of-mass distance vector $\mathbf{r}_{ij} = \mathbf{r}_j - \mathbf{r}_i$, with $\mathbf{r}_i$ the position vector of particle $i$.

The invariants used to characterize the local structures are rotationally invariant combinations of $Q_{l,m}$:

$$Q_l(i) = \left[ \frac{4\pi}{2l+1} \sum_{m=-l}^{l} |Q_{lm}(i)|^2 \right]^{1/2}, \tag{3.8}$$

and

$$W_{l(i)} = \sum_{m_1,m_2,m_3,m_1+m_2+m_3=0} \begin{pmatrix} l & l & l \\ m_1 & m_2 & m_3 \end{pmatrix} \quad Q_{lm_1}(i) Q_{lm_2}(i) Q_{lm_3}(i), \tag{3.9}$$

where the coefficients in the matrix in $W_l$ corresponds to the Wigner $3j$ symbols [121]. The $W_l$ commonly used are the ones normalized as

$$\hat{W}_l(i) = W_l / \left[ \sum_{l=-m}^{m} |Q_{lm}(i)|^2 \right]^{3/2}. \tag{3.10}$$

The FCC (face-centered-cubic), HCP (hexagonal-closed-packing) and icosahedral clusters each correspond to specific values of the bond order parameters that allow us to distinguish them [122], in Table 3.1 we show this values.

Furthermore, to better characterize the local structure we use the algorithm *Topological Cluster Classification* [11] (see Section 2.3).

## 3.3 Results

### 3.3.1 Reentrant behavior

We begin our analysis by investigating the reentrant behavior of the diffusion coefficient as a function of temperature in this system with directional interactions. To this end, we simulate the patchy particles with different coverage going from purely hard-spheres to square-well at different temperatures (see Fig. 3.3) and we measure the dimensionless diffusion coefficient $D\tau/\sigma_L^2$. In Fig. 3.4a), we show this diffusion coefficient for systems with $n = 6$ patches, as a function of the reduced temperature $k_BT/\epsilon$, for a number of different values of the patch coverage fraction $\chi$. In the limit of high $\chi$, we recover the case of an isotropic square-well model in the supercooled regime, and find reentrant diffusive behavior [85, 86], where the system crosses over from an attractive glass to a repulsive one. The point where a system can be called an attractive glass or a gel is not clear, and it is point of controversy [123]. Though percolation is a clear sign of a gel at high densities or packing fractions percolation is indistinguishable from the high packed arrangement of the particles. In here, we use the term *attractive glass* to name the arrested state at low temperature. The fact that this phase may be a continuation of the gel phase at low density [123] is not a fundamental distinction for our results.

Upon decreasing $\chi$, we observe an overall decrease in the diffusion, as shown in Fig. 3.4a) eventhough it retains its reentrant behavior. This observation has been seen as well in a recent mean-field solution for a simpler patch geometry consisting of two patches [124]. The maximum in the diffusion rate shifts to lower temperatures as $\chi$ decreases. This behavior can be understood from the observation that particles with lower coverage fractions form fewer bonds and lower temperatures are required before bonding can similarly affect the dynamics.

In the case of 12-patch particles (Fig. 3.4b) we see a similar decrease in diffusivity by decreasing patch size, but the shift in the maximum is less pronounced. We observe similar trends for the other patch geometries.

### 3.3.2 Fixing the surface coverage

Once we have explored the effect of the size of the patches on dynamics, we now focus in the comparison between geometries. Fixing the same size of patches for different $n$ will lead to a complete different coverage and hence not a clean comparison of the geometries. A reasonable way of comparing the patch geometries is to fix the amount of surface covered by the patches $\chi$. While less surface is covered it is harder to form bonds. Same surface covered corresponds to compare the systems with the same second virial coefficient:

$$\frac{B_2}{B_2^{HS}} = 1 - \chi^2 \left[(1 + r_c)^3 - 1\right] \left[\exp(1/(k_BT/\epsilon)) - 1\right], \tag{3.11}$$

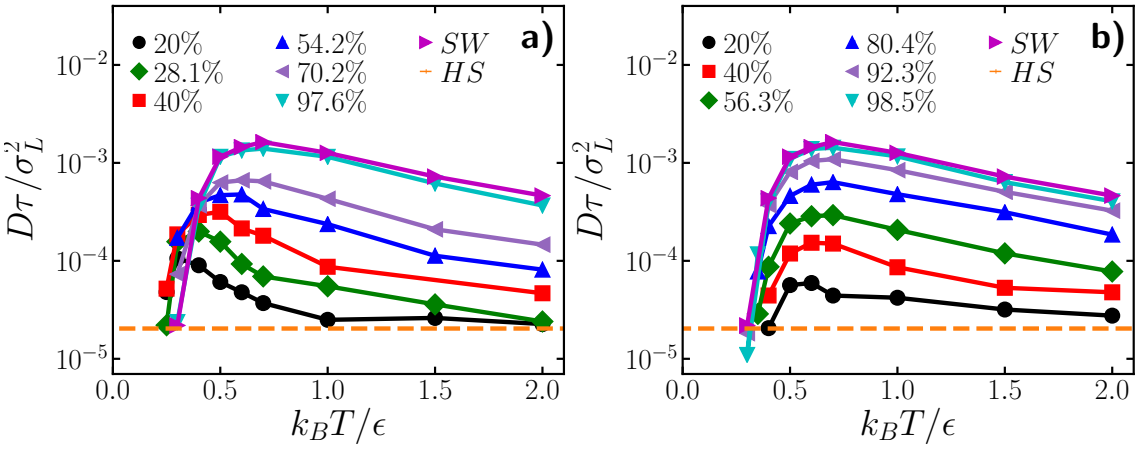


Figure 3.4: Translational diffusion coefficient calculated for a system of 6 patches a) and 12 patches b). Dashed lines correspond to the HS limit and the right triangles to the SW limit.

where $B_2$ corresponds to the second virial coefficient of hard spheres. This expression is only valid before the patches overlap. Comparing at the same virial coefficient can be seen as an extension of the law of corresponding states. Indeed it has been previously shown that $B_2$ is a suitable scaling variable for patchy systems that can form only one bond [125].

Hence, we compare systems at the same coverage fraction $\chi = 20\%$ and $\chi = 40\%$. Note, that the results shown in here correspond to $\chi = 40\%$ but similar results were found in the $20\%$ case. However, the $\chi = 40\%$ case shows clearer reentrance at higher temperatures as can be seen in Fig. 3.4, and the changes with temperature can be better appreciated. The reentrance in $\chi = 20\%$ is shifted to lower temperatures which are computationally slower.

In Fig. 3.5a) we plot the diffusion constant as a function of the patch geometry for different temperatures. Surprisingly, we see that the diffusion coefficient is largely independent of the patch geometry, except when the patch geometry matches icosahedral order (i.e. $10_{ico}$, 11 or 12 patches). In the latter case, we instead see an extreme slowdown of the system at low temperature. Note that for several patch geometries (13, 14, 18, and 20-patch), we observe crystallization at the lowest temperatures investigated. These points have been omitted from Fig. 3.5a). In the inset of Fig. 3.5a) we show the behavior of the two 10-patch geometries with temperature. The icosahedral placement ($n = 10_{ico}$) presents slower dynamics at low temperatures when compared to the 10-patch geometry obtained from the spherical code ($n = 10$). This implicates that there is a strong change in the local structure when the patches match with the icosahedral order. In the following, we will show only the results of the $10_{ico}$ geometry, as the other 10-patch geometry essentially follows the trend of all other non-icosahedral patch placements.

To make a more complete analysis of the dynamics, we measure in each system the intermediate scattering function $F(k,t)$, which characterizes the relaxation time in the system at different length scales specified by the wave vector $k$. In Fig. 3.5b), we plot these correlation functions for temperature $k_BT/\epsilon = 0.4$,

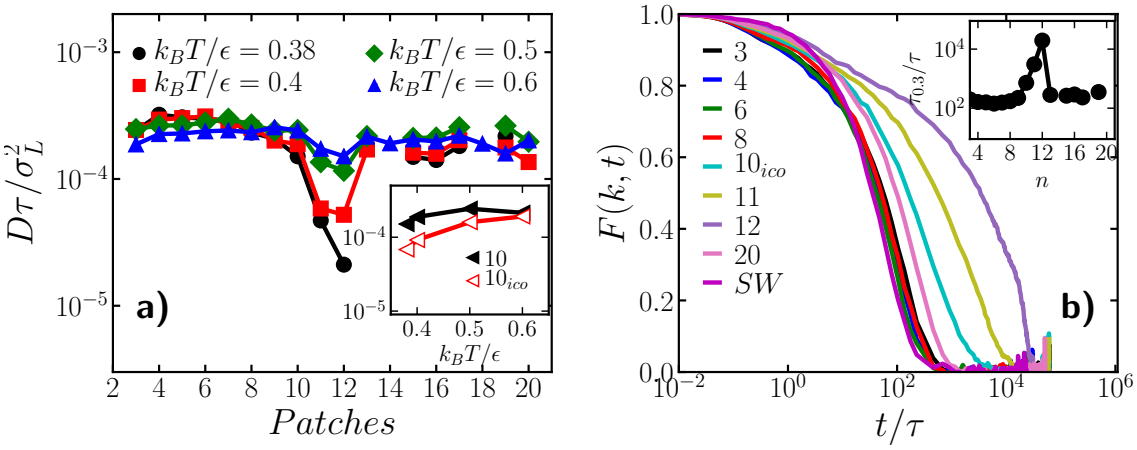


Figure 3.5: a) Diffusion coefficient as a function of number of patches, at different temperatures, for patchy particles with a fixed patch coverage fraction $\chi = 40\%$. Missing points correspond to crystallized systems. The inset shows the diffusion coefficient as function of temperature for the $n = 10$ and $n = 10_{ico}$ cases. b) Intermediate scattering function of the same systems, for a wavevector $q$ corresponding to the first peak of the structure factor, at fixed temperature $k_BT/\epsilon$=0.4. The inset shows the relaxation time $\tau_0.3$ as a function of the number of patches.

at the value of $k$ corresponding to the first peak in the structure factor. We observe an approximate collapse of the correlation functions for most geometries, while the $10_{ico}$, 11, and 12-patch systems are clear outliers which relax much more slowly. We show this clear slowing down by measuring the relaxation time $\tau_{0.3}$. We show in the inset of Fig. 3.5b) the behavior of $\tau_{0.3}$ as a function of the number of patches, where the $10_{ico}$, 11, and 12-patch cases clearly show larger relaxation times, while the other geometries show approximately the same $\tau_{0.3}$.

To confirm that the collapse of correlation functions is independent of the probing length $k$, we plot in Fig. 3.6 the relaxation times as a function of $k$. Clearly, most systems relax at approximately the same rate, regardless of the length scale. However, the relaxation dynamics of the $10_{ico}$, 11, and 12-patch particles are much slower, with the 12-patch system being roughly two orders of magnitude slower. Remarkably, the relaxation time is significantly more affected by icosahedral patch placement than the diffusion time, which only varies by about one order of magnitude at the same temperature (red line in Fig. 3.5a). This suggests a strong breakdown of the Stokes-Einstein relation (SER) [126]. This relation states that translational diffusion coefficient and the viscosity are inversely proportional: $D \propto \frac{1}{\eta_c}$, where $\eta_c$ is the coefficient of shear viscosity (more information about the SER will be given in the next Chapter). At the same time $\eta_c$ is proportional to the relaxation time. Most of the glass-formers deep in the supercooled liquid experience a break down of the SER. This break down has been linked to the emergence of structured domains in the supercooled liquid [126].

In addition, the exceptionally slow dynamics of the 12-patch system correlate with a significantly larger degree of bonding in the system. In Fig. 3.7a), we plot the number of bonds $N_b$ per particle as a function of temperature for the different patch geometries, as well as the square-well system. As expected, in the patchy systems, bond formation is more restrictive than in the square-well system and hence lower temperatures are required to form an equivalent number of bonds.

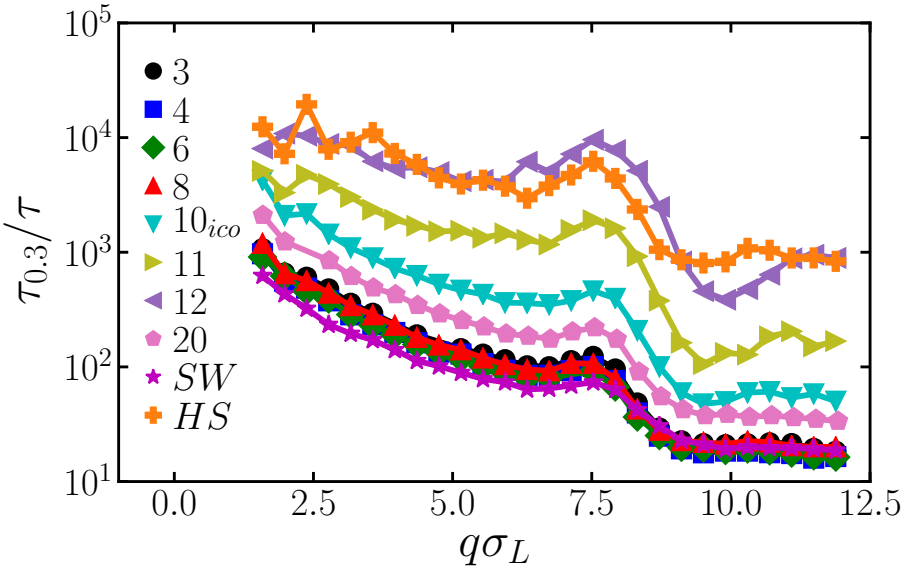


Figure 3.6: Wave vector dependence of the relaxation time $\tau_{0.3}$, at a temperature $k_BT/\epsilon = 0.4$.

This is consistent with the overall shift to lower $k_BT$ of the dynamical features seen in Fig. 3.4b) for low coverage fractions. The shapes of the curves are similar and it is indeed possible to obtain a master curve, presented in the inset of Fig. 3.7a), once the temperature is rescaled by the temperature $T(N_b = 2)$ at which 2 bonds per particle are attained. This suggests that the number of bonds scales trivially with an activation temperature for all geometries. It is now logical to suspect that the diffusion can be trivially rescaled for all the geometries. Interestingly, the collapse does not occur for the diffusivity, this presented in Fig. 3.7b). Even so, by comparing the systems with the same number of bonds per particle, the diffusivity is slowest in the 12-patch case. Hence, the slow down behavior of the icosahedral geometry does not directly scale as a function of the bonding pattern indicating non-trivial changes in the local structure.

### 3.3.3 Local Structure

The previous dynamical results shown compelling proof that icosahedral order is influencing dynamics. In this section we focus on the exploration of the local structure. We show a progressive analysis of the structure: from a general perspective to quantifying in detail the types and geometries of the clusters in the systems.

We start our structural analysis by calculating the angular distribution of the particles with their neighbors. We define the set of neighbors of particle $i$ as the particles within a distance $r_{ij} < r_c$, where $r_c = 1.03\sigma$ , in addition we define the angle $\theta_n = \cos(\mathbf{r}_{ij} \cdot \mathbf{r}_{ik})$ as the angle between two neighbors of particle $i$. We define

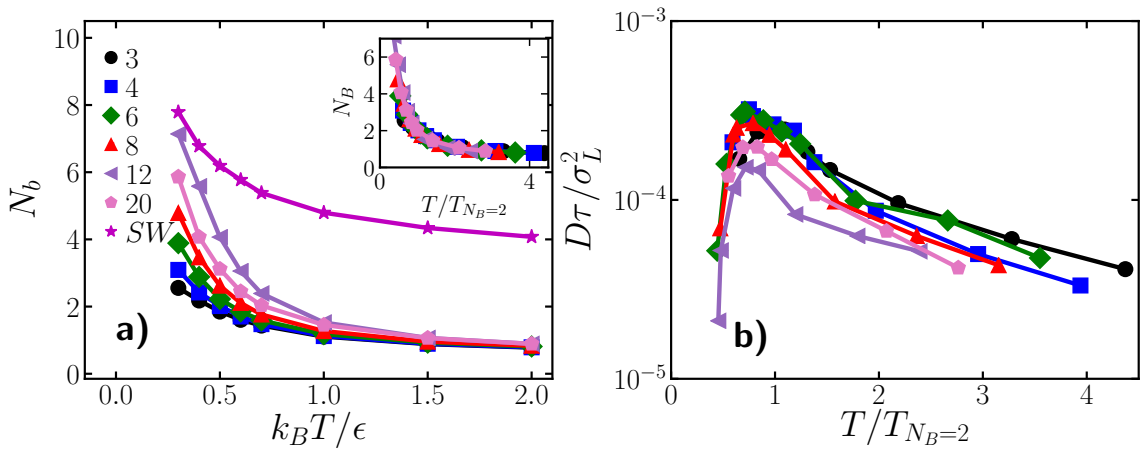


Figure 3.7: a) Number of bonds per particle as a function of temperature for different patch geometries, with $\chi = 40\%$. SW indicates the square-well system. The inset plot shows the number of bonds per particle with rescaled temperature $T/T(N_b = 2)$. For each patch geometry, the temperature is normalized with the temperature at which the system forms an average of two bonds per particle. b) Diffusion coefficient as a function of rescaled temperature for different patch geometries.

the angular distribution function as:

$$f(\theta) = \frac{1}{N}\sum_{i=1}^{N}\sum_{j\neq k}^{N_b}\cos(\mathbf{r}_{ij}\cdot\mathbf{r}_{ik}), \tag{3.12}$$

where $N_b$ is the number of neighbors of particle $i$, and $\mathbf{r}_{ij(k)}$ the unitary vector between the central particle $i$ and its neighbor $j(k)$.

In Fig. 3.8 we show the distribution function of some of the geometries studied at a fixed temperature $k_BT/\epsilon = 0.4$. Once more with the exception of the 12-patch case, the other geometries present the overall same structural features as the angular distributions are on top of each other. Note that, the dashed lines in the figure correspond to the angles found in a perfect icosahedral cluster. The $n = 12$-patch case has a sharp increase of neighbors at those specific angles, in particular at $\theta = 180°$.

In order to have more information about the local structure, we characterize the value of the BOP for each particle for all our systems. We find that the better BOP for finding icosahedral clusters are $Q_6$ and $\hat{W}_6$ that have non-zero values for perfect icosahedral, shown in table 3.1, $Q_6 = 0.663$ and $\hat{W}_6 = -0.170$. These values provide a reference point for finding icosahedral structure in the supercooled liquid. The 12-patch case shows at low temperatures a trend around the corresponding values of the perfect icosahedral cluster. This is not clearly found in the other cases.

In order to quantify local icosahedrality we define a particle to be embedded in an icosahedral environment when its $Q_6 > 0.5$ and $\hat{W}_6 < -0.1$. Even though these 'cut-off limits' seem to be arbitrary we will show that they globally capture the number of particles involve in icosahedral clusters. We show in Fig. 3.9 the

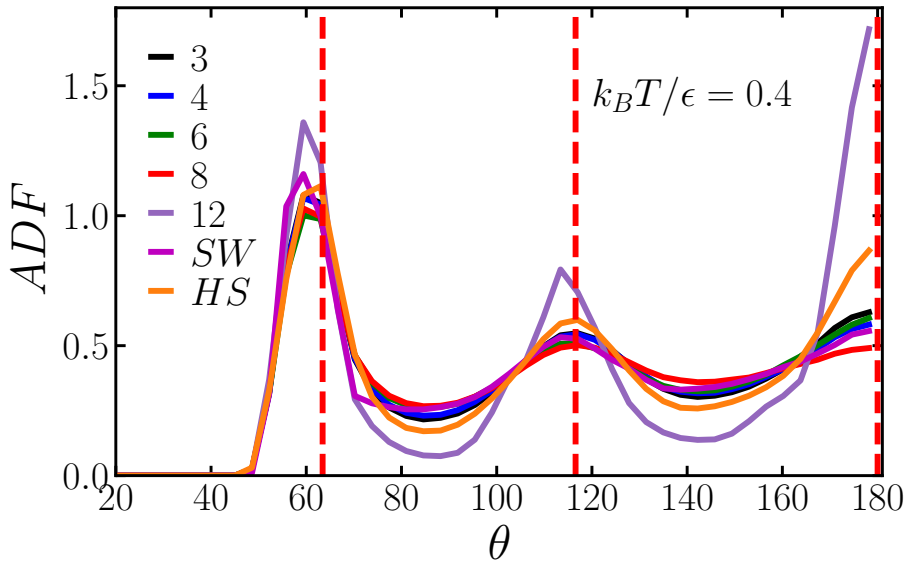


Figure 3.8: Angular distribution function corresponding to different $n$. Dashed lines correspond to the angles found in a perfect icosahedra.

number of particles involved in icosahedral environment as a function of temperature for some of the studied geometries. In the inset we show a scatter plot of $Q_6$ and $\hat{W}_6$ for the $n = 12$-patch case, where the red dot correspond to the values of the perfect icosahedra. At low temperatures the fraction of particles involved in icosahedral environments sharply increases in the 12-patch case. While the other geometries behave similarly between them. At high temperatures, the systems goes towards the repulsive limit reaching icosahedral values corresponding to a system of hard-spheres.

Both of the previous methodologies are known to be 'agnostic methods' for analyzing the local structure, due to none of them assume any particular local structure, and they can collect information of any arbitrary order [25]. Nevertheless, they are good indicators of the changes on the local structure. To look more directly for specific local structures, we explored in more detail the changes on local structure with the Topological Cluster Classification (TCC) algorithm [11]. This algorithm characterizes the local structure in a detailed manner by capturing different structural motifs or clusters from 3 particles to more complex ones made from 13 particles.

In this part of the analysis, we look for TCC motifs matching either icosahedral order (13A), defective icosahedral clusters (10B) or crystalline order (face-centered cubic (FCC), hexagonal close-packing (HCP), or the 9X cluster matching body-centered cubic (BCC), as they are shown in Fig. 3.10.

As we have shown before, icosahedral clusters occur in great numbers in the 12-patch case. Interestingly, hard-sphere binary systems with size ratio close to $q = 0.833$ at high packing fractions stabilize crystal structures belonging to Laves phases ($MgZn_2$, $MgCu_2$, and $MgNi_2$) [127]. One of the components of these phases are icosahedral clusters with specific location of small(large) particles. In

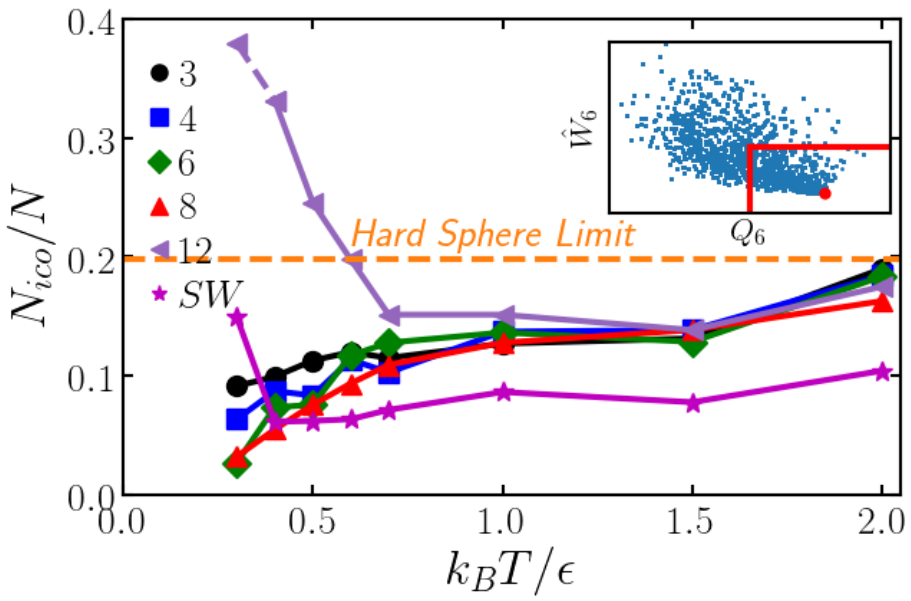


Figure 3.9: Fraction of particles in an icosahedral environment for a fixed temperature of $k_BT/\epsilon = 0.4$. Dashed orange line corresponds to a system of hard-spheres with the same properties. Inset shows the scatter plot of $Q_6$ and $\hat{W}_6$ for the 12-patch case. The red dot correspond to the values of the perfect icosahedral cluster and the red lines show the limits taken for defining an icosahedral environment.

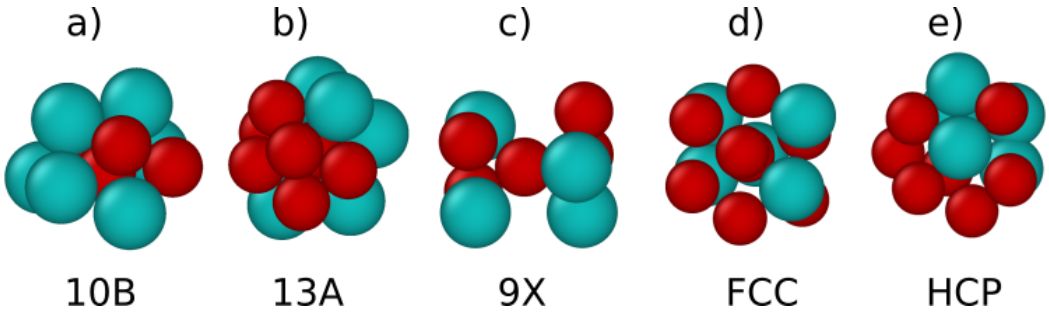


Figure 3.10: Illustration of some of the clusters captured by TCC. a) defective icosahedra (10B), b) icosahedral cluster (13A), c) body-centered cubic (BCC) corresponding to cluster 9X, d) face-centered cubic cluster (FCC) and e) hexagonal close-packing cluster (HCP).

particular, there are two local environments with an icosahedral topology, both with a small particle in the center. Hence, it is logical to suspect that in the 12-patch case crystallization might occur.

In order to ensure that the slowing down on dynamics of the $12-$ patch is not related with Laves-phases, we identify local icosahedral environments matching these crystals. We identify the local "Laves-like" clusters, by counting all icosahedral clusters with a small particle at the center, and an arrangement of large and small particles in the surrounding shell which matches one of these two environments.

In Fig. 3.11, we show the fraction of particles that are part of at least one cluster of each type, for a fixed temperature $k_BT/\epsilon = 0.4$ and for all patch geometries. As expected, for systems where crystallization occurred (14-patch and 18-patch), we

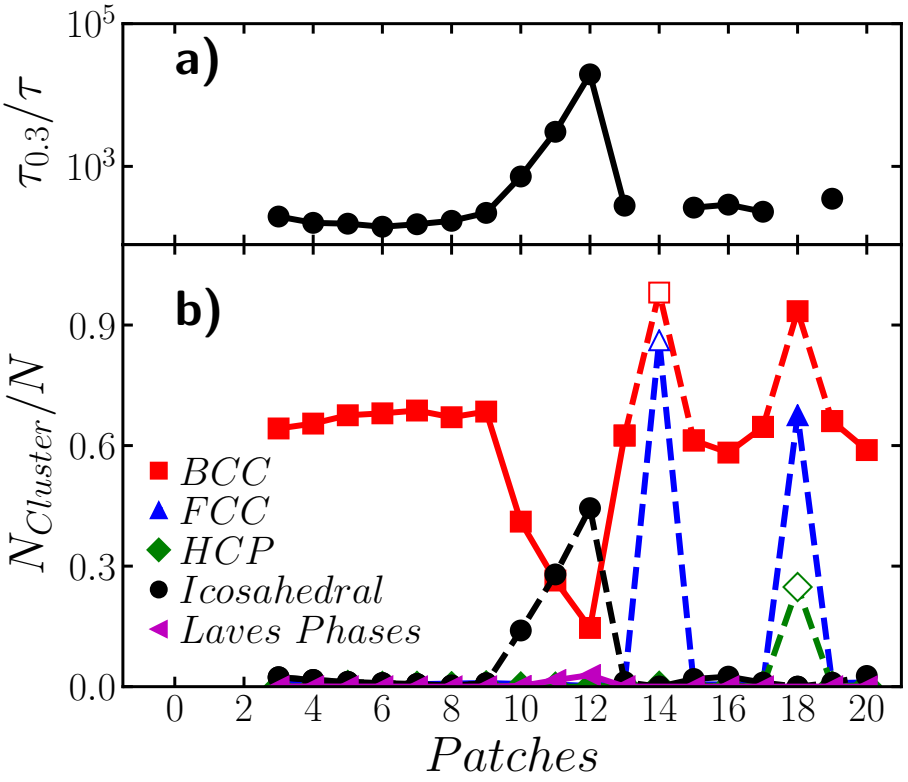


Figure 3.11: Fraction of particles that are part of local structural motifs with specific symmetries, as obtained using Topological Cluster Classification [11]. a) Different structural motifs at a fixed temperature $k_BT/\epsilon = 0.4$. The top panel in a) shows the corresponding relaxation time $\tau_{0.3}/\tau$. Note that the systems with 14 and 18 patches have partially crystallized into an FCC structure.

see large peaks in the populations of "crystal-like" clusters (FCC, BCC, HCP). In contrast, the other systems show little crystallinity, with the exception of the BCC motif, which is present in all fluids and does not indicate crystallinity on its own [11]. Icosahedral order is only observed in significant amounts for the $10_{ico}$, 11, and 12-patch systems (which all match icosahedral symmetry), with the 12-patch system showing the largest fraction of icosahedral motifs. On top of Fig. 3.11 we show the relaxation time $\tau_{0.3}$, where it follows the same trend as the number of particles involved in icosahedral clusters. At the same time, these systems also display a strong drop in BCC ordering. This can be understood from the observation that the appearance of a structural motif can inhibit the prevalence of other local structures [128], and hence assist in avoiding crystallization [129,130]. Indeed, in hard-sphere fluids, the five-fold order that is present in icosahedral clusters strongly anticorrelates with BCC ordering [130]. The fraction of Laves phase clusters is negligible in all systems (i.e. a few isolated motifs of this type per configuration), hence the systems are safe of crystallizing in Laves phases at these conditions.

Now, we show the behavior of the number of icosahedral clusters as a function of temperature for different patch geometries. In Fig. 3.12a), we show the fraction of particles in icosahedral motifs as a function of temperature. In the limit of high temperatures (i.e. the hard-sphere limit), we find that a significant fraction ($\approx 12\%$) of the particles are part of an icosahedral motif. As the temperature de-

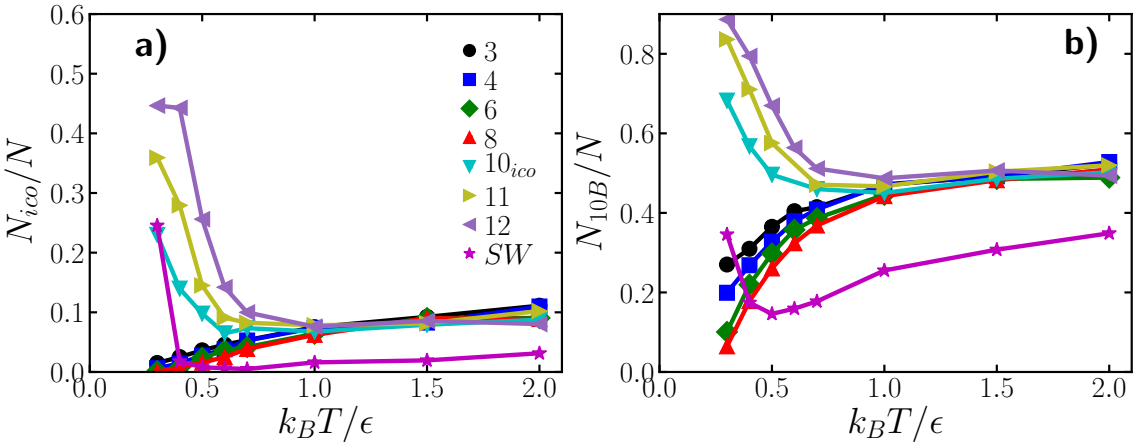


Figure 3.12: a) Fraction of particles in icosahedral clusters as a function of temperature for different patch numbers. The dashed horizontal line indicates the value in the hard-sphere limit. b) Corresponding defective icosahedral clusters as a function of temperature.

creases, the number of icosahedral motifs initially decreases in a similar fashion for all patch geometries. In this regime, the patches essentially act, on average, as a weaker square well, and aid in the cage-breaking that enforce the reentrant behavior observed in Fig.3.4. However, at low temperatures, the $10_{ico}$, 11, and 12-patch systems start to display a strong enhancement of local icosahedral order, reaching values well beyond the hard-sphere level while all other patch geometries continue to further suppress icosahedral motifs. Interestingly, at very low temperatures, the square-well system also enhances icosahedral order and does so quite suddenly, possibly hinting at a phase separation [123].

It is important to note that perfect icosahedral cages are not the only structures enhanced by $10_{ico}$, 11, and 12-patch particles. Intuitively, we expect the patchy interactions to have a positive effect on the concentration of any local structure which is commensurate with the chosen patch geometry. As such, there are other local structures with imperfect icosahedral order, such as defective icosahedra, whose concentration is strongly correlated with the appearance of perfect icosahedral clusters, as it is shown in Fig. 3.12b). As many of these structures incorporate the five-fold symmetry associated with the 12-patch geometry, these additional structures are all likely to contribute to both slowing down the dynamics suppressing crystallization [24, 107, 131].

### 3.3.4 Crystallization

For specific patch numbers ($n = 13, 14, 18, 20$), we find crystallization at the lowest temperatures investigated ($k_BT/\epsilon \lesssim 0.5$). Specifically, we find two distinct crystal structures: a binary CsCl crystal, and a FCC crystal consisting of large particles. The CsCl structure, which consists of two interspersed simple cubic lattices, only appears in the system with $n = 20$ patches. In this structure, each particle has eight nearest neighbors of the opposite species, arranged on the vertices of a cube. The emergence of this crystal structure can be understood from the fact that the

20 patches are arranged on the vertices of a dodecahedron. This arrangement contains subsets of 8 patches that are arranged perfectly on the vertices of a cube, and hence this patch arrangement is highly compatible with the CsCl structure. We only observe the formation of FCC crystals at low temperatures for a few patch geometries ($n=13, 14, 18$), all corresponding to a relatively large number of patches. This structure is stable in the hard-sphere limit, and is evidently further promoted by the interactions corresponding to these patch geometries.

In order to check whether the other geometries are in their equilibrium phase. We used an FCC configuration taken from the case $n = 18$ (which crystallizes into FCC) as an initial configuration for all the patch geometries. The orientation of the particles was randomly assigned at the beginning of the simulation. For the systems where we found crystallization, the simulations with an FCC seed remain crystalline. In contrast, for the other patch geometries after short time the systems melt back into a liquid. From this, we conclude that for most patch geometries, crystallization into the FCC structure is disfavored in the investigated regime.

## 3.4 Conclusions

Our results show that, patchy particles display appropriate characteristics to disrupt the local structure. Specifically, we prove that by boosting icosahedral order the systems go to more arrested states, this reflected in the extreme slowdown on dynamics at low temperatures. Patchy particles with icosahedral interactions ($n=12$, $n=11$ and $n=10_{ico}$) enhance this type of ordering.

In both of the arrested regimes, at high and low temperature, icosahedral clusters and its extension the defected icosahedral, both seem to play crucial role in the arrest. At high temperatures where all the particles behave similarly and their overall diffusion rate is the same, they all present relatively high values of icosahedral. This backs up the observation dynamical slowdown driven by the rise of long-lived structures [74, 132]. In the regime of low temperatures, the systems that show a sharp increase of these structures present a drastic decrease in their diffusion coefficient. This leads us to assure that icosahedral ordering is one of the key ingredients for controlling dynamics and moreover they are a tool to go deeper into the supercooled liquid, either experimentally or in simulations.

Remarkable, the patch geometries that do not match with local icosahedral order do not have a noticeable impact on dynamics. And in those systems, it is not the location and number of the patches that matter, it is the percentage covered by the patches that constitutes the leading factor in controlling the dynamics. This extreme sensitivity of dynamics to local icosahedral structures highlights the important role these motifs play in the kinetic arrest of disordered systems. Moreover, the inherent incompatibility of icosahedral order with long-ranged crystalline order suggests that these systems are also virtually guaranteed to avoid crystallization.

## 3.5 Acknowledgments

Some of the figures and text were reproduced from Ref. S. Marín-Aguilar, H. H. Wensink, G. Foffi, and F. Smallenburg, "Slowing down supercooled liquids by manipulating their local structure", *Soft Matter*, vol. 15, no. 48, pp. 9886-9893, 2019. [14] with permission from the Royal Society of Chemistry.

Additionally, I would like to thank Frank Smallenburg for providing me with the EDMD code for simulating patchy particles.

Chapter 4

# Patchy Particles: Rotational Dynamics

This chapter is based on the publication:

S. Marín-Aguilar, H. H. Wensink, G. Foffi, and F. Smallenburg, "Rotational and translational dynamics in dense fluids of patchy particles", *The Journal of Chemical Physics*, vol. 152, no. 8, pp. 084501, 2020. [15]

## 4.1 Introduction

In the previous chapter, we have shown that the addition of directionality to the interactions can be used to modify the local structure of supercooled liquids and, as a consequence, their translational dynamics change. Patchy particles have proven to be a great tool for this purpose. Despite still being spherical in shape, the patchy particles are inherently anisotropic and impose preferred local particle arrangements in the system. As the orientation of the particles is now distinguishable, they perform both translational and rotational motion and both of these can be slowed down by the interparticle interactions.

The overall dynamical behavior of glassy systems displays important deviations from the fluid one. These differences are key to understand the physical mechanism of the dynamical slowdown (see Section 1.1.1). As we have mentioned before, one of them is the relaxation time behavior in the glassy regime. In the fluid regime the relation between this relaxation time and the diffusion coefficient follows the Stokes-Einstein relation (SER), which states that these two quantities are inversely proportional $D \propto 1/\tau_T$, where $D$ corresponds to the diffusion coefficient and $\tau_T$ to the structural relaxation time. As we have pointed out before, most of the fluids deep into the supercooled liquid regime present a break down of the SER [126].

While the SER considers only the translational dynamics, the rotational counterpart is captured by a similar relation called the Stokes-Einstein-Debye (SED)

relation. Based on the model proposed by Debye [133] concerning the rotational dynamics of polar molecules, the SED relation states that the rotational diffusion coefficient is inversely proportional to the viscosity as:

$$D_r = \frac{k_B T}{8\pi\eta_c a^3}, \tag{4.1}$$

where $D_r$ corresponds to the rotational diffusion, $k_B$ the Boltzmann constant, $T$ the temperature of the system and $a$ corresponds to the diameter of the particle.

The solution of the Debye rotational diffusion equation for the reorientation of a molecular dipole give us a relation between the rotational diffusion and the rotational relaxation time [13]. Here, the rotational relaxation time can be extracted from the long-time decay of a time rotational correlation defined as:

$$C_l(t) = \langle P_l[\mathbf{u}(t) \cdot \mathbf{u}(0)]\rangle \tag{4.2}$$

where $P_l$ are the Legendre polynomial of $l$ degree, and $\mathbf{u}(t)$ is a unitary vector which indicates the direction of the dipole moment at time $t$. Each $l$ will have a corresponding relaxation time and in general they are related as [40]:

$$\frac{\tau_l}{\tau_{l+1}} = \frac{l+2}{l}. \tag{4.3}$$

And the relation between the rotational diffusion and the rotational relaxation time is [13]:

$$D_r = \frac{1}{l(l+1)\tau_l}, \tag{4.4}$$

where $l$ is the $l$-th order of the Legendre polynomial. Therefore, the SED can be written as:

$$\tau_l k_B T = \frac{8\pi\eta_c a^3}{l(l+1)}. \tag{4.5}$$

Here we remark that the viscosity is proportional to the structural relaxation time [126]. Essentially, the SED states that the structural and rotational relaxation time are proportional $\tau_T \propto \tau_R$. As in the case of the SER, for most of the fluids deep in the supercooled liquid regime and into the glassy regime, the SED relation also tends to break. It is important to note that, in the derivation of both relations a particle is considered embedded in a viscous fluid and there are no considerations of the interactions with other particles. In the glassy regime, the environment of the particles has an enormous effect on its dynamics, such is the case of the cage effect. Hence, it is not shocking that these relations break down in the glassy regime.

Eventhough, both relations break, rotations and translations do not necessarily slow down at the same rate and moreover the two relaxations may become arrested at significantly different temperatures or packing fractions [134–136]. The mechanism of the decoupling between relaxation behaviors is complex and dependent on the interactions and the shape of the particles [137–140]. Moreover,

the exact method used for probing the rotational dynamics results in different decoupling [13,136,141,142].

In the case of dense systems of spherical patchy particles, an interesting contrast arises. While the translational motion of a particle is hindered both by the repulsive cores of its neighbors and the attractive bonds it has formed with them, rotational motion is purely hampered only by the attractive bonds. As a result, it is natural to expect a decoupling between translational and rotational motion, at least when the temperature is high enough for the repulsive forces to dominate. This is in sharp contrast to the glassy behavior of low-valence patchy particles at low densities, where any dynamical slowdown is essentially dominated by the time scale at which the bonding network changes, typically leading to strong glass forming behavior [89,91,117,143,144].

Here, we examine the interplay between rotational and translational relaxation in dense suspensions of patchy particles. We use molecular dynamics simulations to investigate patchy particles with two distinct patch geometries. The first favors icosahedral local structures, and hence promotes dynamical slowdown, while the second promotes an octahedral symmetry, which has little effect on the dynamics (as it was shown in Chapter 3).

We show that the rotational relaxation behavior is dependent on the geometry of the patches, and hence on the local structure. We also find that for the systems that enhance icosahedral ordering, the rotational behavior is controlled by the interplay between the icosahedral formation and the number of bonds. Additionally, we show that the rotational relaxation decouples from translational relaxation in nearly all cases. We conclude that while translational dynamics are controlled by collective effects, the rotational relaxation is purely dependent on the local structure.

## 4.2 Model and Methodology

### 4.2.1 Simulation

To model the patchy particles we use the Kern-Frenkel model [10] (see section 3.2.1). In order to explore the rotational dynamics with different patch geometries we focus on systems with two different number of patches: $n=6$ and $n=12$. For both cases the location of the patches is such that the minimum distance between any two patches is maximized, identical to the geometries in Chapter 3. This results in the patches being located at the vertices of an octahedron and an icosahedron respectively [118], as shown in Fig. 4.1.

We use Event Driven Molecular Dynamics (EDMD) [91, 94, 95] to simulate the patchy particles systems (see Chapter 2). As in the previous chapter, all the systems are binary mixtures of $N=700$ particles with size ratio $q=\sigma_S/\sigma_L=0.83$ where $\sigma_{S(L)}$ is the diameter of the large(small) particle and composition $x_L=0.5$.

| $n$ | $\theta_O$ | $\theta_F$ |
|---|---|---|
| 6 | $\simeq 45°$ | $\simeq 54.73°$ |
| 12 | $\simeq 31.72°$ | $\simeq 37.37°$ |

Table 4.1: Values of the angles where the patches start to overlap $\theta_O$ and the corresponding one when the total surface is covered $\theta_F$ for the 6-patch and the 12-patch cases.

The systems were equilibrated at constant temperature for at least $10^4\tau$, where $\tau$ is our time unit $\tau = \sqrt{m\sigma_L^2/k_BT}$. After equilibration, we simulate the dynamics at constant energy for at least $10^5\tau$. We perform our measurements in this last step.

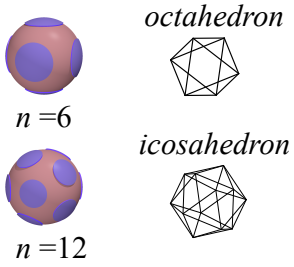


Figure 4.1: Patchy particles with $n=6$ and $n=12$ patches. Next to each of the cases we show the polyhedron whose vertices correspond to the patch locations.

In this Chapter we will focus on the effect of the patches in the rotational dynamics in the glassy regime. For this, we explore in detail different patch sizes (modulated by the angle $\theta$, see Fig.3.1). This model, as mentioned previously, allows us to interpolate between two limit cases: hard spheres systems when $\theta=0$ and square-well particles when the total surface is covered by the patches. Here, it is important to note that the angle where the patches cover the total surface $\theta_F$ and the angle where the patches start overlapping $\theta_O$ depend on the number of patches $n$ and its location. In particular, the angle $\theta_O$ has an important effect on the rotational dynamics. In table 4.1 we show the values of these two angles for both of the geometries used in this Chapter.

### 4.2.2 Analysis

In this Chapter, one of the main discussion points is the coupling or decoupling of the translational and the rotational relaxation times. In order to have a clearer picture of the translational relaxation behavior of these systems, we measure the translational relaxation time. To do so, we calculate $\tau_{0.3}$ by fitting a stretched exponential to the long time behavior of the intermediate scattering function. In order to clearly distinguish between the rotational relaxation and the translational relaxation we will denote $\tau_{0.3}$ as $\tau_T$ in this Chapter.

#### 4.2.2.1 Rotational dynamics

Based on the Debye model, the reorientation of a molecule can be described by the time dependent correlation function [12]:

$$C_l(t) = \frac{1}{N}\sum_{j}^{N} P_l\left(\hat{\mathbf{u}}_j(t)\cdot\hat{\mathbf{u}}_j(0)\right) \tag{4.6}$$

where $P_l$ is the Legendre polynomial of $l$-th degree and $\hat{\mathbf{u}}$ is a fixed unit vector which rotates along with the particle. In the patchy particle case we define the unitary vector $\hat{\mathbf{u}}$ as the vector that points to a specific patch in the particle, such that the dot product $\hat{\mathbf{u}}(t)\cdot\hat{\mathbf{u}}(0)$ is calculated between the initial direction of the patch and the rotated one after a time $t$.

Assuming that the reorientation of a particle is due to infinitesimal uncorrelated steps, the correlation function for all $l$ degrees decays exponentially and is directly related with the rotational relaxation time [145, 146]:

$$C_l(t) = \exp\left[-l(l+1)t/\tau_l\right], \tag{4.7}$$

where $\tau_l$ is the rotational relaxation corresponding to the $l$-th degree Legendre polynomial. Moreover, the correlation can be directly measured from experiments, as $C_1$ can be related to the spectral bandshapes measure in infrarred absorption and $C_2$ to Raman light scattering [40]. In this Chapter we will denote $\tau_R$ as the rotational relaxation time corresponding to the second Legendre Polynomial.

It should be noted here that in this study of the rotational correlations, we deliberately do not account for the symmetry of the particle. The rotational correlation function simply checks whether an average particle has rotated with respect to its original orientation, even if the new orientation has (different) patches pointing in the same directions as in the original one. This implies we are looking at the ability of the particle to rotate, rather than find a new configuration that is fully independent of its starting orientation. For example if a particle with the patches located in the vertex of an octahedron rotates $90^\circ$ around an axis that passes through any patch it will arrive to a configuration where the patches are located in the same way of the initial configuration, even if the particle has rotated.

## 4.3 Results

### 4.3.1 Translational relaxation time

We begin our study by exploring the translational relaxation behavior for both geometries and a wide range of temperatures. As was shown in Chapter 3 the reentrant behavior in the phase diagram of systems with short range interactions

is retained after the addition of directional interactions (i.e. for patchy particles). This was reflected in the changes on diffusion coefficient along temperature. Additionally, the translational relaxation time is expected to capture as well the reentrance. In order to confirm this, we calculate the translational relaxation time $\tau_T(\tau_{0.3})$ for the two studied geometries and different temperatures.

In Fig. 4.2 we show the structural relaxation time for both geometries. At low temperatures, the system is in an arrested state driven by the attractions with their neighbors and thus the relaxation time grows. Upon increasing the temperature, the systems regains fluidity and the value of the relaxation time decreases. Finally, at higher temperatures the relaxation time increases again due to the arrest of the system driven by repulsions. The dependence of this behavior on the size of the patch is also captured by the $\tau_T$: smaller angles which are closer to the hard-sphere scenario lead to stronger dynamical arrest.

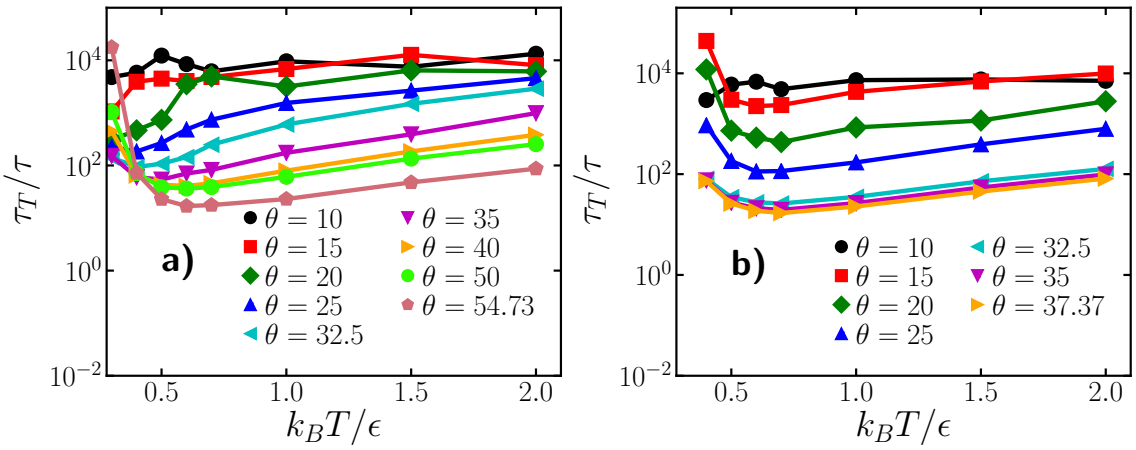


Figure 4.2: Translational relaxation times $\tau_T$ as a function of $k_BT/\epsilon$ for the a) 6-patch and b) 12-patch system.

### 4.3.2 Rotational Dynamics

We now turn our attention to rotational dynamics. To do so, we calculate the orientational correlation function (Eq. 4.6). We focus on the second degree correlation $C_2$ which captures the decay of the second Lengendre polynomial. This correlation is the most commonly used due to the possibility of comparison with experiments [40, 147]. We show in Fig. 4.3 the decay of $C_2$ found in our patchy systems. As we mentioned previously, in the Debye approximation these correlations decay exponentially. However, in the patchy-particle case we notice that the decay is not exponential and it displays different behaviors. One of the main differences with the Debye approximation is that in there the rotations occur in small uncorrelated steps and in our systems the rotations get correlated at longer-scales due to the complexity of the environment of the particles. Moreover, when a bond is broken large rearrangements in the orientation are expected, which makes the rotational dynamics strongly dependent on the current orientation of the particles. This as consequence disrupts the smooth exponential decay. Nev-

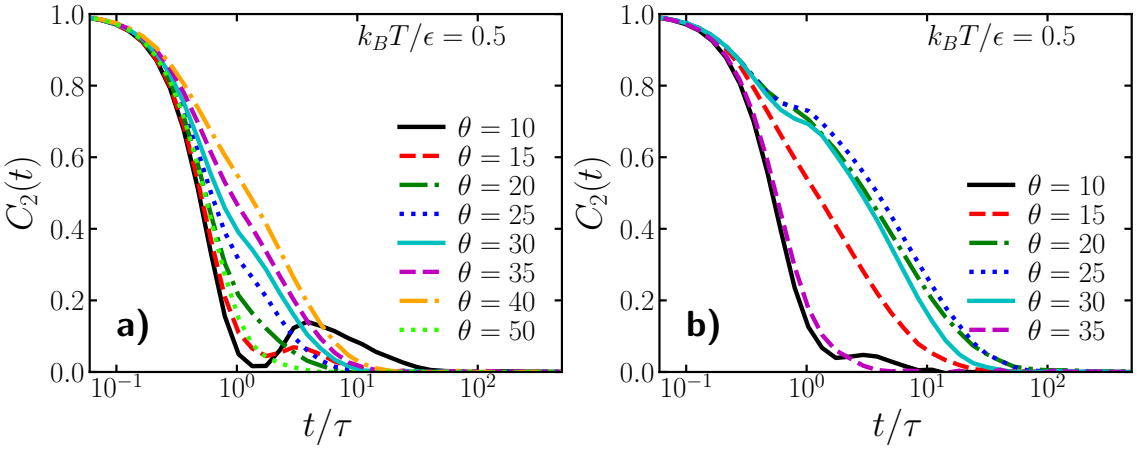


Figure 4.3: Rotational correlation function for the a) 6-patch system and b) 12-patch system.

ertheless, valuable information of the rotational behavior is extracted from this anomalous decay.

The shape of $C_2$ shows at least two deviations from the exponential decay. The first of them is found at small angle $\theta$, the rotational correlation function first decays rapidly, and then after a short time shows a sudden increase. Note that the same behavior happens on larger $\theta$, but at higher temperatures. We attribute this behavior to the presence of free spinners: particles which rotate around the same axis for a long period of time. As the only interactions that affect the rotation of the particles are attractions by the patches, free spinners occur when the system forms very few bonds, such that patch-patch collisions are rare, hence the angular velocity does not change and the particle continues to spin around the same axis. Once there is a patch interaction, either an attractive or a repulsive collision, the angular velocity changes and so does the rotation axis. Naturally, this behavior predominantly happens when either the patches are very small, or the temperature is high and there are few bonds. On the other hand at lower temperatures or larger patch size, patch collisions are more common and hence, the particles do not spin for a long time, loosing rapidly the free-spinners behavior.

In order to ensure that this specific behavior is due to the contribution of free spinners, we explore in greater detail the time scale of the sudden increase and the correlation in the ideal gas limit. For the latter, we go back to the definition of the rotational correlation in the ideal gas limit. Suppose that a patchy particle rotates around the axis $z$ with an angular velocity $\omega$, in the ideal gas limit there are no interactions and the value and direction of the angular velocity is constant. The probability of a particle rotating to $\omega t$ follows the Maxwell-Boltzmann distribution. Hence, the rotational correlation at time $t$ will be:

$$C_l(t) = \left(\frac{1}{2\pi}\right)^{3/2} \int P_l(\mathbf{u}(t)\cdot\mathbf{u}(0)) \exp\left[-\frac{|\omega|^2}{2}\right] d\Omega \tag{4.8}$$

By solving this equation for $l = 2$ and different times we recover the behavior of the correlation $C_2$ corresponding to free-spinners shown in 4.4 a). At short times the correlation decays and then it increases to a fixed value.

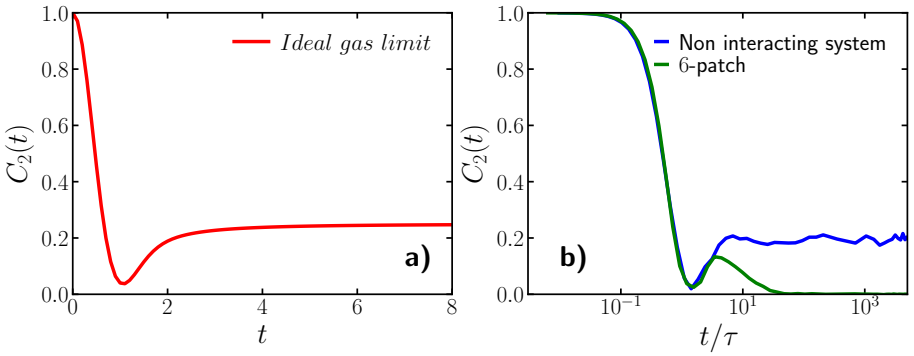


Figure 4.4: a) Decay of the rotational correlation according to Eq. 4.8, $I$ and $\omega$ are taken as 1. b) Rotational correlation functions of a system of hard-sphere particles and the 6-patch case with an opening angle of $10^\circ$ and $k_BT/\epsilon = 0.4$. In both cases, the packing fraction is fixed at $\eta = 0.58$.

Moreover, we can retrieve a similar result by calculating the rotational correlation in a system with isotropic interactions. To do so, let us define a vector $\mathbf{u}$ pointing a specific direction on each of the particles of a hard-sphere or a square-well system. We simulate this system at the same conditions as the patchy particles and we calculate the rotational correlation.

In Fig. 4.4b) we show the decay of $C_2$ of a system of hard spheres. As in the patchy systems there is a fast decay of the correlation and then a sudden increase corresponding to the rotation of the free spinners, this is in agreement with the theoretical approach from Eq. 4.8 shown in Fig. 4.4a). In the same figure we show one of the patchy systems where the local minimum in the correlation function is present. The time where the correlation reaches the local minimum indeed matches with the solution of the free spinners. This confirms our conclusion that this behavior in the patchy-particle case results from the presence of free spinners in the system.

The second behavior captured by the decay of the $C_2$ which deviates from the exponential decay is better appreciated in the 12-patch case (Fig. 4.3b)). For intermediate values of $\theta$ the correlation presents a plateau. This plateau represents the slowing down of rotational dynamics due to bonds with neighboring particles. For small angles, bonds are rare, and hence the rotations are unlikely to be blocked by their neighbors. In contrast, in a regime where the angles are not overlapping but they are covering a considerable amount of surface, the particles are likely to have more bonds. Hence, in order to fully decorrelate from the initial orientation several bonds have to break, leading to a slow down in rotational dynamics. Finally this plateau disappears in the regime where the patches overlap. There, the particles can easily rotate passing from one patch to another without the need of breaking bonds and thus the rotational relaxation time decreases again. As one might expect, this plateau becomes more pronounced at lower temperatures, where bonds take longer to break. Additionally, at sufficiently low temperatures the plateau also arises in the six-patch system, but mostly for large (non-overlapping) values of $\theta$. As a result of these effects, we observe a reentrant behavior in the rotational relaxation time as a function of the size of the patch.

#### 4.3.2.1 Relaxation time as a function of $\theta$

In order to show this reentrance explicitly, we measure the rotational relaxation time $\tau_R$. To do so, we fit a stretched exponential, avoiding the regime where the correlation goes up due to free spinners. We define $\tau_R$ as the time at which the correlation function decays to a value of $0.3$. This definition is taken to be consistent with the definition of the translational relaxation time and due to the complex non-exponential decay of the rotational correlation.

In Fig. 4.5 we show the dependence of $\tau_R$ on $\theta$ for both systems. The dashed vertical lines show the overlap angle $\theta_O$. As mentioned previously, the dependency shows a reentrant behavior, where at intermediate angles the relaxation time increases due to the formation of a plateau in the correlation function and at larger angles the rotational relaxation decreases.

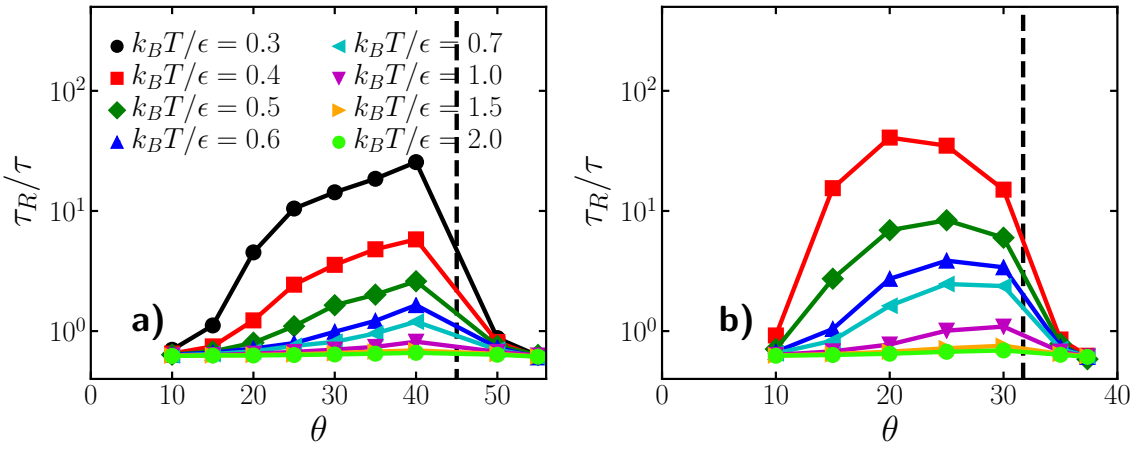


Figure 4.5: Rotational relaxation times $\tau_R$ as a function of the patch opening angle of the system a) $n = 6$ and b) $n = 12$. Dashed lines correspond to the overlap angle of each.

At first glance both geometries seem to have the same reentrant behavior, though a careful observation shows that the behavior at low temperatures is qualitatively different. Even though for both geometries, there is an angle where the relaxation time is maximized, the place of the maximum in the rotational relaxation time depends on the geometry.

For the 6-patch case, the slowest rotational dynamics is found just below the overlapping angle: $\tau_R$ increases essentially monotonically until the patches overlap, and then drops sharply as the particles are now more free to rotate without breaking any bond. This type of behavior is present in all the temperatures studied. Furthermore, it is the most intuitive: particles with small angles form fewer bonds, so in order to decorrelate the particles do not have to cross the energy barrier imposed by the attractive interactions and particles rotate easily. On the other hand, larger patches lead to more bonds, and several bonds must break to rotate, hence rotational dynamics slow down. Once $\theta > \theta_O$, the patches overlap and the particles are free to rotate without breaking any bonds, resulting in faster relaxation.

In contrast, for the 12-patch case the optimal angle is found well below the overlapping angle $\theta_O$, around a value of $\theta \simeq 20°$-$25°$ at low temperatures. While going to higher temperatures the maximum in the relaxation time shifts to larger angles below $\theta_O$. At high temperature both geometries show essentially the same behavior.

The shift at low temperatures may be once more related with changes in the local structure. As we show in Chapter 3 locating the patches in an icosahedral manner modifies the local structure, promoting the appearance of icosahedral clusters. This effect is particularly strong at low temperatures where we see the changes in the rotational relaxation in the 12-patch case. If an increase of icosahedral clusters is found around patch sizes $\theta \simeq 20 - 25$, this could cause the shift of slower rotational dynamics to these angles. We explore this in more detail in Section 4.3.4 where we will show the changes in the local structure as a function of the characteristics of the patches.

#### 4.3.2.2 Relaxation time as a function of temperature

In Chapter 3 we showed that the translational dynamics of systems of short range patchy particles present a clear reentrance in the dynamics as a function of temperature due to the crossover between two arrested phases driven by attractions and repulsions. A logical question arises in the study of rotations: is the same type of reentrance present in the rotational dynamics as a function of temperature? In order to answer this question we explore the rotational relaxation time at different temperatures.

In Fig. 4.6 we show $\tau_R$ for both patch geometries as a function of temperature. At low temperatures the rotational relaxation slows down roughly one order of magnitude in comparison to higher temperatures. This is understandable as at higher temperatures, the particles tend to rotate easily and thus the relaxation time drops.

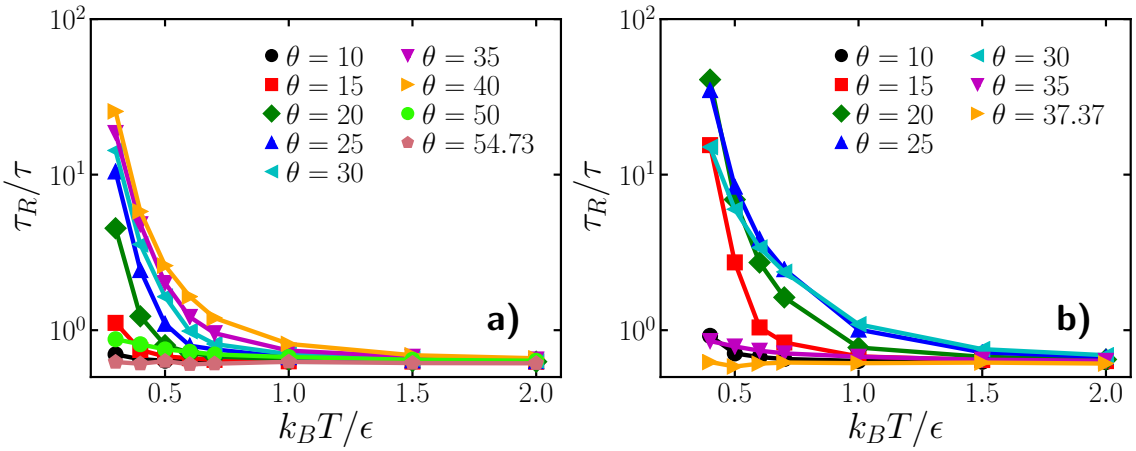


Figure 4.6: Rotational relaxation times $\tau_R$ as function of $k_BT/\epsilon$ for a) the 6-patch system and b) the 12-patch system.

Remarkably the time scales of the two types of relaxation (translational and rotational) are completely different. Comparing the scale of the translational relaxation shown in Fig. 4.2 with the rotational relaxation from Fig. 4.6, we notice that the latter is significantly faster. With the exception of the lowest investigated temperatures, $\tau_R$ is at least an order of magnitude smaller than $\tau_T$. Moreover, the temperature-dependence of $\tau_R$ shows a stark contrast to that of $\tau_T$: the reentrance is not present in the rotation relaxation. Together, these observations show that the two time scales are essentially decoupled unless the temperature is extremely low.

While the Stokes-Einstein-Debye relation points that the structural relaxation is proportional to the rotational relaxation in the fluid, in the glassy regime is well known the relation breaks down. However in the patchy systems the relation between the two types of relaxation follows a non-trivial functionality highly dependent of the size and the geometry of the patches. This is shown in Fig. 4.7 where we show the ratio between $\tau_R$ and $\tau_T$ as a function of temperature. The SED relation is broken as consequence of an interplay of the effects present in these systems with strong preferred directions and short range interactions. First, the reentrance behavior in the translational relaxation disrupts strongly the relation between the two types of dynamics as the rotational one do not present the reentrance as a function of temperature. Moreover, the rotational behavior depends strongly of the size of the patches. This dependency is not seen in the translational relaxation, where $\tau_T$ decreases monotonically as the patch size increases.

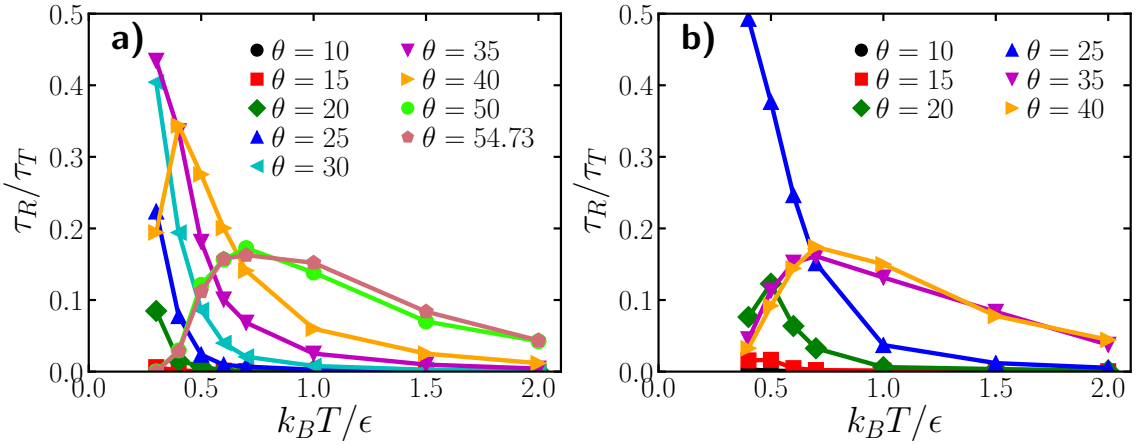


Figure 4.7: Translational relaxation time as a function of the rotational relaxation time of the 6-patch and the 12-patch case.

Although the breakdown of the SED was expected, it is interesting to observe that even at extremely low temperatures, where most particles are strongly bonded, the particles still manage to rotate almost freely on relatively short time scales. In addition, the big gap between the two time scales provides an indication of the mechanism of the relaxation. While the translational relaxation needs collective motion for a particle to break the cage and diffuse in the system, the rotational relaxation seems to be mainly controlled only by local rearrangements within its local cage. In the next section, we explore this in more detail.

### 4.3.3 Dynamical Monte Carlo

The time scale of the rotational relaxation points at a rather local relaxation mechanism. In order to confirm this hypothesis, we use a simple model to approximate the rotational relaxation of each particle in its local cage. We start from an equilibrated configuration from the molecular simulations. Next, we fix the positions of all particles except for a single one. We then sample the rotations in one local cage by performing a Monte Carlo simulation on only the chosen particle. During each simulation step, the particle is moved with small rotational and translational displacements, while keeping all other particles fixed. The step size for both types of moves is chosen to be sufficiently small to ensure a high acceptance rate ($\gtrsim 90\%$), such that the dynamics of the particles resemble a Brownian motion trajectory. Additionally, the small step size avoids the possibility of "jumping" between two distinct bonded configurations without a change in energy.

Due to the high acceptance rate, this algorithm resembles a dynamical Monte Carlo (DMC) scheme [148].

After $10^5$ steps, the chosen particle is returned to its initial configuration and the same procedure is performed on another particle. While doing the rotational movements we calculate the rotational correlation in the same way as we did in the molecular dynamics, but as a function of the number of MC steps instead of as a function of time. With this methodology, we sample the average rotational relaxation of all particles in their respective cages, under the assumption that this relaxation is an entirely local process, as we have frozen the positions of all the other particles.

We normalize the rotational relaxation time $\tau_{DMC}$ by dividing it by the typical relaxation time of a free rotor $\tau_{FR}$ calculated in the same way. In Fig. 4.8 we show the local dynamical Monte Carlo rotational relaxation time $\tau_{DMC}$ divided by the corresponding $\tau_{FR}$ as function of the angle $\theta$. Comparing the results with Fig. 4.5 we see that the qualitative behavior of the rotations is reproduced by the local DMC approach. In the 6-patch case the relaxation time increases with the size of the patch until it finds its maximum shortly before the overlap angle, and then decreases rapidly. In contrast, for the 12-patch case the maximum in the relaxation time shifts to lower angles, ending up around $\theta \simeq 25^\circ$ for the lowest temperatures. Note that in the DMC simulations, the particles behave diffusively at short time scales, as opposed to the ballistic behavior that occurs in EDMD for short times. Hence, the DMC simulations have significantly longer rotational relaxation times at high temperatures, resulting in a more limited variation in $\tau_{DMC}$ as compared to the $\tau_R$ measured in EDMD. Nonetheless, these results show that the local DMC simulations capture the qualitative behavior of the rotational dynamics in our molecular dynamics simulations. In combination with the large discrepancy in time scales between the rotational and translational dynamics, this confirms that the rotational relaxation of the system is largely decoupled from the translations. Rather than being controlled by global rearrangements, rotational diffusion is dominated by local rearrangements within the translational cage that surrounds a particle.

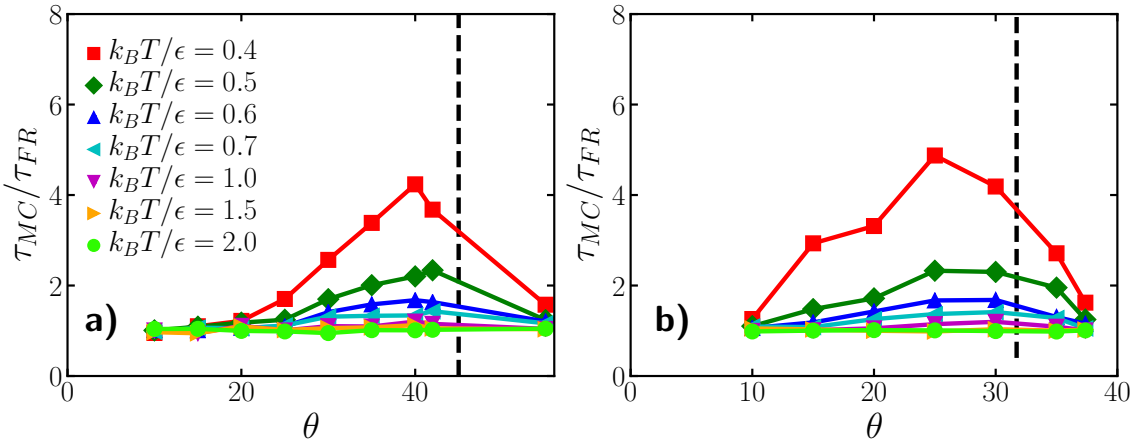


Figure 4.8: Rotational relaxation time $\tau_{DMC}$ obtained from local cage dynamical Monte Carlo simulations. All relaxation times are normalized by the value $\tau_{FR}$ for a free rotator in a simulation with the same step size. Data are shown for both a) 6 patches and b) 12 patches.

As the model captures the geometry of the cage and this result can also be seen as an indicator that the local structure is playing an important role in changing the rotational motion in particular the $n = 12$ case. Additionally, it seems that the local structure is sensitive to the size of the patch as the maximum on the relaxation time of the 12-patch case shifts to smaller angles. In the next section we will examine in detail the prevalence of icosahedral clusters in the 12-patch case as a function of the angle and temperature.

### 4.3.4 Structural Analysis

For the 12-patch system, both the EDMD and DMC simulations show a local maximum in relaxation time for relatively small patch sizes. To examine the origin of this feature, we focus our attention on the local structure of the 12-patch systems.

As in the previous Chapter, we use the *Topological Cluster Classification* algorithm [11] to explore the presence of local icosahedral order in our systems. These same local structures may contribute to the anomalous rotational dynamics. In Fig. 4.9 we show the fraction of particles which are part of an icosahedral environment, as a function of $\theta$. We see a strong maximum in the number of icosahedral structures around a patch angle of $\theta \simeq 15^\circ$ at low temperatures. In this regime, a larger fraction of the particles will be enclosed by an icosahedral cage, offering the possibility to bond to a large number of neighbors slowing down the rotational relaxation. This significantly slows down both rotational and translational relaxation, consistent with Figs. 4.2 and 4.5.

It is important to note that cage structure is not the only factor determining the rate of rotational relaxation, as the number of bonds formed by the particles also plays an important role. After all, for any given cage structure, particles bound by a larger number of attractive bonds are expected to rotate more slowly. In Fig. 4.5b) we show the energy per particle of the 12-patch case. As one might

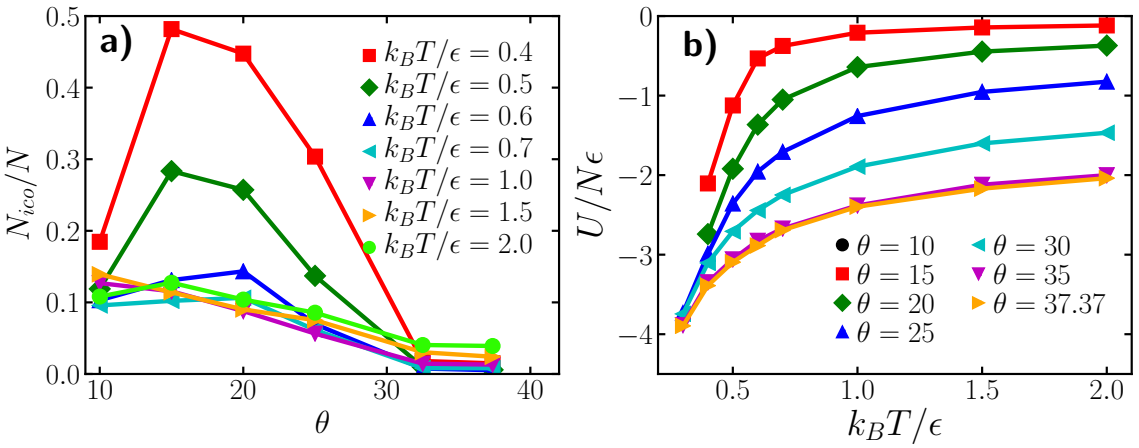


Figure 4.9: a) Fraction of particles that are part of icosahedral clusters in the 12-patch system, for different patch sizes $\theta$ and reduced temperatures $k_BT/\epsilon$. b) Energy per particle for 12-patch systems with different patch sizes $\theta$. Note that for a fully bonded particle $U/N\epsilon = -6$.

expect, larger patches lead to a larger number of bonds in the system. Hence, while around $\theta = 15°$ more particles can be found in a (potentially highly bonded) icosahedral environment, the average particle has more bonds when $\theta$ is higher. The rotational relaxation time thus stems from a combination of factors, including the fraction of icosahedral cages (which is maximized for relatively small angles), and the number of bonds (which is maximized for larger angles). Together, these factors contribute to the peak in $\tau_R$ shown in Fig. 4.5b).

## 4.4 Conclusions

In general, the overall relationship between translational and rotational dynamics in supercooled liquids is complex and highly dependent of the details of the interactions and the shape of the particles. Systems of patchy particles are no exception to this rule. Here, we have explored the interplay between local structure, rotational relaxation, and translational relaxation in dense fluids of spherical patchy particles. In particular, we focused on two specific patch locations, one that is capable of enhancing icosahedral ordering ($n=12$) and the second one that do not promote this ordering ($n=6$).

The tangled dynamics of the patchy particle systems are reflected in the relation between translational and rotational dynamics. The rotational relaxation is much faster than the translational relaxation, such that the two relaxations are effectively uncoupled and the Stokes-Einstein-Debye relation is broken. However, the decoupling is dependent of both the size of the patches and the temperature. One reason for this is the fact that the translational dynamics show a reentrance as a function of temperature that it is not present in the rotational dynamics. At high temperatures as the system forms few bonds the particles can rotate freely. Our results show that in contrast to the translational relaxation mechanism, which needs collective rearrangements to fully decorrelate, the particle orientations can

relax by simply adjusting their orientation within its local environment. This last mechanism is corroborated by the results of the local dynamical Monte Carlo simulations, which qualitatively reproduce the rotational behavior of the full system. Moreover, it shows the relevance of the local structure.

A second reason for the strong difference between relaxation times is that the rotational relaxation is as well dependent of the size of the patches and their locations. Which is in agreement with the role of the local structure on rotational dynamics as these two characteristics of the patches promote in different degrees preferred local structures. The slowest dynamics, both in terms of translations and rotations, are observed when the system forms a large number of icosahedral clusters. An important observation is the existence of an optimal patch size ($\theta \simeq 15°$) which enhances icosahedral order. Indeed, this optimal patch size is close to the case where we observe the slowest translational relaxation. Hence, tuning patch sizes provides an additional route to manipulating the dynamics of glassy fluids by tuning their local structure.

Our results show that rotational relaxation in patchy particle systems is essentially governed by local rearrangements. And its dynamics is a consequence of the interplay between the geometry of the local structure and the number of bonds the particle is involved in, which can or can not arrest the rotational motion. Moreover, patchy particles have proven to be an ideal tool to control dynamics, and not just the translational motion as shown in Chapter 3, the rotational dynamics can be as well controlled by changing the geometry of the local cage. The results shown in this Chapter show a clear way of templating the dynamics of the rotational degrees of freedom. This could be extended to other colloidal systems capable of changing the local structure such as colloidal particles with anisotropic shapes.

## 4.5 Acknowledgments

Some of the text and images from this chapter were reproduced from S. Marín-Aguilar, H. H. Wensink, G. Foffi, and F. Smallenburg, "Rotational and translational dynamics in dense fluids of patchy particles", *The Journal of Chemical Physics*, vol. 152, no. 8, pp. 084501, 2020., with the permission of AIP Publishing.

Chapter 5

# Patchy Particles as monodisperse glasses

In the previous Chapters we have used binary mixtures of patchy particles to explore the glassy behavior. In this Chapter, we will exploit the ability of this type of particles to change the local structure in order to use them as monodisperse glass formers.

## 5.1 Introduction

In general, a fluid that is subjected to extreme conditions of low temperatures or high density enters to the glassy regime if it avoids crystallization. In that regime, the system is structurally similar to a liquid, in that it lacks long-range order, but at the same time its dynamical behavior deviates from the liquid one. This is mainly due to the increasingly strong confinement of the particles by their neighbors which slows down their dynamics with only slight changes in the structure. In order to avoid crystallization and enter to the glassy regime several methods have been proposed. We can classify them into three families: kinetic, thermodynamic and topological mechanisms [149].

The kinetic mechanisms are methods aimed at slowing down the crystalization rate. As there is a competition between the arrest and crystallization while going into the glassy regime, slowing down the crystallization rate allows the system to get arrested before a crystal can form. This can be achieved in experiments by modifying the chemical potential or by modifying the surface tension. The thermodynamic route takes a different approach and it is mainly concerned of mixtures. For example, by adjusting the composition and size ratio of the components it is possible to get a mixture (eutectic mixture) where its melting temperature is smaller than the one for the pure components and other compositions [150, 151]. As consequence, the fluid is thermodynamically stable in denser regions and arrest happens without any crystallization. Finally, the topological

mechanism relies on reinforcing structures that are incompatible with crystal lattices and can not be replicated in 3-dimensions and lead to geometrical frustration. Note that, different approaches to avoid crystallization end up being part of the three families at the same time or a combinations of them.

An ideal glass former would follow the thermodynamic route where its melting point would be located below the region where the system gets arrested [152]. In other words, at low temperatures and high densities the fluid should still be thermodynamically stable compared with the crystal phase. In that ideal case, the system will presumably preserve its 'liquid-like' structure. One way of achieving this is by using particles where the valence is controlled as in network glasses made of patchy particles [91, 92].

Most simulation studies on supercooled liquids rely on the use of mixtures with different size ratios and compositions to avoid crystallization. This methodology belongs at the same time to the three categories. Although this method works well, it promotes a more complex behavior as the contributions to dynamics and structure from each of the components are entangled. For example, the diffusion rates of each of the components are different, and in general we can define observables per component, which at the end might have different behaviors. A direct solution to this problem is the use of monodisperse systems. However, most of the monodisperse fluids tend to rapidly crystallize in the glassy regime and to avoid this, additional tricks that suppress crystallization must be implemented.

Based on the topological mechanism, it has been found that carefully designed anisotropic interactions in monodisperse systems can favour local structures incompatible with long range order in three dimensions suppressing crystallization in the fluid [107, 153, 154]. This can be achieved by adding many-body interactions to the potential [153–155] or with oscillatory interactions [106, 156–160]. In particular, the promoted local structures are typically icosahedral [156, 157, 161] and tetrahedral ones [153, 155, 159]. Both of these cannot be used to fill an infinite three dimensional space, and hence tend to counteract crystallization.

Here, we propose the use of patchy particles as a route towards the design of a monodisperse glass former. This idea is based on the observation that binary systems of patchy particles have proven to be a great tool for exploring and controlling the interplay between structure and dynamics of supercooled liquids [15,110] (see Chapters 3 and 4). The directionality embedded in their potential is capable of modifying the local cage and this could be used to prevent crystallization. Specifically, in the case where the patches are located in an icosahedral geometry, they dramatically increase the number of icosahedral local structures in the system, and slow down the dynamics. However, it is also interesting to explore a geometry that is not related to icosahedral order but could preserve the 'liquid-like' structure. Therefore, we propose two different geometries to be used as monodisperse systems: the well-known 12-patch case that enhances icosahedral clusters in the system and the 8-patch case, a geometry that is not directly related to any specific crystal structures and neither to the tetrahedral or icosahedral structures.

For both of these, we explore in detail the structural and dynamical characteristics. Intriguingly, both systems are capable of avoiding crystallization at low temperatures. However, the disruption of the 12-patch case changes the overall structure causing it to strongly deviate from the structure of a simple liquid. While the 8-patch case requires lower temperatures to avoid crystallization, the changes on the local structure are much more subtle, and preserves an overall liquid-like structure factor.

## 5.2 Model and Methodology

### 5.2.1 Simulation

As in previous Chapters, we use Event Driven Molecular Dynamics [91, 94, 95] to simulate monodisperse patchy-particle systems. The patchy interactions are implemented following the Kern-Frenkel [10] model. In this Chapter we explore two different monodisperse patchy systems: the first composed of particles with $n = 8$ patches and the second of particles with $n = 12$. The patches are located on the vertex of a square antiprism and an icosahedron respectively. These geometries are shown in Fig. 5.1.

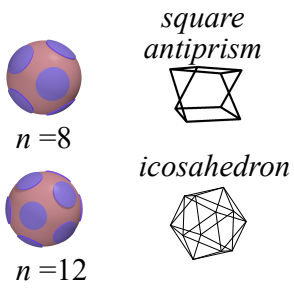


Figure 5.1: Patchy particles with $n = 8$ and $n = 12$ patches. For each geometry, we show both the particle, and the polyhedron associated with the placement of the patches.

In the previous Chapters, we found that the best way of comparing different patch geometries is by fixing the fraction of the particle surface area covered by the patches $\chi$ (See Chapter 3). Based on that, we fix $\chi = 40\%$ for both systems. We use a short-ranged interaction $r_c = 1.031\sigma$, where $r_c$ is the range of the potential and $\sigma$ the diameter of the particles. Our systems consist of $N = 700$ particles and we explore the systems in the high-packing-fraction regime $\eta \geq 0.56$. Additionally we explore a wide range of temperatures to locate the temperature range where the system is in a fluid phase. We equilibrate each system at fixed temperature for at least $10^4\tau$, where $\tau$ is our time unit $\tau = \sqrt{m\sigma^2/k_BT}$, where $T$ is the temperature, $m$ is the mass of a particle and $k_B$ is Boltzmann's constant. Finally, we simulate the systems with fixed energy for at least $10^5\tau$.

## 5.2.2 Analysis

### 5.2.2.1 Structural Analysis

As we are interested in the ability of the systems to avoid crystallization by promoting structures that are incommensurate with crystallization, we explore in detail the local and global structure of both geometries.

In scattering experiments, the way the light scatters from the interaction with the particles in a system give us information of its global structure. In simulations, the same information can be extracted from the calculation of the structure factor $S(k)$, which can be computed as follows:

$$S(k) = \langle \rho(-\mathbf{k})\rho(\mathbf{k}) \rangle = \frac{1}{N} \sum_{j=1}^{N} \sum_{l=1}^{N} \exp\left[i\mathbf{k}.\mathbf{r}_{jl}\right], \tag{5.1}$$

where $\rho(k)$ corresponds to the Fourier transform of the density, $k$ is a wave vector and $r_{jl}$ the joining vector between particle $j$ and $l$. The $S(\mathbf{k})$ in a plane shows a clear fingerprint of the structure: for an homogeneous liquid we find an arrangement of rings corresponding to the homogeneous scattering of the particles, while a crystallized system shows well-defined peaks reflecting the anisotropy of the structure. We characterize the values of the average $S(\mathbf{k})$ in the $xy$-plane to better distinguish among the phases.

In addition, we characterize the phase behavior of our systems using bond orientational parameters [122,162] (see Sec. 3.2.3.2). In particular we focus on the calculation of the six-fold order parameter $Q_6$. This because the systems under consideration are most likely to crystallize into close-packed lattices such as a faced-center-cubic lattice (FCC) or an hexagonal-closed-packing (HCP) lattice. $Q_6$ is a good tool to distinguish between phases as a function of temperature, since the typical crystal lattices have a non zero $Q_6$ value (FCC lattice, $Q_6 = 0.57452$ and for a perfect HCP lattice $Q_6 = 0.48476$), while the fluid phase yields $Q_6$ values close to $0$. Moreover, crystallization is accompanied by a discontinuous jump in $Q_6$ across the transition.

Finally, we characterize the specific local environment of the systems using the *Topological Cluster Classification* algorithm [11](see Section 2.3).

### 5.2.2.2 Dynamical Behavior

In addition to the phase behavior and fluid structure, we are interested on the dynamical aspects of the systems in the fluid phase. Ideally, as glass formers at low temperatures their dynamical behavior will reflect the typical characteristics of a glassy material (see Section 1.1.1). To explore this point we perform an exhaustive exploration of dynamics. We start by calculating the mean square displacement $MSD = \left\langle \frac{1}{N} \sum_{i=1}^{N} \left[\mathbf{r_i}(t) - \mathbf{r_i}(0)\right]^2 \right\rangle$. In addition, we calculate the time-dependent

intermediate scattering function (ISF) to quantify the relaxation behavior, and fit it with a double stretch-exponential:

$$f(t) = \alpha \exp\left[-(t/\tau_a)^{\gamma_a}\right] + (1-\alpha)\exp\left[-(t/\tau_b)^{\gamma_b}\right], \tag{5.2}$$

where $\alpha$, $\gamma_{a(b)}$ and $\tau_{a(b)}$ are fitting constants. From this fit we then extract the relaxation time $\tau_{0.3}$ as the time where the correlation has decayed to $0.3$ and the non-ergodicity parameter $f_q = 1-\alpha$ corresponding to the height of the plateau.

Finally, since the systems have orientational degrees of freedom we characterize the rotational dynamics using the same methodology as in the previous Chapter. Specifically, we calculate the decay of the rotational correlation $C_2$:

$$C_2(t) = \frac{1}{N}\sum_{j}^{N} P_2\left(\hat{\mathbf{u}}(t)\cdot\hat{\mathbf{u}}(0)\right), \tag{5.3}$$

where $\hat{\mathbf{u}}$ is a unitary vector pointing to a specific patch and $P_2$ the second Legendre polynomial. From this correlation function, we extract the rotational relaxation time $\tau_r$ as the time where the correlation has decayed to $0.3$.

## 5.3 Results

### 5.3.1 Square Well

We start our study by introducing a simple reference system with liquid-like structure. The best candidates for this are the square-well systems due to the fact that they are simple fluids with interactions that are highly similar to the patchy-particle systems we consider here. Square-well systems are composed of spherical particles with homogeneous interactions and strong correlations [163], i.e. its interactions are short-ranged and the physics of the system is well captured from the first coordination shell, this is reflected in the good predictions made by the MCT approach which have as input the structure factor (see Section 1.2). We explore the behavior of a monodisperse square-well (SW) system with the same interaction range as the patchy-particle systems and fixed packing fraction $\eta = 0.56$. This will allow us to compare our patchy-particle models directly to a comparable monodisperse system with isotropic interactions.

First, we characterize the phase behavior as a function of temperature. We start our simulations from a compressed fluid state, for a range of different temperatures, we let them equilibrate and then we characterize the structure by calculating the $Q_6$ order parameter. The global structural features show a reentrant phase behavior with temperature. This reentrance is captured by the $Q_6$ order parameter. In Fig 5.2 we show the values of the bond order parameter $Q_6$ as a function of temperature for the square-well system. Values close to $Q_6 = 0$ are characteristic of a fluid phase where there is no long-ranged order. In contrast,

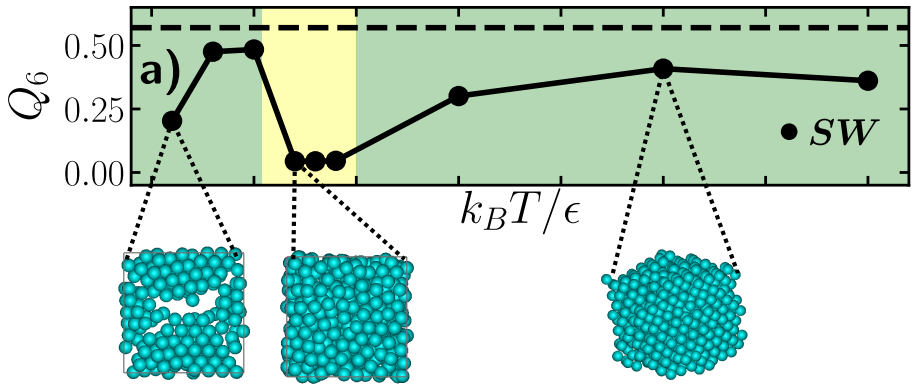


Figure 5.2: $Q_6$ calculation as a function of temperature for the SW. Yellow regions correspond to a fluid phase and green regions to a crystallized phase, dashed line is the $Q_6$ value of a perfect FCC lattice. Below each region we illustrate the phase with a corresponding snapshot. Note that, at the lowest temperature we see signs of phase separation.

values near $Q_6 = 0.57$ indicate a crystal phase. At low temperatures the square-well system crystallizes into an FCC structure. Additionally, at the smallest temperature analyzed, we see a drop in $Q_6$. By exploring visually the system we find signs of a phase separation as shown in the bottom image of Fig. 5.2, in which part of the system forms empty voids corresponding to a gas phase [123]. At intermediate temperatures, between $k_BT/\epsilon = 0.6$ and $0.7$ the system remains in a disordered liquid state. Finally, at temperatures $k_BT/\epsilon > 0.7$ the system crystallizes once more into an FCC crystal.

This reentrant crystallization behavior for spherical particles with short-ranged attractions has previously been observed in both experiments and simulations [164, 165]. Moreover, it is reminiscent of the reentrant glass behavior shown by short-ranged binary systems with similar interactions (see Section 1.4.2).

The different phases in the SW systems are also well captured by the structure factor. We show in Fig. 5.3 a) the $S(k)$ of the SW system at a low temperature where we find crystallization and one corresponding to a liquid at intermediate temperature. The structure factor of the SW liquid is smooth, confirming its homogeneous nature, and it will be our structural reference point.

In contrast, the crystal phase presents localized peaks at certain wavelengths corresponding to the translational order in the crystal. Note that the high degree of noise in the $S(k)$ is related to the defects and dislocations (spontaneously formed) in the crystal. In Fig. 5.3 b) and c) we show the corresponding non-averaged structure factor in the $xy$-plane for the crystal and the liquid respectively. Indeed, the anisotropic ordering of the crystal phase is clearly visible in Fig. 5.3 b). Note that, due to spontaneous crystallization, there can be multiple domains and the $xy$-plane is not necessarily associated with a symmetry plane of the crystal.

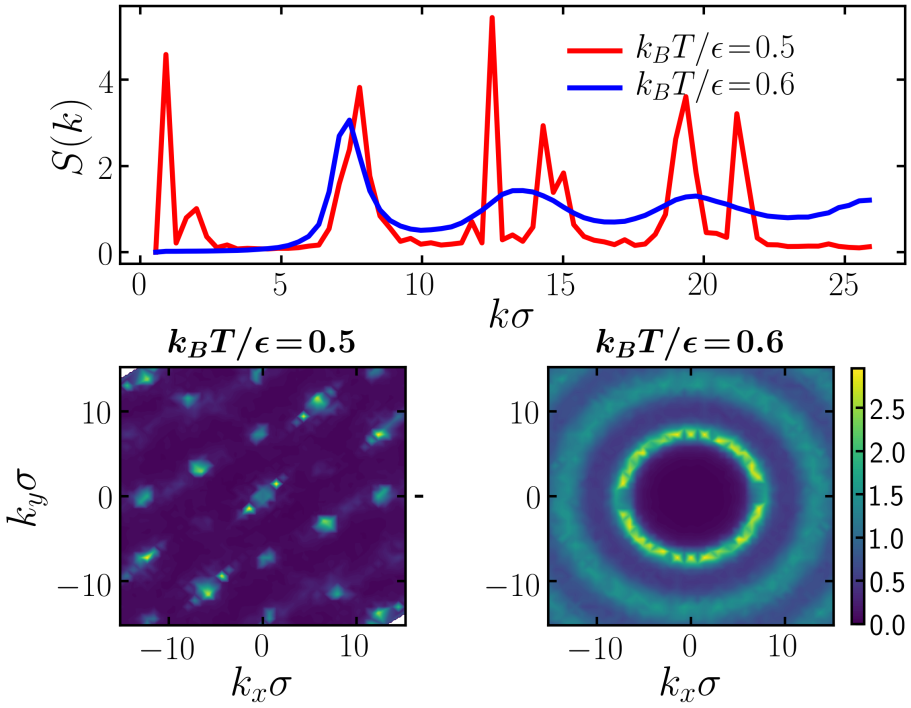


Figure 5.3: a) Structure factor of the square well system with potential range of $r_c=1.03\sigma$ of a crystallized system at $k_BT/\epsilon=0.5$ and a liquid system at $k_BT/\epsilon=0.6$. b) Structure factor of the same crystallized system in the $xy$-plane. c) Structure factor for the corresponding liquid state.

### 5.3.2 Patchy particle systems

We now turn our attention to our patchy models. First, we analyze the phase behavior of the monodisperse system with $n=12$ patches. In Fig. 5.4 a) we show $Q_6$ as a function of temperature. As expected, at high temperatures the system crystallizes into an FCC crystal, $Q_6$ takes values close to the FCC limit. In this regime the attractions from the patches have little effect and the particles behave approximately as hard spheres. A different picture is found upon cooling below $k_BT/\epsilon \leq 0.6$, where $Q_6$ is approximately $0$ indicating the system is in a fluid phase. The directionality imposed by the patches plays an important role at low temperatures where the local structure is modified, this is enough to avoid crystallization. As a consequence the system remains in a fluid phase for all remaining temperatures ($k_BT/\epsilon \leq 0.6$).

The changes in the local structure are enough to avoid crystallization. However, they also have a profound effect on the global structure, as indicated by the $S(k)$. In Fig. 5.5 we show the $S(k)$ for each of the temperatures where the system is in the fluid phase. It is important to remark that the 12-patch exhibits a split in the second peak, which is most obvious at the lowest temperatures. This is a a sharp difference from the isotropic case (Fig. 5.3).The splitting of the second peak has been related to the appearance of icosahedral and tetrahedral ordering [72] in binary and monodisperse systems [159].

As our second patchy model, we investigate the case of $n=8$ patches. Anal-

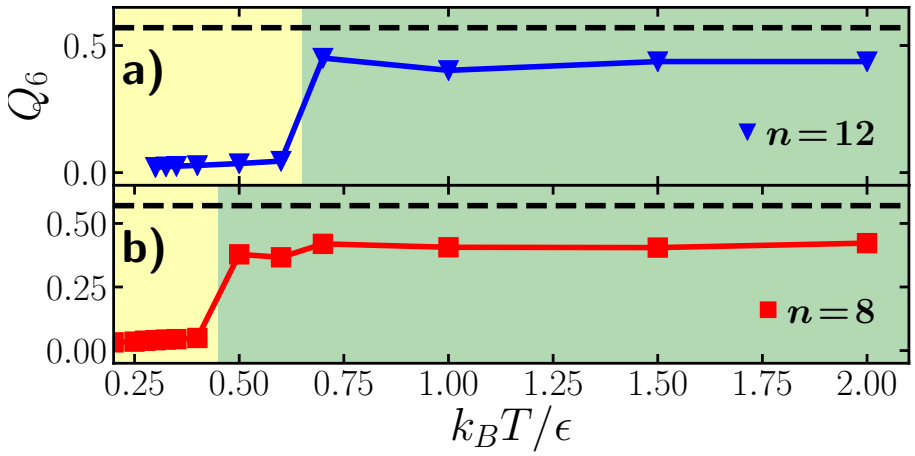


Figure 5.4: $Q_6$ calculation as a function of temperature for the two patchy cases investigated at fixed packing fraction, a) $n=12$ patches and b) $n=8$ patches.

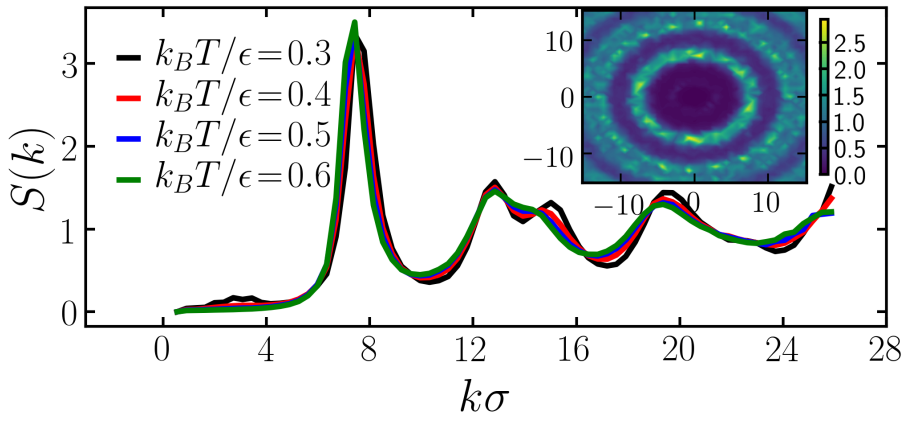


Figure 5.5: Structure factor of the 12-patch system at temperatures where the system has not crystallized. The inset shows the structure in the $xy$-plane at temperature $k_BT/\epsilon = 0.3$.

ogous to the previous case, the 8-patch particles also avoid crystallization in the low-temperature regime, although this is reached only at temperatures below $k_BT/\epsilon \leq 0.4$ as shown in Fig. 5.4 b). However, the structure of the system evolves very differently from the 12-patch case. We show in Fig. 5.6 a) the structure factor at the temperatures where the system is in a fluid phase. The $n=8$ case presents 'typical' liquid-like structure factor related to a liquid. In particular, the first peak is not as sharp as in the 12-patch case and more importantly there is no splitting of the second peak. We compare the structure of our reference system with the $n=8$ case. The latter essentially maps on top of our reference system, this is shown in Fig. 5.6 b). This is a remarkable difference with the proposed monodisperse glassy systems found in the literature [153, 155–157, 159, 161], that are focused on facilitating icosahedral ordering. The 8-patch case is capable of avoiding crystallization without changing the global homogeneous structure of a liquid.

We now explore in detail the changes in the local structure, focusing in the formation of icosahedral clusters for all our systems. To do so, we use the *Topological Cluster Classification* algorithm [11] to characterize the local structure. In Fig. 5.7

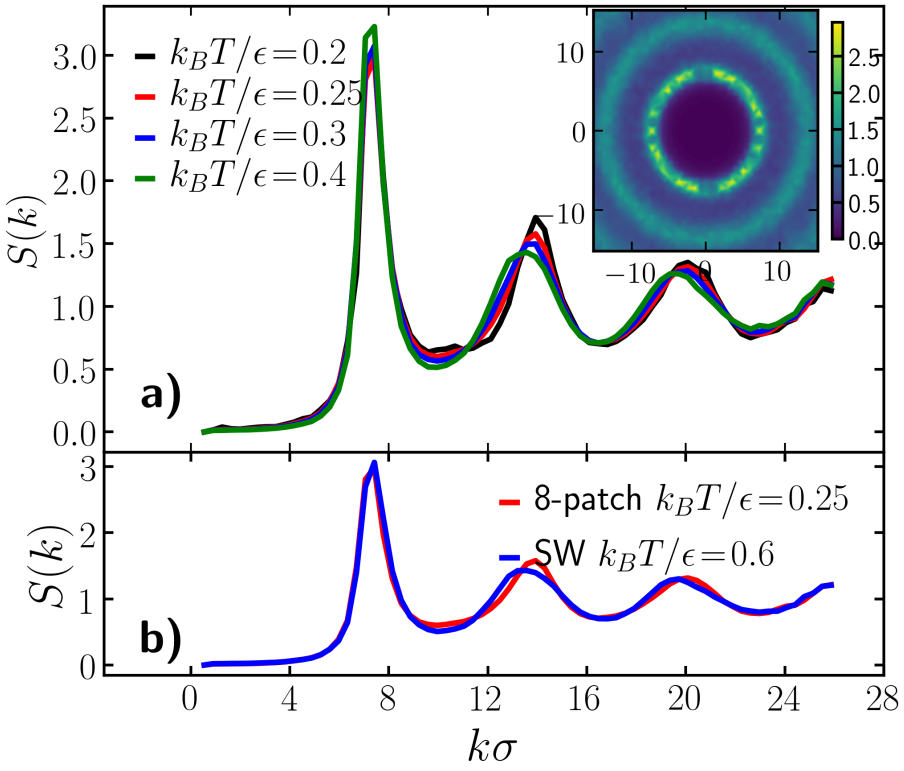


Figure 5.6: a) Structure factor of non crystalline 8-patch systems. The inset shows the structure factor in the $xy$-plane corresponding to $k_BT/\epsilon = 0.3$. b) Comparison between $S(q)$ of the 8-patch liquid and a SW liquid.

we show the fraction of particles involved in icosahedral clusters as a function of temperature for the three studied cases. The missing points correspond to the temperatures where the system crystallizes. As expected, the $n = 12$ shows an increase of the number of icosahedral clusters at low temperatures. However, for the 8-patch case and the SW the number of icosahedral clusters is on average very close to 0.

Both the 8-patch and 12-patch geometries are able to avoid crystallization at sufficiently low temperatures. Nevertheless, the two patch geometries have dramatically different effects on the local structure. While the 12-patch interactions boost the number of icosahedral clusters in the system, leading to profound changes in the global structure factor, the effect of the $n = 8$ patches in the local structure are subtle, and the overall liquid structure remains unchanged. However, these subtle changes are enough to avoid crystallization at low temperatures.

As this is a new route to avoid crystallization without enhancing icosahedral ordering, the 8-patch case is an interesting and elegant candidate for a monodisperse simple glass former. In the following section we show a detailed characterization of the 8-patch dynamical features at different packing fractions.

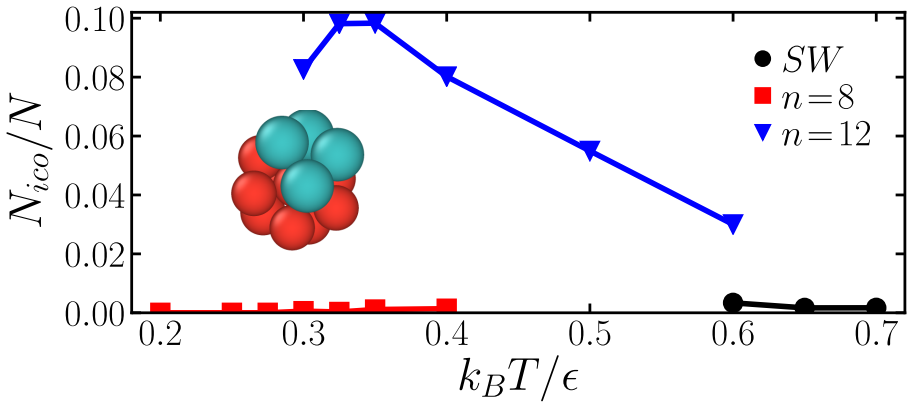


Figure 5.7: Fraction of particles in an icosahedral cluster as a function of temperature for the temperatures where the system is a fluid.

### 5.3.3 Dynamical behavior of the monodisperse 8-patch system

We start this section by exploring the temperature dependence of the energy and pressure for three different packing fractions $\eta = 0.56$, $0.57$ and $0.58$. The results are shown in Fig. 5.8 a) and b) respectively. Note that at higher packing fractions, the system crystallizes for temperatures above $k_BT/\epsilon = 0.3$. In the fluid phase, the potential energy $U$ of the system is not strongly dependent on the packing fraction, and it increases monotonically with temperature. Note that the potential energy is related to the average number of bonds as: $N_b = -U$ and the maximum $N_b$ correspond to the number of patches, i.e. 8. The trend of the potential energy points out that at the smallest temperature the particles are almost fully bonded.

In Fig. 5.8 b), we plot the pressure $P$ for the same systems. At the lower packing fractions, the pressure comes close to vanishing, indicating that we approach a gas-liquid binodal, which marks the temperature below which the system will attempt to phase separate into coexisting gas and liquid phases. However, for packing fraction $\eta = 0.58$, the pressure levels off at low temperatures, suggesting that we avoid the binodal at that packing fraction. Note that such a transition has also been noted for glassy binary mixtures of square-well particles [123]. Additionally, we see the same behavior in our monodisperse SW systems.

Now, we turn our attention to the dynamical behavior of the $8$-patch system. To this end, we compute the MSD. At the lowest packing fraction $\eta = 0.56$, the system displays glassy features, this is shown in Fig. 5.9a) where we show the MSD for the system at $\eta = 0.56$. At short times, the particles undergo ballistic motion. Later, at intermediate times, the particles are caged by their neighbors resulting in an approximate plateau in the MSD. Although the plateau is not as clear as in other glass formers, the particles are still caged by their neighbors. We will show this in more detail with the ISF. Finally, at larger time scales, the dynamics crossover into the diffusive regime. At higher packing fractions the dynamical behavior is qualitatively the same, though dynamics are slower as the systems are deeper in the glassy regime and the plateau is better appreciated.

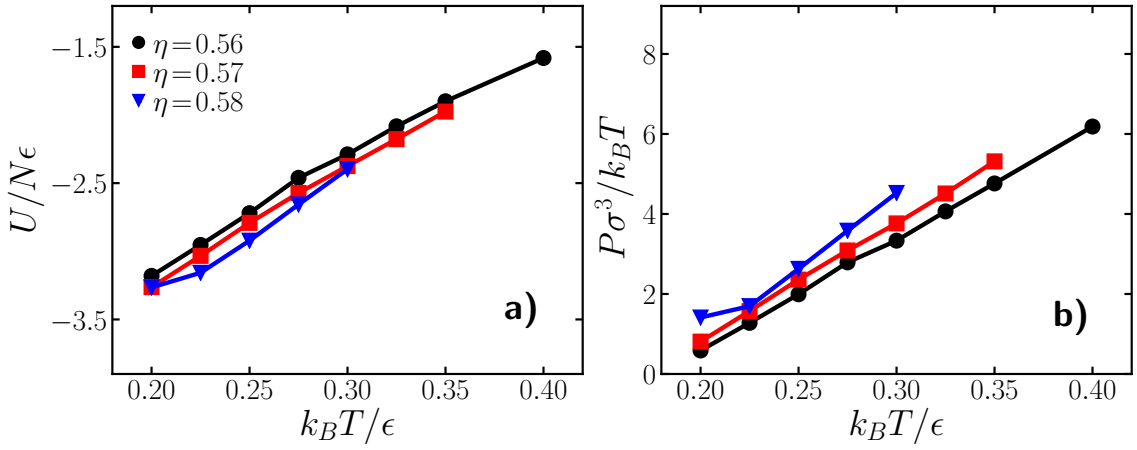


Figure 5.8: a) Average energy per particle as a function of temperature of the 8-patch system. b) Dimensionless pressure of the same systems.

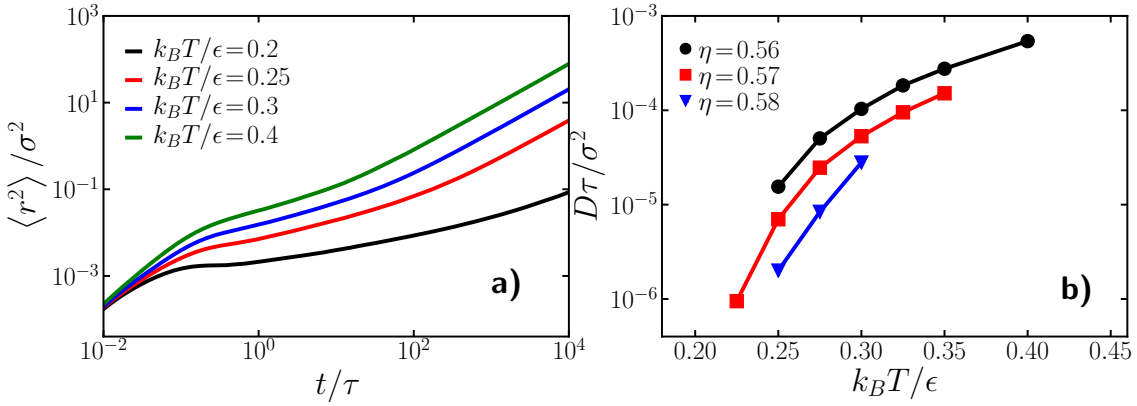


Figure 5.9: a) Mean squared displacement of the $n = 8$ patch at temperatures where the system is a fluid and a fixed packing fraction $\eta = 0.56$. b) Diffusion coefficient of all temperatures and packing fractions investigated.

To provide an overview of the dynamics of all the 8-patch systems, we measure the diffusion coefficient for all the different temperatures and packing fractions where the system is in the fluid phase. In Fig. 5.9 b) we show the dimensionless diffusion coefficient $D\tau/\sigma^2$. At the lowest temperatures all systems have extremely slow dynamics as reflected in the small values of the diffusion coefficient. When going to slightly higher temperatures the system regains fluidity and the diffusion increases. This is the expected behavior of a glass-former that at low temperatures its dynamics slows down in this case in the limit of high temperatures crystallization takes place as it is the favored phase in the hard-sphere limit.

In order to have a clearer picture of the structural relaxation of this systems we explore the ISF. In Fig. 5.10 we show the ISF corresponding to the wavelength of the first peak of the $S(k)$ for $\eta=0.56$. When going to lower temperatures the system needs more time to fully decorrelate. Note that at even lower temperatures we can no longer equilibrate our simulations. The decay of the ISF also shows a small plateau, which is more clearly visible at lower temperatures as shown in

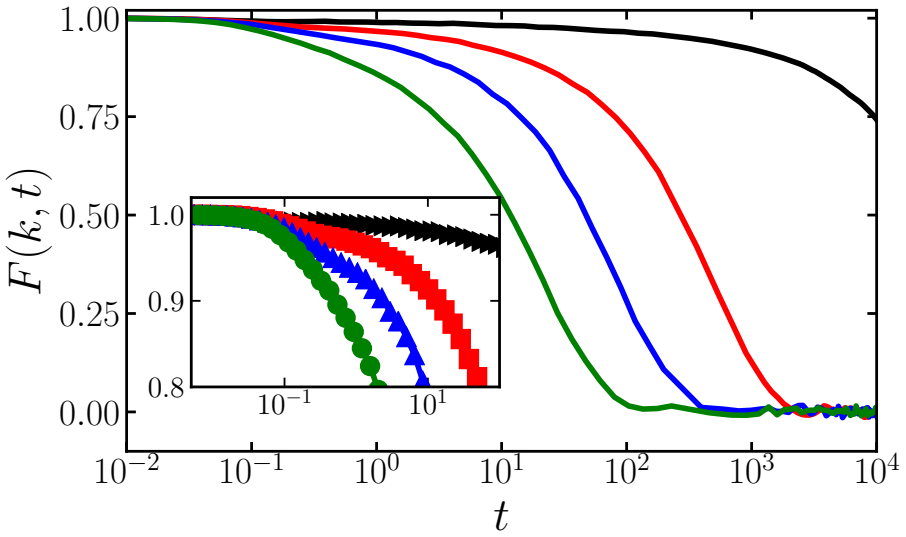


Figure 5.10: Intermediate scattering function of the 8-patch case at $\eta = 0.56$, inset corresponding to a zoom to the region where the first decay in the ISF happens.

the inset of Fig. 5.10. The height of the plateau is extremely close to 1, indicating that the particles are tightly caged by the attractions with their neighbors at short times.

To have a clearer picture of the relaxation behavior and the role of the caging, we calculate the relaxation time $\tau_{0.3}$ as a function of the wavelength $k$. The results are shown in Fig. 5.11 a), where we plot $\tau_{0.3}(k)$ for the three different packing fractions and two different temperatures. For all investigated state points, the relaxation time shows a peak at the wavelength $k$ corresponding to the first peak of the $S(k)$. This indicates that the slowest density fluctuations that appear in our systems are on the length scale of the local cages, while fluctuations at all other length scales relax more quickly

Another feature we can extract from the intermediate structure factor is the non-ergodicity parameter $f_k$. The $f_k$ is dependent of the wavelength and it provides further information about the cage effect. In an true ideal glass, the system never decorrelates, the particles are completely arrested by their neighbors and they cannot escape their cages. In this case, the system is in a non-ergodic state as it cannot explore the phase space anymore. All of this is reflected in the ISF, which presents a plateau that do not decay over the time scale of the measurement. The non-ergodicity parameter $f_k$ measures the value of the ISF where the correlation stops decorrelating and present a plateau. Furthermore, the height of this plateau is a measure for the freedom of the system to exhibit fluctuations at a chosen wavelength, and hence the rigidity of the system. In a glass the $f_k$ will have values greater than $0$ while in a complete fluid phase, the ISF do not have a plateau and $f_k = 0$.

In the supercooled-liquid regime where the system is able to decorrelate from the initial configuration we take the $f_k$ as the value of the correlation where the plateau is found. Moreover, the non-ergodicity parameter can be used to dis-

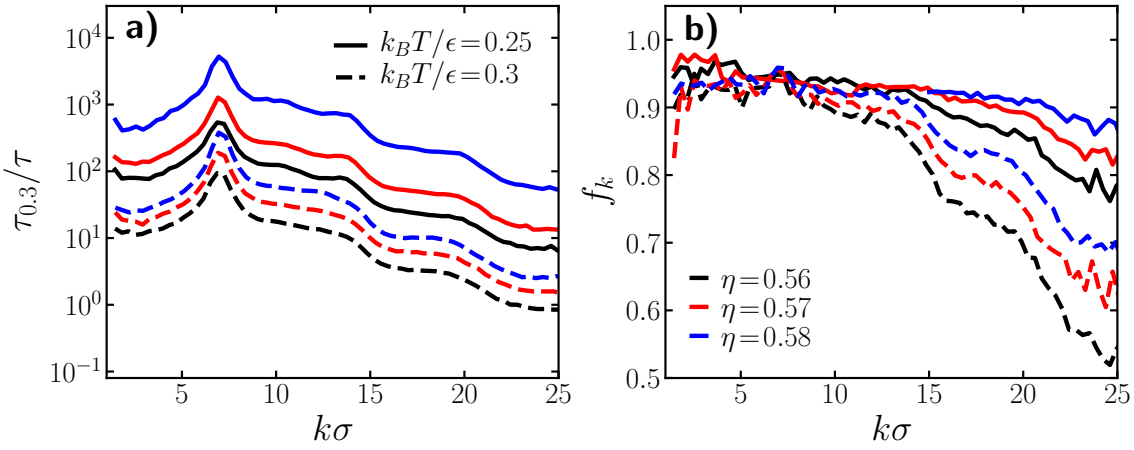


Figure 5.11: a) Relaxation time as a function of $k$-vector. Continuous lines correspond to $k_BT/\epsilon = 0.25$ and dashed lines to $k_BT/\epsilon = 0.3$, different colors correspond to different packing fractions $\eta$. b) Corresponding non-ergodicity parameter.

tinguish between different types of arrest: the behavior of $f_k$ as a function of $k$ depends on the 'type' of glass (repulsive or attractive). Typically, in an attractive glass $f_k$ is close to 1 and decays slowly with $k$. Meanwhile, in a repulsive glass, the non-ergodicity parameter decays quickly with $k$ and reaches lower values than in the attractive case [166].

Here, we calculate the non ergodicity parameter $f_k$ by fitting the ISF with a double stretched exponential function as in Eq. 5.2. In Fig. 5.11 b) we show the behavior of $f_k$ at the two lowest temperatures for each packing fraction. Remarkably, as we see in the decay of the ISF, the plateau is close to 1, this behavior extends to different $k$ values, indicating that the structure of the system is highly rigid until bonds start breaking. As one might expect, this is particularly true at the lowest temperature, where the particles are highly bonded. This behavior is typical for an attractive glass, where the dynamical arrest of the system is driven by strong short-ranged attractions [166, 167].

Another feature that is interesting to explore in our monodisperse glass-former is the relation between dynamics and relaxation behaviors through the Stokes-Einstein relation (SER) and the Stokes-Einstein-Debye relation (SED). These relations break down in most fluids in the glassy regime as a consequence of the emergence of complex dynamics and dynamical and structural heterogeneity (see Section 1.1.1). Here, we explore the two relations for the monodisperse patchy particle systems.

We start with the SER relation which states that the structural relaxation time is inversely proportional to the diffusion time in a diluted regime [126]. To explore this relation we calculate the relaxation time $\tau_{0.3}$. In Fig. 5.12 we show the structural relaxation time as a function of the diffusion coefficient. Surprisingly, the SER relation is remarkably well preserved in all systems we consider here, showing an almost perfect linear relation between $\tau_{0.3}$ and $D$.

To check for a possible breakdown of the SED relation, we first calculate the

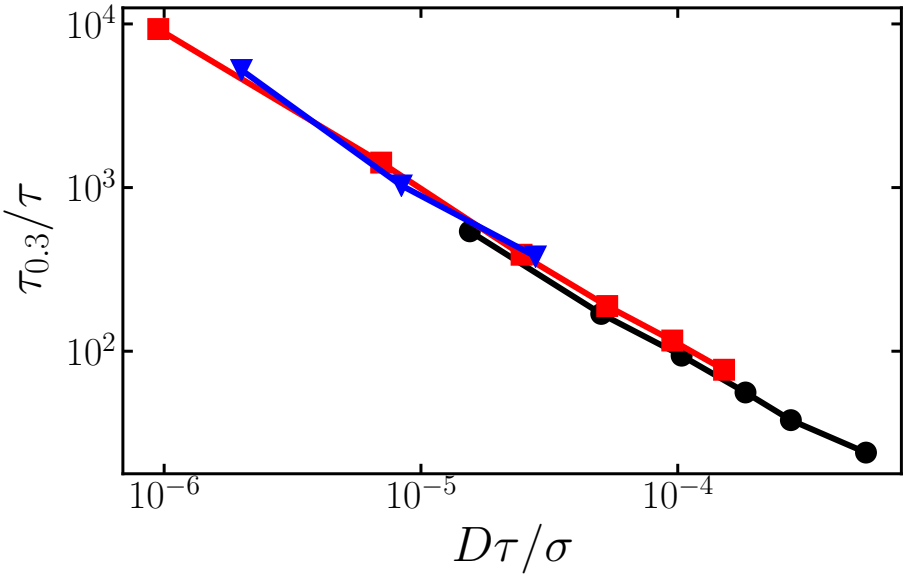


Figure 5.12: Relaxation time $\tau_{0.3}$ as a function of the diffusion coefficient $D\tau/\sigma$.

rotational correlation function $C_2$. In Fig. 5.13 a) we show the behavior of the rotational correlation. As in the binary mixture case (See Chapter 4) at the lowest temperatures the correlation shows a plateau at short times. This corresponds to the regime where the particle can no longer decorrelate from its initial orientation due to the strong interactions with their closest neighbors. This is expected to occur when the particles need to break several bonds before they can rotate away from their initial orientation. This behavior is stronger in the monodisperse case where we can see that the correlation decays at longer times compared to the binary mixture.

From the decay of $C_2$ we measure the rotational relaxation time $\tau_r$. The SED relation states that the rotational relaxation time is proportional to the structural relaxation time. In Fig. 5.13 b) we show the relation between these two relaxation times. We find that the SED relation is still approximately valid in the patchy monodisperse glass former. However, the rotational relaxation time $\tau_R$ appears to grow slightly faster than $\tau_{0.3}$, the two time scales remain on the same order through all packing fractions. The strong slowdown in the rotational dynamics at low temperatures allows the relation to hold through even at low temperatures. This is in contrast to the binary mixture case (Chapter 4), where the crossover of glasses entangles the relation between the two types of motion and hence causes a breakdown of the SED.

## 5.4 Conclusions

We have shown that systems of patchy particles can be used as monodisperse glass formers. In particular we explored two different cases: $n = 12$ patches and $n = 8$. While both of this geometries are capable of avoiding crystallization, the

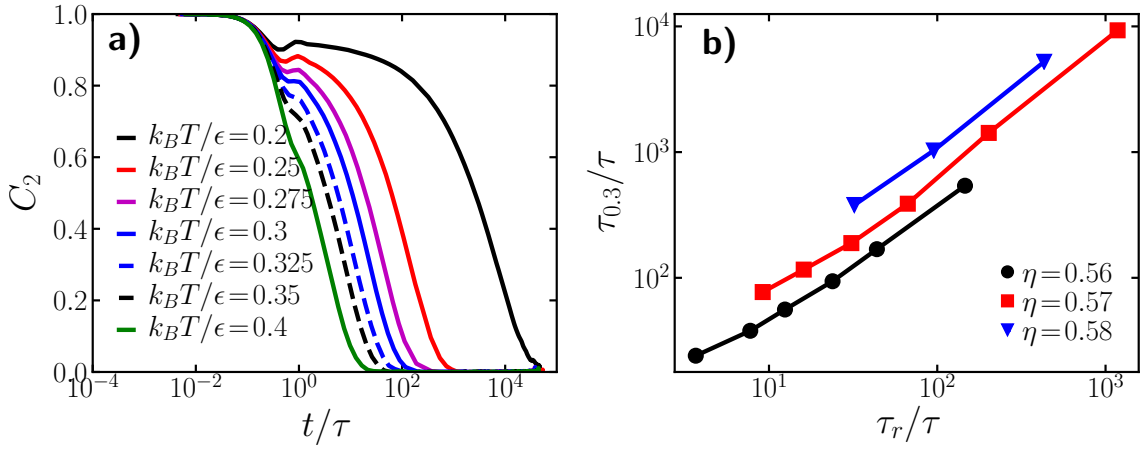


Figure 5.13: a) Rotational correlation function $C_2$ of the $n=8$ patch at $\eta=0.56$. b) Structural relaxation times $\tau_{0.3}$ as a function of the rotational relaxation time $\tau_R$ for all the 8-patch systems in fluid phase.

$n=12$ promotes strong structural changes. In particular, it promotes icosahedral clusters which change the overall structure leading to a strong deviation from the structure of a 'simple liquid'. In contrast, the 8-patch system shows both the ability to avoid crystallization at low temperatures and preserves the overall liquid structure.

The 8-patch case at high packing fractions display several of the key features of a glass former. These are captured by the intermediate scattering function where a plateau is developed at high packing fractions and low temperatures. In particular, the 8-patch case behaves as a typical attractive glass: the non-ergodicity parameter has large values close to 1, and the rotational correlation shows a clear plateau at short times meaning that the particles get trapped both translationally and orientationally in the cage made by their neighbors.

Despite its clear glassy features, it is interesting to note that both the Stokes-Einstein relation and the Stokes-Einstein-Debye relation hold in the glassy regime of our monodisperse patchy systems. This suggest that mean-field theoretical approximations could be accurate to predict the behavior of this type of glass-former as they work better on systems where these relations are only mildly violated [160, 168].

Our results show that patchy particles can be used to avoid crystallization. Moreover, they can help to shed some light on glass formers where the SER and the SED relations are not strongly broken. Our results open the door to the design of monodisperse glasses, where the interplay between local structure and dynamics can be studied in detail without having to consider multiple species of particles.

Chapter 6

# Tetrahedrality dictates dynamics in hard-sphere mixtures.

This chapter is based on the publication:

S. Marín-Aguilar, H. H. Wensink, G. Foffi, and F. Smallenburg, "Tetrahedrality dictates dynamics in hard sphere mixtures", *Phys. Rev. Lett.*, vol. 124, no. 24, pp. 208005, 2020. [16].

## 6.1 Introduction

In the previous Chapters we have shown the effect of the local structure on dynamics of supercooled-liquid patchy particles. We showed that the versatility of patchy particles allows us to control and modify the local structure, which in turn changes the translational and rotational dynamics in binary and monodisperse systems. Additionally, we have seen that some structures, such as icosahedral cluster, emerge with the slowing down of dynamics. Since it is clear that the structure is highly correlated to dynamics in the glassy regime, the logical question to answer is whether it is possible to predict the dynamical behavior of a system in the glassy regime only by its structural information.

In order to answer this question, we would like to have a simple model that displays clear structural changes and that at the same time could be easily compared with experiments. In general, patchy particles have proven themselves to be a good model for exploring the interplay between structure and dynamics. However, despite the growing experimental control over the synthesis of patchy particles [90, 119, 120], dense non-crystalline patchy particle systems are still not easily realizable and experimental comparisons are still missing. With this in mind, we turn our attention to one of the simplest glass formers that can be compared with experiments: the hard spheres.

Hard spheres are arguably the most fundamental model system in colloidal science, for theory, simulation, and experiment alike. Their interaction is only (and infinitely) repulsive when the particles are at a distance equal to their diameter. Hence, the behavior of hard spheres does not depend on temperature and only on the packing fraction. These characteristics help to simplify some of the complex theoretical approaches used to describe physical phenomena. The use of hard spheres has led to a better understanding of a wide variety of complex physical behaviors such as entropy-driven phase transitions, crystal nucleation, and, of course, the glass transition [38,169–175].

However, monodisperse hard spheres crystallize into simple close-packed crystals at high packing fractions [81]. And hence, mixtures with different size ratios and compositions are needed to avoid crystallization. The dynamics of hard-sphere mixtures change significantly upon varying the size and number ratios of the different species [176–178]. Intuitively, mixing spheres of different sizes results in different geometrical constraints on the possible local packings of particles, and hence this will lead to different local structures.

In this Chapter, we examine the link between local structure and dynamics in simulations of hard-sphere mixtures. In particular, we simulate binary and polydisperse mixtures over a wide range of packing fractions and compositions (or polydispersities), and attempt to link variations in the local structure to the dynamical slowdown. We find that icosahedral clusters are not capable of predicting the changes in dynamics of systems that are not extremely deep in the glass regime. Moreover, other complex structures also appear while going to the glassy regime following the trends of icosahedral clusters, although none of these structures are capable of capturing all the changes on dynamics of hard-sphere mixtures by themselves. However all of them can be decomposed into tetrahedral clusters: the smallest possible three-dimensional local cluster. Previously, simple order parameters based on the notion of tetrahedra [9,179,180] have been proposed showing good correlations with dynamics. Here, we propose to quantify the structure via the tetrahedrality of the local structure (TLS), a simple idea which consists of counting the number of tetrahedral clusters around each particle. We show that the TLS captures a universal structure in hard spheres and performs extremely well as a predictor for both the global and the local dynamics of dense hard-sphere mixtures.

## 6.2 Model and Methodology

We use Event-Driven Molecular Dynamics [94] to simulate a wide variety of hard-sphere mixtures at constant number of particles $N$, volume $V$, and energy $E$. We explore binary mixtures with size ratios $q = \sigma_S/\sigma_L$, where $\sigma_L = 1$ corresponds to the diameter of the large particles and $\sigma_S$ to the small particles, ranging from $0.6$ to $0.85$ in steps of $0.05$. Additionally, we vary the composition of the system $x_L = N_L/N$, where $N_L$ is the number of large particles and $N$ the number of particles, from $x_L = 0.2$ to $0.65$ every $0.05$. The combination of both parameters

gives us at least $60$ different systems.

To get a wider picture of hard-sphere mixtures, we also explore polydisperse systems with different polydispersities. These systems are composed of $15$ different types of particles, characterized by different sizes, taken from binning a Gaussian distribution with mean value of $1$ and standard deviation chosen between $0.01$ and $0.2$. The values of the standard deviation correspond to a polydispersity between $1\%$ to $20\%$. Note that due to the relatively small polydispersities used here, the smallest particles in the system always have a diameter of at least $0.4\sigma$. For larger polydispersities, it may be necessary to use e.g. a lognormal or Schultz distribution to avoid negative particle sizes

For each of the mixtures, we explore a wide variety of packing fractions $\eta$ starting from $0.52$ upto $0.59$, ranging from a fast moving fluid to deep inside the glassy regime. Most of our simulations have $N=700$ particles except for the slowest binary mixtures where we perform larger simulations upto $N=10000$ particles and the polydisperse systems which have $N=2000$ particles. We simulate our systems for at least $10^5\tau$ where $\tau$ is our time unit given by $\tau=\sqrt{\beta m\sigma^2}$, with $\sigma$ the diameter of the large spheres (for binary mixtures), or the average sphere size (for polydisperse mixtures), and $\beta=1/k_BT$ with $k_B$ Boltzmann's constant and $T$ the temperature.

### 6.2.1 Analysis

#### Global Dynamics

As we are interested in the interplay between dynamics and structure in glassy hard spheres, we explore both properties. In particular, we characterize the dynamical behavior of our systems by calculating the dimensionless diffusion coefficient $D\tau/\sigma^2$ which is related to the mean square displacement through the Einstein relation:

$$D\tau/\sigma^2 = \lim_{t\to\infty}\frac{1}{6Nt}\left\langle\sum_{j=1}^{N}\left[r_j(t)-r_j(0)\right]^2\right\rangle, \tag{6.1}$$

where $r_j(t)$ is the position of particle $j$ at time $t$. We define the diffusion time $\tau_D$ as the time that a particle needs to diffuse approximately $1\sigma_L$. We can extract it from the inverse of the diffusion coefficient as:

$$\tau_D=\sigma_L^2/D\tau \tag{6.2}$$

In order to explore in more detail the relaxation behavior we also calculate the Intermediate Scattering Function (ISF). From there, we extract the $\alpha$-relaxation time by fitting a stretched exponential to its long time decay: $A\exp[-(t/\tau_\alpha)^\gamma]$, where $A$, $\tau_\alpha$ and $\gamma$ are fitting constants and $\tau_\alpha$ corresponds to the $\alpha$-relaxation time.

We characterize the local structure by using the 'Topological Cluster Classification' algorithm (TCC) [11]. As we will explain in the following sections, we are now interested in the tetrahedrality of the local structure. The calculation of this new parameter is based on the same modified Voronoi construction of the TCC (see Sec. 2.3). However, we will define it in detail in the results section.

**Dynamical heterogeneity**

Finally, we will explore in detail the emergence of dynamical heterogeneity in hard-sphere mixtures.

The heterogeneities are time dependent as the system evolves. At short times, the heterogeneity is weak as the particles are starting to diffuse, and the dynamics looks more homogeneous. Later, at a time interval $t^*$ the system presents the maximal heterogeneities, as some regions will be more arrested by their cages and the system will be divided into regions with faster dynamics than other. Finally, at long timescales the particles escape the cages and the heterogeneities are weak again.

In simulations, one elegant way of distinguishing between different dynamical regions is through the calculation of dynamical propensity [181,182]. The idea is to quantify the displacement of the particles on an interval $\Delta t$ that is not originated by thermal fluctuations. To do so, thermal fluctuations are averaged out, by generating $N$ runs starting from the same equilibrated configuration but with different random velocities according to the Maxwell-Boltzmann distribution. The dynamical propensity $D_i$ is the 'ensemble' average of the squared displacement of each particle. This is a quantity dependent of time, and the maximal differences between regions will be at time $t^*$. By choosing that time, each particle can be colored by their $D_i$ value. In the glassy regime, this will lead to a clear distinction between different dynamical regions.

## 6.3 Results

### 6.3.1 Local Structure and Dynamics of Binary Hard-Sphere mixtures

We begin our study by exploring the structure and dynamics of dense binary hard-sphere mixtures at fixed packing fraction $\eta = 0.575$. For each choice of $q$ and $x_L$, we characterize the dynamical behavior by calculating the diffusion time $\tau_D$. Note that, at extreme size ratios close to 1 or less than 0.5 the systems are prone to crystallize into an FCC crystal or into a coexistence between FCC of large spheres and a fluid consisting mostly of the small ones. As we are interested only in the glassy dynamics we avoid those crystallizing regions.

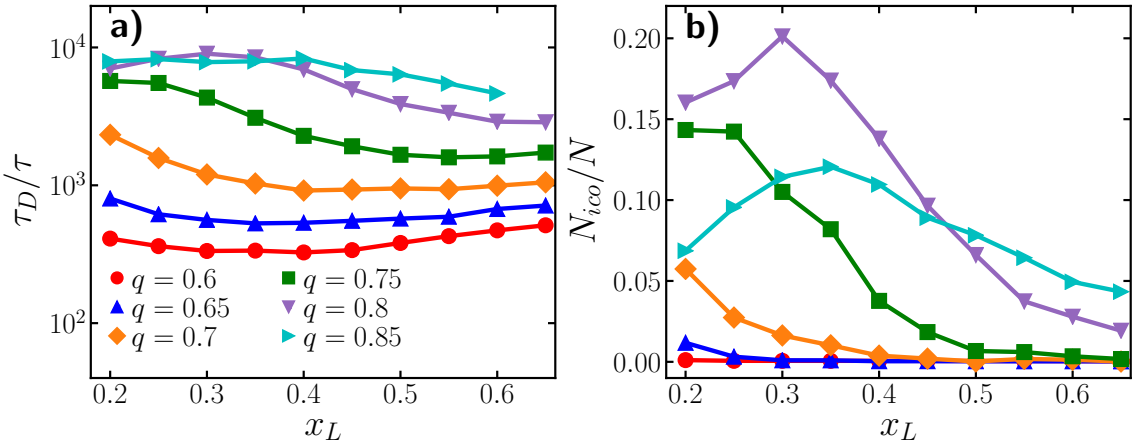


Figure 6.1: a) Diffusion time $\tau_D$ as a function of composition $x_L$ for binary hard-sphere mixtures with various size ratios $q$ as indicated. b) Fraction of particles inside an icosahedral cluster for the same systems. The inset shows a typical icosahedral cluster.

The dynamics of binary hard-sphere mixtures are known to vary significantly upon changing the composition $x_L$ and size ratio $q$ [176, 177]. We confirm those dynamical changes with the calculation of $\tau_D$. In Fig. 6.1 a) we plot the diffusion time $\tau_D$ as a function of the composition $x_L$ for each of the size ratios $q$. The dynamical behavior of the binary mixtures is highly dependent of the composition of the systems and in general it presents a complex, non-monotonic behavior between the diffusion time and composition. Moreover, each size ratio shows qualitatively different behaviors. For mixtures with a small size ratio $q \lesssim 0.75$, the diffusion time is a convex function of $x_L$, showing a clear single minimum. In contrast, for higher size ratios, a maximum in the diffusion times appears at smallest compositions $x_L$, those systems correspond to the ones with the slowest dynamics. Note that, even though the packing fraction is fixed for all the systems, the dynamics varies more than one order of magnitude depending on the size ratio.

In previous Chapters, we have shown that icosahedral clusters play an important role on controlling the dynamical slowdown of supercooled liquids. In particular, for the patchy-particle case in the high temperature limit we found that a considerable number of particles were involved in icosahedral clusters $\simeq 20\%$ (see Chapter 3). With this information, we can hypothesize that the strong variation in diffusivity can be related with changes on the local structure. We can expect different stable local structures as the combination of different size ratios and compositions impact the geometry of the local packings. In particular, we will first focus on the changes on icosahedrality (number of particles involved in icosahedral clusters). Ideally, the icosahedrality of a system can be used to predict dynamical behavior if it varies accordingly to the changes on dynamics.

To explore this conjecture, we use the Topological Cluster Classification algorithm [11] to quantify the number of particles involved in icosahedral clusters. In Fig. 6.1 b) we show this quantity as a function of the composition for each size ratio at the same packing fraction $\eta = 0.575$. The results show that effectively, the number of icosahedral clusters and so the local structure are highly dependent

on composition. However, to explore whether icosahedrality can be used as a dynamical predictor, we will describe in detail the relation of icosahedrality with the fastest and the slowest systems.

First, we start with the slowest systems. The mixture with the highest number of icosahedral clusters, $q = 0.8$ and $x_L = 0.3$, corresponds to the one with the largest value of diffusion time $\tau_D$, i.e. the slowest system. This is on agreement with our previous results that relate the slowdown on dynamics with an increase of icosahedral clusters (Chapter 3). However, this specific mixture ($q = 0.8$ and $x_L = 0.3$) is close to the region where crystallization into Laves phases are stable [127]. These phases have in their unit cell an icosahedral cluster, hence as we approach to the region where icosahedral order is part of the preferred structure, the system slows down and the number of icosahedral clusters increase. We simulate larger systems with $N \geq 2000$ particles to explore the possibility of crystallization into Laves phases. Indeed, in some of our large simulations we find crystallization [127, 183]. These crystals are detected using a machine-learning based order parameter [184]. Note that in the system used to measure the quantities shown in Fig. 6.1, we do not find any signs of crystallization.

In the regime of slow dynamics, icosahedrality is highly sensitive to the changes on dynamics. Contrary to the fast dynamics regime, where we can see that despite the different dynamics, the number of icosahedral clusters is 0 for almost all the compositions of our fastest systems (size ratios $q = 0.6$ and $q = 0.7$). Note that these two size ratios are presumably not deep in the glassy regime as their dynamics are fast compared to the ones of larger size ratios.

The increase on the number of icosahedral clusters is dependent of how deep the system is in the glassy regime. Hence, icosahedrality is not a good predictor of the overall dynamical behavior of hard spheres outside the region deep in the glass.

**Additional complex structures**

As we have previously shown, icosahedral clusters have become important in the study of glasses [5, 6, 14, 185] because of their five-fold symmetry, their long life times in arrested systems and most importantly their increasing prevalence while going deeper in the glassy regime. However, as we have shown in Fig. 6.1 b) the slowest systems of hard spheres at $\eta = 0.575$ have at most $30\%$ of the particles involved in icosahedral clusters, Additionally, the fastest ones, although they are in the glassy regime, do not have icosahedral clusters. Hence, a logical question to ask is: are there any other clusters related to the changes in dynamics?. Indeed, recent work has shown that a variety of complex clusters in hard-sphere mixtures can also have long lifetimes [74] and they could be also related to the changes in dynamics. Based on that, we explore in greater detail the local structure of hard spheres. To do so, we characterize all the clusters detected by the TCC [11, 24]. We pay special attention to the clusters with long life times [74].

From the analysis of all these clusters we find that there is a whole family

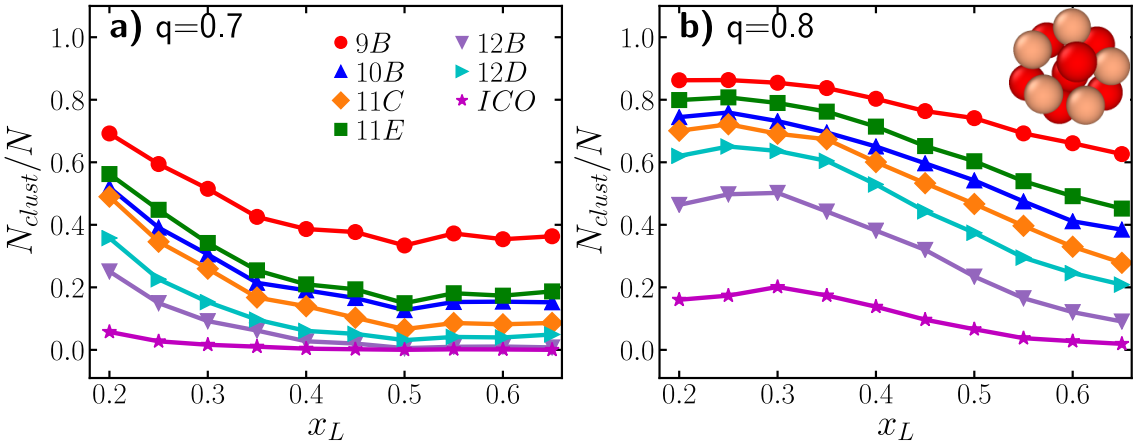


Figure 6.2: Clusters correlated with the appearance of icosahedral cluster in hard spheres for a) $q=0.7$ and b) $q=0.8$. Inset corresponds to the $12B$ cluster, the five-member ring is shown in different color.

of structures that commonly appear together with perfect icosahedral clusters. This family follows the same trends as the icosahedral ones and some of them are related with the long-lived structures in hard spheres. Moreover, almost all of them have in their structure rings of 5 particles, characteristic of the icosahedral clusters as shown in Fig. 6.2 b) where we show the five-member ring of the cluster $12B$. In Fig. 6.2 a) and b) we show some of these clusters for size ratio $q=0.7$ and $q=0.8$. Intuitively, it is therefore likely that each of these clusters contributes, to some degree, to the slowdown of the system. However, it is hard to assign a particular contribution for each of them. And, in terms of experimental realization the distinction between all of these clusters can be difficult. A more simple structure or parameter is missing to quantify and capture all the changes on hard-sphere mixtures.

### 6.3.2 Tetrahedrality of the Local Structure

Based on the previous information we can disentangle the complex structure of the systems by turning our attention to the smallest cluster in 3 dimensions: the tetrahedron. Some of the clusters in the family, we have found in the previous section, are formed by several tetrahedral clusters assembled together. We define a tetrahedral cluster as a group of four particles where each pair of particles are considered nearest neighbors, an schematic picture of a tetrahedral cluster is shown in Fig. 6.3. We use the same modified Voronoi contruction of the TCC algorithm [11](see Section 2.3) to define the nearest neighbors. In general, the modifications attain the avoidance of counting second-shell neighbors and allow distorted rings of four particles. Some structures can be decomposed in more tetrahedral clusters than others. One example of this is the icosahedral cluster where the central particle belongs to 20 different tetrahedrons as it forms a tetrahedron with each of the faces of the icosahedral.

Considering the different morphologies of the structures we define a new order parameter: the Tetrahedrality of the Local Structure (TLS). As essentially all

particles are involved in multiple tetrahedral clusters, we quantify their tetrahedrality by measuring the average number $\langle n_{\rm tet} \rangle$ of tetrahedra a particle is involved in. Well packed and symmetric clusters as the icosahedral one will present higher tetrahedrality values. Depending on its environment each particle will have a different value of tetrahedrality represented by $n_{\rm tet}(i)$.

Hence, natural questions to ask are: how the tetrahedrality of the local structure (TLS) is related to the overall dynamical behavior?, and more importantly, can TLS predict local and global dynamical behavior?. In the following sections we will discuss in detail all the aspects of the TLS.

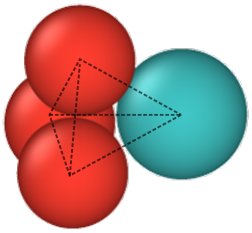

Figure 6.3: Schematic image of a tetrahedral cluster, dashed lines indicate that each particle is nearest neighbors to the other three particles.

### 6.3.3 TLS and the global dynamics

In order to answer how the tetrahedrality correlates with the global dynamics, we calculate the average number of tetrahedra per particle:

$$\langle n_{\rm tet} \rangle = \frac{1}{N} \sum_{i=1}^{N} n_{tet}(i), \tag{6.3}$$

where $n_{tet}(i)$ corresponds to the number of tetrahedra the particle $i$ is involved in.

In Fig. 6.4 we show $\langle n_{\rm tet} \rangle$ for each binary mixture for $\eta = 0.575$. Remarkably, this simple structural order parameter captures the behavior of the diffusion time almost perfectly, reproducing both the convexity of $\tau_D$ for low $q$ and its maximum at high $q$ shown in Fig. 6.1 a).

In order to test the tetrahedrality and the diffusion time at higher and lower packing fractions, we calculate $\langle n_{\rm tet} \rangle$ for all the studied binary mixtures at different packing fractions $\eta = 0.52$, $0.54$, $0.56$, $0.57$ and $0.58$. In Fig. 6.5 we show the $\langle n_{\rm tet} \rangle$ and $\tau_D$ as a function of composition for a packing fraction of $\eta = 0.56$ and $0.58$, for both packing fractions the overall tetrahedrality captures well the changes on dynamics. Similar results are found for the other packing fractions.

There is a clear correlation between the tetrahedrality and dynamics for all the packing fractions investigated. This can be better seen by calculating the diffusion time as a function of $\langle n_{\rm tet} \rangle$. In Fig. 6.6 we show all the diffusion times as a function of $\langle n_{\rm tet} \rangle$ for all mixtures per packing fraction. We find that the well behaved correlation we see in Fig. 6.1 and Fig. 6.5 is reflected in all our data per packing fraction collapsing onto the same line. From this remarkable collapse we can

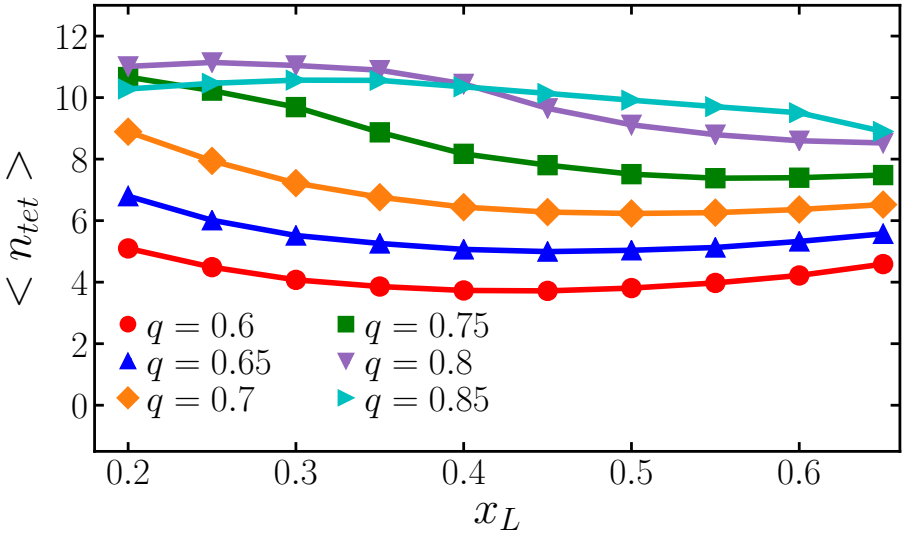


Figure 6.4: Average number of tetrahedral per particle of binary hard-sphere mixtures with packing fraction $\eta = 0.575$.

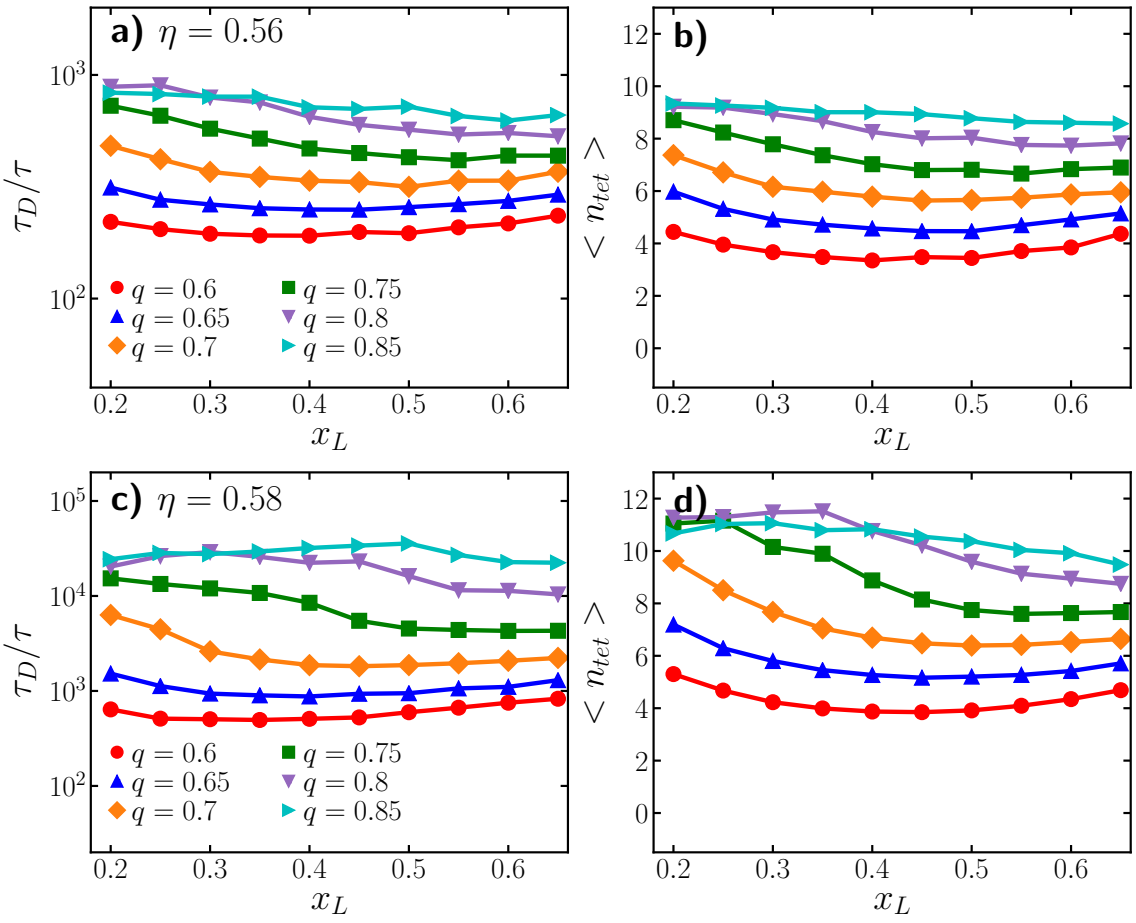


Figure 6.5: a) Diffusion time $\tau_D$ as a function of composition $x_L$ for binary mixtures at $\eta = 0.56$. b) Average number of tetrahedra per particle for the same systems. c) and d) show the corresponding results of binary mixtures at $\eta = 0.58$.

prove that for each packing fraction, $\langle n_{\rm tet} \rangle$ provides an excellent predictor of the diffusion time, revealing an approximately exponential relationship between $\tau_D$ and $\langle n_{\rm tet} \rangle$ (dashed lines). Note that for each packing fractions there are at least 60 different systems.

Moreover, we calculate the number of tetrahedra and the diffusion time for all our polydisperse systems at different packing fractions with polydispersities ranging from 1% to 20%. Surprisingly, the data from the polydisperse systems follow exactly the same relation as the binary mixtures, shown in Fig. 6.6 as closed symbols. The tetrahedrality is capable of predicting the dynamical behavior of a wide diversity of hard-sphere mixtures, from binary mixtures to polydisperse systems.

Another interesting point is that the collapse is well-behaved at relatively low packing fractions where the dynamics are fast and the systems are just entering the glassy regime. The tetrahedrality allows us to have a clear picture of the changes in dynamics way far from the glassy regime. This was not the case for the icosahedrality as the system needed to be deep in the glassy regime to have a significant number of icosahedral clusters.

All the previous results strongly suggest that the dynamical behavior of hard-sphere mixtures of roughly similar sizes is universal and that tetrahedrality captures well the slight changes in the local structure that can be related to the changes on dynamics. Note, however, that this likely does not apply to all possible size ratios. For example, for more extreme size ratios than the ones studied here, demixing could occur due to stronger depletion effects [186].

The relation between $\tau_D$ and $\langle n_{\rm tet} \rangle$ for all the packing fractions follow an exponential relation which resembles to a Vogel-Fulcher-Tamman equation (VFT). The VFT equation proposes a relation between the relaxation time and the temperature in an Arrhenius form [51]:

$$\tau(T) = \tau_0 exp\left(\frac{\alpha}{T - T_0}\right), \tag{6.4}$$

Interestingly, we can approximately collapse the data for all packing fractions in Fig. 6.6 by assuming the diffusion time follows a VFT relation. In our case we do not have a temperature dependency but instead we have the packing fraction one. We can write the diffusion time as a VFT equation:

$$\tau_D = \tau_0(\eta) exp\left(\frac{\alpha \langle n_{\rm tet} \rangle}{\eta^{-1} - \eta_g^{-1}}\right), \tag{6.5}$$

where $\tau_0(\eta)$, $\alpha \simeq 0.03$, and $\eta_g \simeq 0.598$ are fit parameters, with only $\tau_0$ dependent on the packing fraction. The value of $\eta_g$ would correspond to the critical packing fraction where the relaxation time diverges and the system becomes fully arrested.

As the inset of Fig. 6.6 shows, re-scaling the data according to this fit indeed results in an approximate data collapse. However, the assumption of one universal value for $\eta_g$ for all combinations of size ratio and composition is likely not

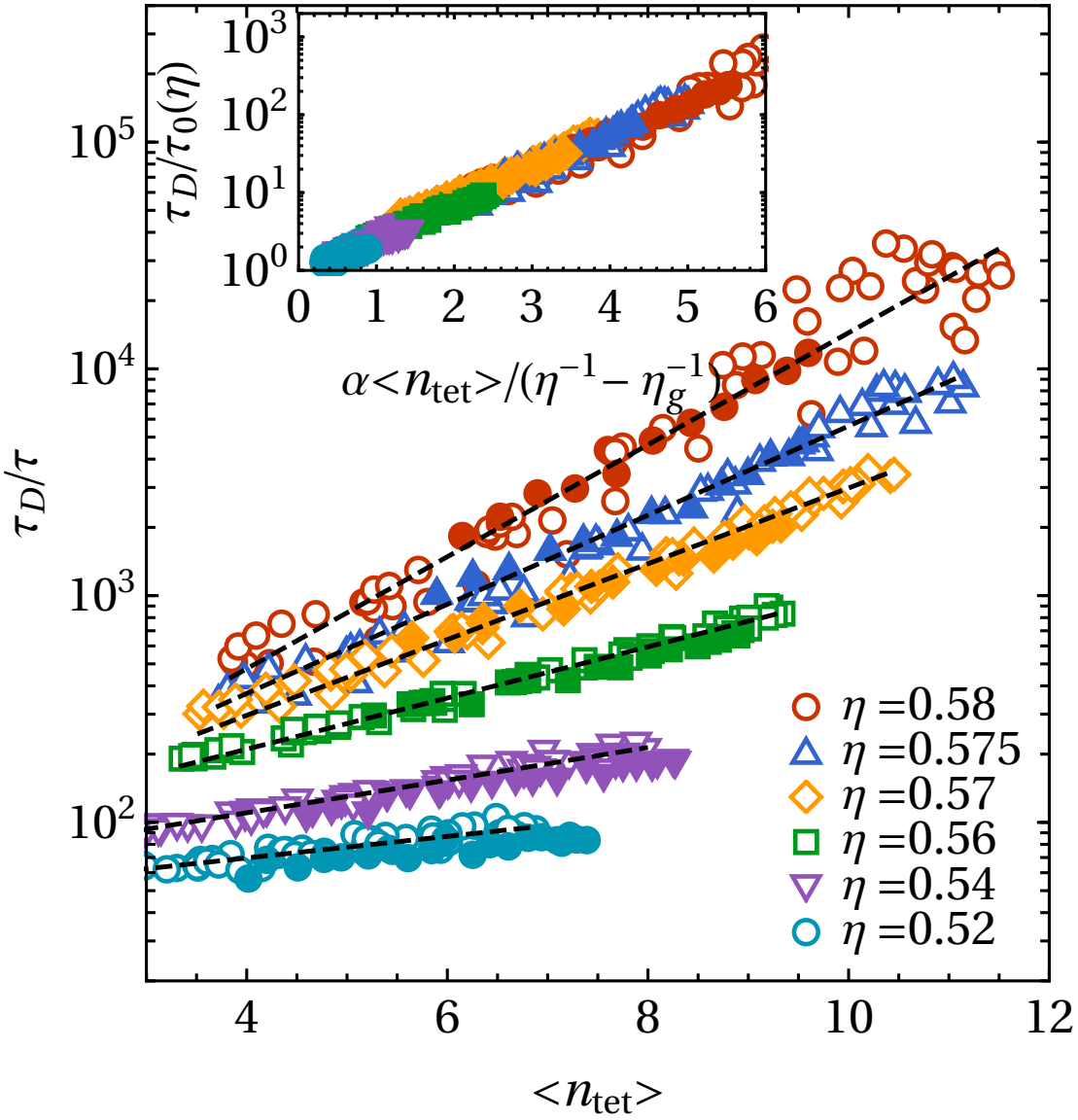


Figure 6.6: Diffusion time for all investigated hard-sphere mixtures as a function of tetrahedrality. Different colors indicate different packing fractions. Within each packing fraction, open symbols correspond to binary mixtures with different size ratios and compositions. Closed symbols are polydisperse systems with different packing fractions. The dashed lines are exponential fits to the binary data for each packing fraction. The inset shows the approximate data collapse obtained by re-scaling the data according to Eq. 6.5.

physical. Moreover, it is unlikely that the diffusion time diverges at the same packing fraction $\eta_g$ for all mixtures as the dynamics are highly dependent of the composition and size ratios and some systems at the same packing fraction are at least one order of magnitude faster than others. Indeed, we perform simulations of some of our (less tetrahedral) systems at packing fractions close to and even beyond $\eta_g$ where we were able to still equilibrate them, and hence Eq. 6.5 must break down for sufficiently high $\eta$. Note that, at those extreme high packing fractions the systems that we can equilibrate correspond to the ones with smaller size ratios and their dynamics per specie starts to be extremely different, hence the data stops collapsing as nicely as in lower packing fractions. Nonetheless, the overall data collapse indicates that Eq. 6.5 approximately captures the increased sensitivity of the dynamics to tetrahedrality as the packing fraction increases.

### 6.3.4 TLS and the $\alpha$-relaxation

All the previous results were obtained from characterizing the dynamics with the diffusion time. However, another commonly time scale used in the study of glassy systems is the $\alpha$-relaxation time as it is also dependent on the caging effect. In Fig. 6.7 a) we show the $\tau_\alpha$ as a function of $\langle n_{tet} \rangle$. At smaller values of $\langle n_{\rm tet} \rangle$ the exponential relation of the dynamical behavior and the structure seems to hold, however at higher $\langle n_{\rm tet} \rangle$ corresponding to the slower systems the relation shows clear deviations. Those systems where the dynamics gets extremely slow are deeper in the glassy regime and we can expect that the Stokes-Einstein relation (SER) breaks down [1, 134, 187, 188].

As we can recall the SER establishes that $\tau_\alpha$ is inversely proportional to the diffusion. Since the diffusion time is the inverse of the diffusion coefficient, the two time scales are proportional: $\tau_\alpha \propto \tau_D$.

In order to determine whether the relation holds in our systems we compare the ratio between $\tau_\alpha$ and $\tau_D$. In Fig. 6.7 b) we show this ratio for the binary mixtures for a fixed composition $x_L = 0.3$ and all the size ratios studied. At high packing fractions there is a clear break down of the relation for the largest size ratios corresponding to the slowest systems. As these two time scales stop increasing proportionally, the relation between $\tau_\alpha$ and $\langle n_{\rm tet} \rangle$ cannot follow the same relation as $\tau_D$ and $\langle n_{\rm tet} \rangle$.

We can also conclude that in general the TLS captures the ability of the particles to diffuse in a dense environment. Furthermore, the relation between $\tau_D$ and $\langle n_{\rm tet} \rangle$ is simple, while the breakdown of the SER promotes a more complex relation between $\tau_\alpha$ and $\langle n_{\rm tet} \rangle$.

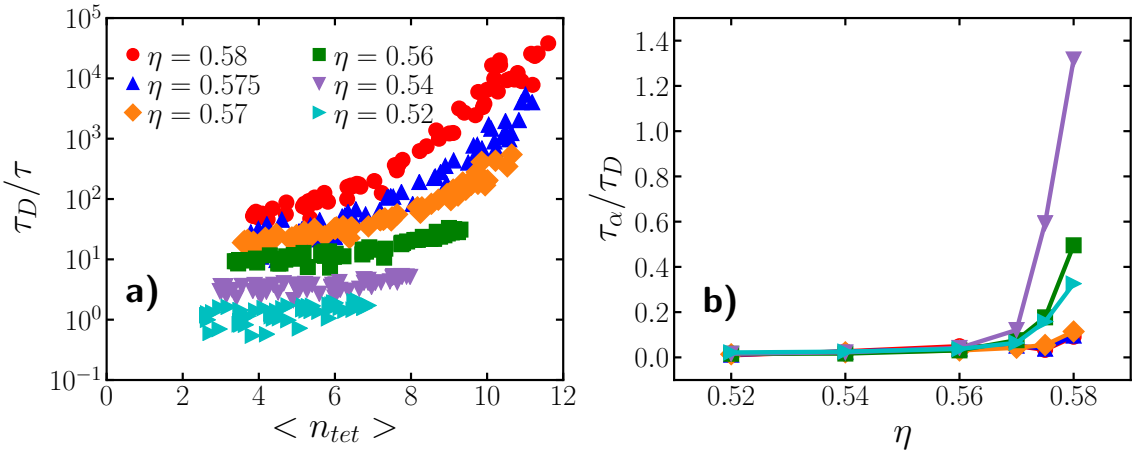


Figure 6.7: a) $\alpha$-relaxation as a function of the average number of tetrahedra per particle for all the binary mixture systems. Different colors indicate different packing fractions. b) $\tau_\alpha/\tau_D$ for binary systems with composition fixed to $x_L = 0.3$, at high packing fractions the Stokes-Einstein relation breaks for the slowest systems.

### 6.3.5 TLS and its lifetime

In order to better understand the role of tetrahedrality, we now turn our attention to the lifetime of the tetrahedral clusters, i.e. the time where the local environment decorrelates. To do so we characterize the decorrelation time of the tetrahedra per particle by calculating the time-dependent autocorrelation function $C_{tet}(t)$:

$$C_{tet}(t) = \frac{\langle n_{tet}(0) n_{tet}(t)\rangle - \langle n_{tet}(0)\rangle \langle n_{tet}(t)\rangle}{\langle n_{tet}^2\rangle - \langle n_{tet}\rangle^2}, \tag{6.6}$$

averaged with all the $N$ particles.

The autocorrelation function give us an estimate of the time where the structure changes. In Fig. 6.8 a) we show the autocorrelation for one of the non-crystalline slowest systems: $q = 0.850$ and $x_L = 0.300$ and all the packing fractions investigated. At short times there is quick decrease on the correlation which after stabilize into a plateau that fully decay at long times.

We extract a decorrelation tetrahedral time by fitting a stretched exponential to the autocorrelation: $A\exp[-(t/\tau_{tet})^\gamma]$, where $A$, $\tau_{tet}$ and $\gamma$ are fitting constants and $\tau_{tet}$ corresponds to the tetrahedral decorrelation time. In Fig. 6.8 b) we show the different time scales: $\alpha$-relaxation time, diffusion time and the decorrelation tetrahedral time of the same size ratio and composition. In Fig. 6.8 b) we can see the breakdown of the SER: at lower packing fractions $\tau_\alpha$ and $\tau_D$ grow at the same rate, at higher packing fractions the relation is broken and $\tau_\alpha$ grows faster than $\tau_D$.

It is interesting to note that $\tau_{tet}$ is significantly shorter than $\tau_D$ for all investigated packing fractions. This can be understood from the fact that $\tau_D$ is a measure of the time a particle needs to diffuse a distance on the order of its own diameter. Clearly, by the time this has happened, the particle will have completely broken

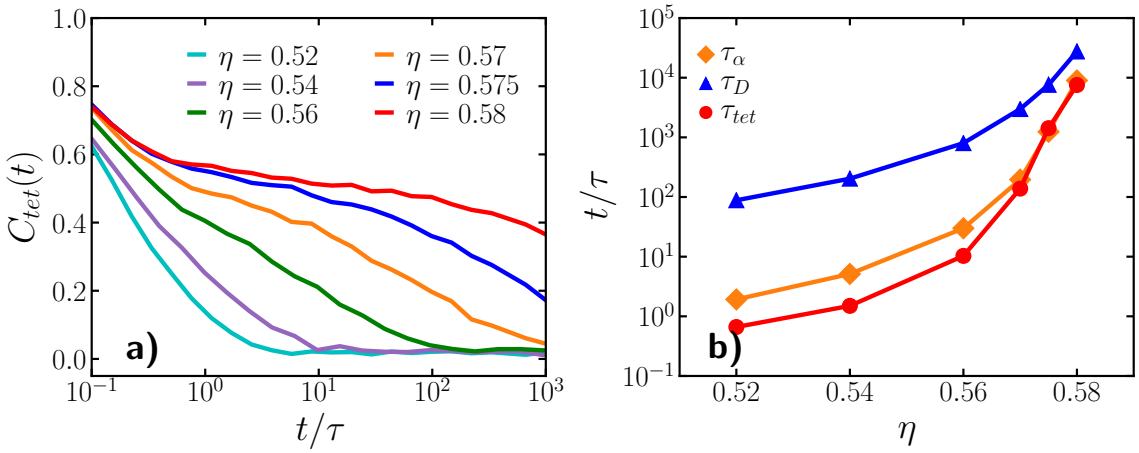


Figure 6.8: a) Time dependent tetrahedral correlation of a binary mixture with size ratio $q = 0.850$ and composition $x_L = 0.300$, different colors denote different packing fractions. b) Comparison between time scales for the same system. Circle markers correspond to the tetrahedral decorrelation time, triangles to diffusion time of all particles and diamonds to alpha-relaxation calculated from the q-vector corresponding to the peak of the structure factor.

free of its initial cage, and the memory of the tetrahedra it was part of, will be lost. Hence, it is understandable that we find values of $\tau_{tet}$ that are smaller than $\tau_D$. In contrast, the decorrelation time $\tau_{tet}$ is on the order of $\tau_\alpha$. The $\alpha$-relaxation time captures the time needed for a particle to escape the cage, just when this happens the system starts loosing memory of the original cage structures. Hence, the decorrelation tetrahedral time coincides with the $\alpha$-relaxation time.

### 6.3.6 TLS and the local dynamics

Thus far we have examined the relationship between globally averaged TLS and diffusivity. Now we turn our attention to the effect of tetrahedrality in the local regime and how this is related to the typical dynamical local changes of the supercooled hard spheres. As we have shown in previous chapters, one of the key features of glassy behavior is the appearance of dynamical heterogeneity, this means that there are regions with faster dynamics than others. It is interesting to explore if the changes in the local dynamics can be associated with variations on the tetrahedrality of the local structure. To this end, we explore the relationship between the number of tetrahedra $n_{\text{tet}}(i)$ a given particle $i$ is involved in, and the absolute distance $\delta r_i = |\mathbf{r}_i(t) - \mathbf{r}_i(0)|$ over which it moves in a given time interval $\delta t$.

This correlation can be quantified explicitly by calculating the Spearman's rank-order correlation $\rho$ [189] as a function of time. This correlation takes values between -1 and 1 and quantifies the monotonic relation between two variables by ranking their values. When $\rho$ is 1 the two variables have a perfectly monotonic growing relation and if it takes a value of -1 the variables decrease monotonically.

We follow the dynamics of one our slowest systems corresponding to $q = 0.85$

and $x_L = 0.3$, we calculate the $n_{\text{tet}}(i)$ and $\delta r_i$ at logarithmic spaced time intervals. Then we calculate the Spearman's correlation between the two variables. In Fig. 6.9a) we show this correlation for each of the species. The correlation between them is negative, meaning that higher values of tetrahedrality are related with smaller values of displacement and viceversa. As we can see from Fig. 6.9a) the correlation grows with time until it reaches a maximal value and after the variables start decorrelating. In Fig. 6.9b) and c) we show a typical snapshot of that system, with particles colored by either their tetrahedrality b) or their displacement c) after a time interval $\delta t = 200\tau$ corresponding roughly to the time of strongest correlation of the small particles. We can see that effectively the regions with lower values of tetrahedrality (red particles in Fig. 6.9b)) are linked to larger displacements (red particles in Fig. 6.9c)).

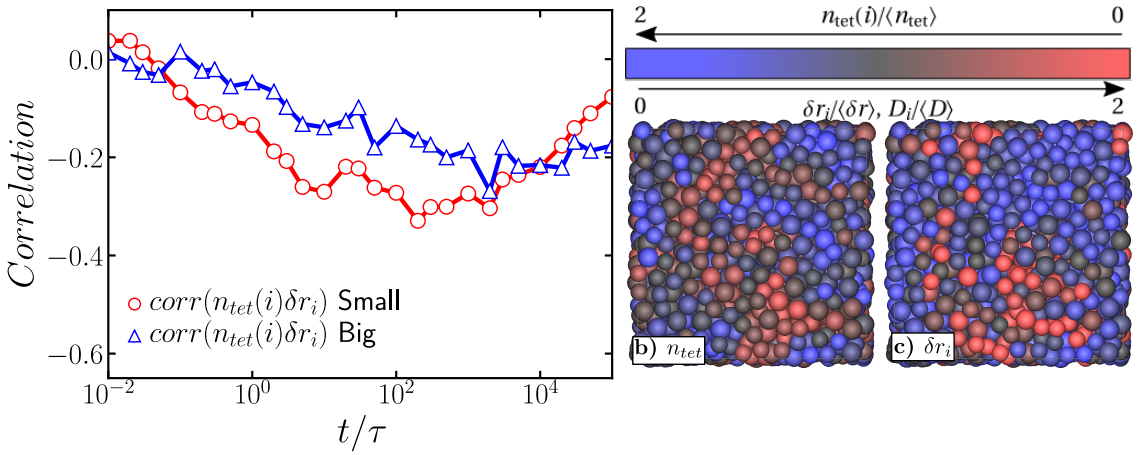


Figure 6.9: a)Spearman's rank correlation between the number of tetrahedral clusters a particle is involved in $n_{\text{tet}}$ and its displacement $\delta r_i$ b,c) Snapshot of a glassy system at packing fraction $\eta = 0.58$, size ratio $q = 0.85$ and composition $x_L = 0.3$, with particles colored according to a) the number of tetrahedra $n_{\text{tet}}(i)$ a particle is involved in, with red particles involved in fewer tetrahedra, and blue particles in more. b) According to the absolute displacement $\delta r_i$ after a time interval $\delta t = 200\tau$ in one trajectory, with red indicating fast particles and blue indicating slow ones.

However, the correlation is noisy. This is because examining the displacement in a specific trajectory provides only a limited view of particle mobility. After all, in a given trajectory, the ability of a particle to move depends not only on its environment, but also on the initial velocities of all particles. To average out this thermal noise, we measure the dynamic propensity $D_i$ of a particle: its average absolute displacement, taken over an ensemble of simulations starting from the same initial configuration [99, 185, 190]. We perform $\sim$ 200 simulations starting from the same equilibrated configuration, each of the simulations start with different velocities to average the thermal noise. In Fig. 6.10 we show the improvements to the correlation by calculating the dynamical propensity. In Fig. 6.10 b) we color the particles once more accordingly to $n_{\text{tet}}(i)$ to better compare and in Fig. 6.10 c) we color each particle according to $D_i$ (again taken at $\delta t = 200\tau$), and indeed reveal a striking correlation between $n_{\text{tet}}(i)$ and $D_i$. To better quantify the correlation, we now calculate the Spearman's correlation between $D_i$ and $n_{\text{tet}}(i)$. In Fig. 6.10a) we show this correlation for the same system. At very short timescales ($\delta t \lesssim 0.1\tau$), before any particles escape their cages, there is little correlation between local TLS and dynamic propensity. Once the thermal noise is averaged the

correlation is smooth and increases its value. At intermediate timescales, we find a strong negative correlation between $n_{\text{tet}}(i)$ and $D_i$, confirming that particles involved in fewer tetrahedra are more mobile. Finally, for timescales approaching the diffusion time $\tau_D \approx 10^4\tau$, the memory of the initial configuration is lost, the initial tetrahedral clusters are broken up, and the correlations start decaying back to zero.

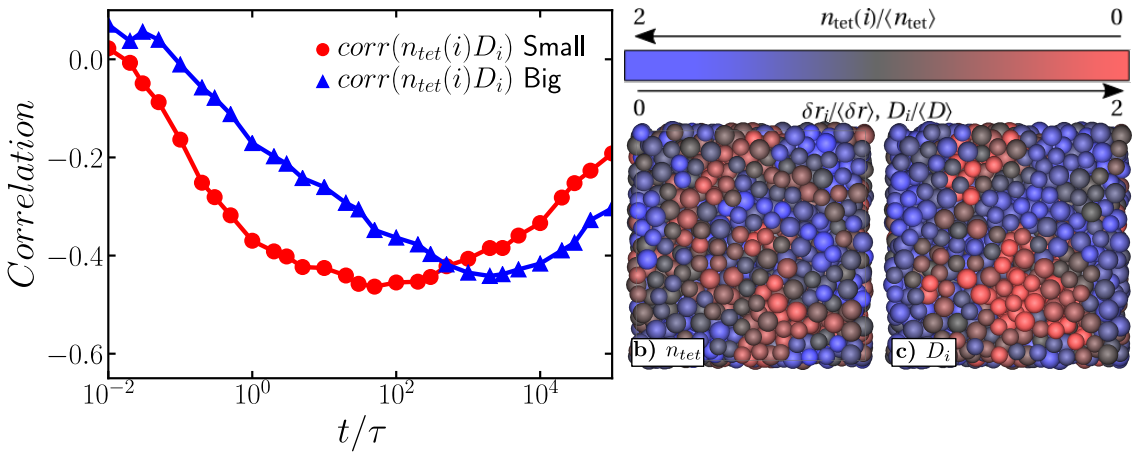


Figure 6.10: a)Spearman's rank correlation between $n_{\text{tet}}$ and its dynamic propensity $D_i$ b,c) Snapshot of a glassy system at packing fraction $\eta = 0.58$, size ratio $q = 0.85$ and composition $x_L = 0.3$, with particles colored according to a) the number of tetrahedra $n_{\text{tet}}(i)$ a particle is involved in, with red particles involved in fewer tetrahedra, and blue particles in more. b) According to the dynamic propensity $D_i$ after a time interval $\delta t = 200\tau$ in one trajectory, with red indicating fast particles and blue indicating slow ones.

The level of correlation between TLS and dynamic propensity demonstrated outperforms most of the purely local observables previously investigated [25]. Moreover,the predictive power of TLS can be enhanced by performing a local averaging of $n_{\text{tet}}(i)$, this is a common practice that has been applied to other local order parameters [25, 185]. To this end, we define $\overline{n_{\text{tet}}}(i, r_c)$ as the mean value of $n_{\text{tet}}(j)$ for all particles $j$ found within a sphere of radius $r_c$ around particle $i$ (including $i$ itself). We calculate the Spearman's correlation with three different cutoff radii $r_c$, we show this results in Fig. 6.11b). We see that the correlation is optimized for $r_c = 2\sigma$, at a value of $\approx 0.63$. In Fig. 6.11a), we color the particles by their value of $\overline{n_{\text{tet}}}(i, r_c = 2\sigma)$. As one might expect, this results in smoother domains of high tetrahedrality, which correlate yet more strongly with the dynamical propensity shown in Fig. 6.10c).

This correlation works particularly well in the slowest systems, though these correlations in other hard-sphere mixtures provides similar results, with weaker correlations for systems with higher diffusivity. In faster systems, dynamics are less heterogeneous, and hence less predictable based on local structure.

In general, local tetrahedrality is an excellent predictor for the dynamics of a particle in the near future in the glassy regime where there is dynamical heterogeneity.

From the results of dynamical propensity we can see that there is a clear arise of dynamical heterogeneity accompanied by the separation of regions with high

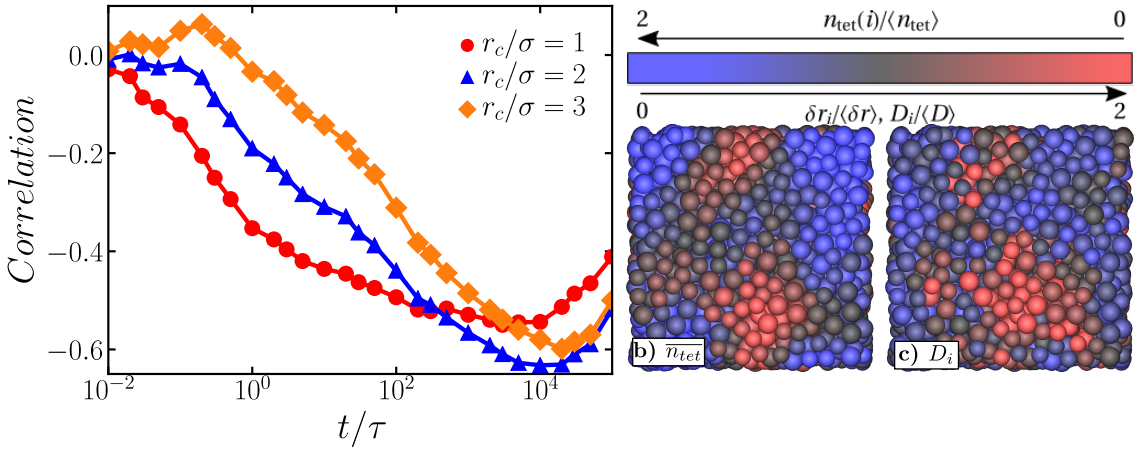


Figure 6.11: a) Snapshot of a glassy system at packing fraction $\eta = 0.58$, size ratio $q = 0.85$ and composition $x_L = 0.3$, with particles colored according to the average tetrahedrality over a spherical region of radius $r_c = 2\sigma$ around each particle. b)Spearman's rank correlation between between locally averaged tetrahedrality and $D_i$ for different radii $r_c$ of the averaging region.

and low values of tetrahedrality. The dynamical correlation length grows as the system increases the packing fraction, however a static correlation length shows a modest increase. We refer the reader to Appendix B where we show a more detailed discussion about the dynamical and static correlation length of one of the slowest systems.

## 6.4 Conclusions

Our results shed some light on the relation between local structure and dynamics in hard spheres. We found that even if icosahedral and other complex structures are present and increase in numbers while going deeper into the glassy regime, they are not capable of capturing all the changes in the dynamics of hard-sphere mixtures. However, the solution for this problem seems to lie in considering a simpler structure: tetrahedral clusters. Depending on the morphology of the local structure, each particle can be part of several tetrahedral clusters. We proposed to characterize this with the tetrahedrality of the local structure which refers to the number of tetrahedra each particle is involved in. We showed that the tetrahedrality of the local structure is a good structural parameter that captures well the slight changes in dynamics of hard spheres over a wide range of packing fractions and size ratios. Globally, the tetrahedrality directly predicts diffusivity at each investigated packing fraction, resulting in a data collapse of a vast variety of hard-sphere mixtures onto one exponential curve using only two global fit parameters. It performs well even with systems that have fast dynamics and are just entering to the glassy regime. All this demonstrates that within this family of hard-sphere mixtures, tetrahedra play a predictable and universal role in determining dynamics.

At the local level the tetrahedrality is closely related to the changes in local dynamics showing large correlations between the local tetrahedrality and the lo-

cal displacement. Local regions with slow dynamics correspond to regions with larger values of tetrahedrality. Additionally, the tetrahedrality presents decorrelation time scales on the order of the alpha-relaxation and in the time scale of the time of the largest heterogeneities, providing more evidence of its relation to the ongoing arrest of the system.

The prediction of the TLS can be directly tested in experimental realizations of colloidal hard-sphere mixtures, using e.g. confocal microscopy [191–196]. Our results may impact attempts to realize the self-assembly of binary Laves phases [183, 197], for which the stability region is in the regime where dynamics are extremely slow. On the theoretical side, the exponential dependence of global dynamics on tetrahedrality is strongly reminiscent of theoretical descriptions of glasses in terms of activation energies for collective rearrangement [62], and random first-order transition theory [1,69,198]. Most importantly, our results demonstrate that the dynamics of hard-sphere mixtures can be predicted purely by looking for the most fundamental three-dimensional building block for the fluid: the simple tetrahedron.

## 6.5 Acknowledgments

Some of the text and images from this chapter were reproduced from S. Marín-Aguilar, H. H. Wensink, G. Foffi, and F. Smallenburg, "Tetrahedrality dictates dynamics in hard sphere mixtures", *Phys. Rev. Lett.*, vol. 124, no. 24, pp. 208005, 2020. 

Chapter 7

# Beyond Tetrahedrality: other models and Machine Learning

## 7.1 Introduction

In the previous Chapter we proposed a new order parameter to quantify the changes on the local structure of supercooled hard-spheres mixtures: the tetrahedrality of the local structure (TLS). This parameter consists of counting the number of tetrahedra a particle is involved in. The TLS works extremely well for predicting the global and local dynamics of a wide variety of hard-sphere mixtures in the supercooled liquid regime. In the local picture the tetrahedrality is highly correlated with the local mobility of the particles outperforming previous parameters used to predict dynamics in hard-spheres. However, in general the smallest structure related to changes in dynamics will presumably depend on the characteristics of the system [185, 199]. For example in Ref. [185], similar strong correlations as ours between dynamical propensity and (larger) locally preferred structures were found for the Wahnström glass former [200], but not for several other model glass formers, such as the Kob-Andersen (KA) mixture [201].

In particular, the Kob-Andersen mixture presents a great challenge for the search for the preferred local structure that correlates with dynamics [185]. This mixture is one of the most used glass-former models for metallic glasses [201]. The peculiarity of this model is that it consists of Lennard-Jones particles with non-additive interactions, which can be expected to impact the local structure. There have been different approaches to find a good structural estimator capable of capturing the dynamical changes of the Kob-Andersen mixture. In particular, machine learning techniques seem to gain importance on predicting the structure [202, 203].

Nowadays with the increase of computational power and the need of handling and learning from huge amounts of data, new computational techniques are needed. One of these is *machine learning* (ML) that allows to extract and 'learn'

information from an input in an 'automatic way'. ML infers from the input information and hence it is based on statistics [204].

In general ML techniques can be divided into two methodologies: supervised and unsupervised machine learning. In the former, *"the aim is to learn a mapping from the input to an output whose correct values are given"* [204, 205]. In contrast, in the latter there is no information about the correct output and only the input is given. In this last method, the goal is to find common characteristics in the input information in order to classify it. The applications of ML vary widely, from data mining to pattern recognition for security, marketing, social media, etc. However, the ideas of ML classification have been applied to supercooled liquids as well. In particular, supervised ML techniques have proven to be useful to recognize regions in glassy systems that are prone to rearrange [206, 207], where information of the rearrangement of a number of particles is given for training.

Reamrkably, unsupervised ML has proven to be a useful tool to classify particles accordingly to information only from their local structure. In particular, it has been used to classify different crystal structures in colloidal systems [208]. And recently, an unsupervised ML methodology based on structural mutual information has been able to distinguish regions correlated with their dynamic propensity [202].

In this chapter, we will first discuss an extension of our proposed parameter TLS, to other glass-former models. In particular, we will show the performance of the TLS in a Wahnström and a Kob-Andersen mixture at different supercooled states. As the Wahnström mixture is an additive binary mixture of repulsive particles, the tetrahedrality shows as good correlations as in the hard-sphere mixtures. However, in the Kob-Andersen mixture the correlations are poorer as the local structure is perturbed presumably by the non-additiviness of the potential.

Finally, we will briefly discuss the use of a simple unsupervised machine learning technique used to distinguish between particles in slow and fast structures. We will show that we obtain similar correlation values for the Wahnström mixture and that for the Kob-Andersen mixture the unsupervised ML outperforms the correlations of the tetrahedrality as the ML is not based in a particular structure and it is capable of distinguishing non-trivial orders.

## 7.2 Methodology

We use the Kob-Andersen [201] and Wahnström [200] models to simulate particles in the glassy regime. Both of them are binary mixtures of Lennard-Jones (LJ) particles. The LJ interaction potential is as follows:

$$U_{ij}(r) = \begin{cases} 4\epsilon \left[ \left(\frac{\sigma_{ij}}{r_{ij}}\right)^{12} - \left(\frac{\sigma_{ij}}{r_{ij}}\right)^{6} \right] & r_{ij} < r_c, \\ 0 & r_{ij} \geq r_c \end{cases} \tag{7.1}$$

where $\epsilon$ is the strength of the interaction, $r_{ij}$ the distance between the particle $i$ and $j$, $r_c$ a cut-off radius and $\sigma_{ij}$ the effective diameter of the particle, if the interaction is between particles of the same specie $\sigma_{ij}$ corresponds to the particle diameter of that specific specie and if the interaction is between different species mixing rules are applied.

The Wahnström model [200] is a binary mixture with composition $x_L = 0.5$ (equimolar composition) with a size ratio of $q = \sigma_{BB}/\sigma_{AA} = 1.2$: $\sigma_{AA} = 1.0$, $\sigma_{BB} = 1.2\sigma_{AA}$ and $\sigma_{AB} = 1.1$. The LJ interaction strength between all pairs of particles is identical: $\epsilon_{AA} = \epsilon_{AB} = \epsilon_{BB}$. The LJ potential is truncated and shifted at the minimum in the potential, such that the interactions are purely repulsive.

The Kob-Andersen model [201] is a non-additive mixture with composition $x_L = 0.8$. The interaction parameters are $\sigma_{BB} = 0.88\sigma_{AA}$, $\sigma_{AB} = 0.8\sigma_{AA}$, $\epsilon_{BB} = 0.5\epsilon_{AA}$, and $\epsilon_{AB} = 1.5\epsilon_{AA}$. The LJ potential is truncated and shifted at a cut-off distance $r_{c,ij} = 2.5\sigma_{ij}$ (where $i, j \in \{A, B\}$), such that the attractive part of the potential is retained.

For both Wahnström and Kob-Andersen, we define the reduced number density $\rho^* = \rho\sigma_{AA}^3$ and reduced temperature $T^* = k_B T/\epsilon_{AA}$, with $k_B$ Boltzmann's constant.

We use molecular dynamics with the LAMMPS [209] package to simulate Kob-Andersen and Wahnström mixtures. For both systems, we use $N = 64000$ particles. The number density $\rho^* = 1.2$ for the Kob-Andersen mixture and $\rho^* = 0.81$ for Wahnström. In order to explore different supercooled states, we explore a wide range of temperatures for both mixtures. In particular for the Wahnström systems we explore temperatures ranging from $T^* = 0.7$ to $T^* = 1.5$ and for the Kob-Andersen mixture temperature from $T^* = 0.55$ to $T^* = 1.0$.

### 7.2.1 Analysis

First, we characterize the typical relaxation time of both systems by extracting the $\alpha$-relaxation time $\tau_\alpha$ from the long-time decay of the Intermediate Scattering Function (ISF).

In order to characterize the local dynamics of both systems we calculate the dynamic propensity $D_i$ (See Chapter 6). We start at least $32$ different simulations with randomize velocities from a Boltzmann distribution accordingly to the specific temperature, all of them starting from the same equilibrated configuration.

We characterize the local structure through the TLS, by counting the number of tetrahedron each particles is involved in following the same methodology from Chapter 6. From the same Voronoi construction of the Topological Cluster Classification algorithm [11] we find the neighbors of the particles and then we count the number of tetrahedra. We define a tetrahedral cluster as four particles such that each of them is considered as nearest neighbors of the others.

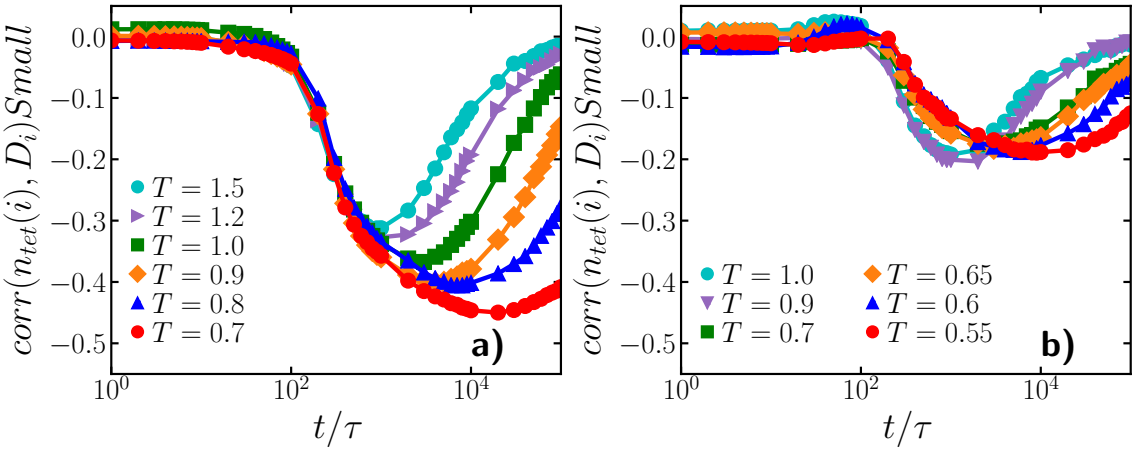


Figure 7.1: Rank correlation between the number of tetrahedra for a particle $n_{tet}$ and the dynamic propensity $D_i$ for small particles of a) Wahnström model and b) Kob-Andersen model. Different colors represent different temperatures. The large particles show similar behavior.

## 7.3 Results

We start by testing the correlation between local tetrahedrality and local mobility in the Wahnström and Kob-Andersen mixtures. We characterize both systems by calculating the dynamic propensity $D_i(\delta t)$ and the number of tetrahedral per particle. Then, we correlate these quantities with a Spearman's rank correlation. The correlation takes values between $1$ and $-1$ and quantifies the monotonic relation between two variables by ranking their values. In Fig. 7.1 a) we show the rank correlation for the Wahnström model corresponding to the small particles and all the temperatures investigated. Interestingly, the correlation shows similar trends as the ones from the hard-sphere mixtures. Note that the Wahnström model is a mainly repulsive model and hence we can expect that the preferred local structures will be similar to the ones from the hard-spheres (See Chapter 1). Similar to what we saw in the hard-sphere case the correlations improve as the system goes deeper in the glassy regime. In this case this happens when the temperature is lower. This is consistent with the fact that at lower temperatures the system becomes slower as the arrest plays a bigger role. Furthermore, the tetrahedrality of the local structure can also be used to predict the local and global dynamics of Wahnström mixtures.

In contrast, in Fig. 7.1 b) we show the Spearman's correlation of the Kob-Andersen system. We see a different scenario for this model. The first point to remark is that the correlation reaches a maximum value of $\simeq -0.2$ which tells us that the two quantities are not strongly correlated. While going to lower temperatures the correlation decreases in value. This indicates in general that the tetrahedral cluster is not the fundamental structure leading the slowdown on dynamics. As we have pointed out before, the Kob-Andersen model has non-additive interactions and we expect that this disrupts the preferred local structures. In principle, however, different simple structures can be responsible of the changes in dynamics.

With this in mind and with the fact that the locally preferred structures in

the Kob-Andersen mixture are composed of subunits made of bipyramids [7,11], we turn our attention to count the number of pyramids a particle is involved in. However the correlation does not improve and it has lower values than the one found for tetrahedrality. The next step would be trying different local structures to find a good candidate as a predictor of the local dynamics, however the non-additiveness of the interaction affects the local structure in a non-trivial way and none of the clusters identified by the TCC seem to correlate strongly with dynamics.

We turn out attention to an elegant methodology which can be able to capture non-trivial structures from structural information: Unsupervised Machine Learning.

## 7.4 Unsupervised Machine Learning

In this section, we will apply the same unsupervised machine learning techniques (UML) from Ref. [208] to the last two glass-former models we have worked with: Kob-Andersen mixture and Wahnström mixture.

The heart of this UML method consists of classifying particles accordingly to their local structure. The first step is to find a proper input that describes the local structure of each particle. As shown in Ref. [208] a good candidate for this are the bond order parameters, similar to the ones used in Chapter 3. Here, we will focus on $Q_{lm}(i)$ as in Eq. 3.7:

$$Q_{l,m}(i) = \frac{1}{N_b(i)} \sum_{j=1}^{N_b(i)} Y_{lm}(\theta_{ij}, \phi_{ij}), \tag{7.2}$$

where $Y_{lm}(\theta_{ij}, \phi_{ij})$ are the spherical harmonics, with $m \in [-l, l]$ and $\theta_{ij}$ and $\phi_{ij}$ are the polar and azimuthal angles of the center-of-mass distance vector $\mathbf{r}_{ij} = \mathbf{r}_j - \mathbf{r}_i$, with $\mathbf{r}_i$ the position vector of particle $i$.

The rotational invariant, which are combinations of $Q_{lm}$ are:

$$Q_l(i) = \left[ \frac{4\pi}{2l+1} \sum_{m=-l}^{l} |Q_{lm}(i)|^2 \right]^{1/2}, \tag{7.3}$$

Finally in order to take into account the information of the local structure of the neighboring particles we define the average $\bar{Q}_l(i)$ as:

$$\bar{Q}_l(i) = \frac{1}{N_b(i)+1} \left( Q_l(i) + \sum_{j=1}^{N_b(i)} Q_l(j) \right). \tag{7.4}$$

Note that this second average has information about the local structure of the second shell.

In order to have a complete structural input we calculate a set of 8 $\bar{Q}(i)_l$ parameters, with $l$ from 1 to 8. Hence, the local structure of each particle will be characterized by a vector $\bar{Q}(i)_l$.

One common technique in ML to classify families with similar characteristics is first to do a dimensionality reduction [204]. To do this we use an autoencoder, which is a neural network trained to reproduce its input as its output. In Fig. 7.2 we show a schematic diagram of the autoencoder. First, the autoencoder reduces the dimensionality of the input in the 'hidden layer' (known as 'bottleneck') through a non-linear projection. Then, a subsequent hidden layer is used as a decoder. The input of this final layer is the lower-dimensionality output and its goal is to recover the initial input. For more information about this process we refer the reader to Ref. [204] and Ref. [208], The parameters of the bottleneck and the training are fixed such that at least 75% of the variance of original input is retained by the output of the autoencoder.

In order to classify the particles according to their structure, only the trained bottleneck is retained. Hence, the data with the lower dimensionality will be used to classify. Finally, a clustering technique is applied for classifying the particles, here we used the *Gaussian mixture model* (GMM). GMM assumes that the input comes from a mixture of $k$ Gaussians with unknown parameters, for more information we refer the reader to Ref. [204]. We use the assumption that the data is a mixture of two Gaussians. The output of the GMM is a list of probabilities $P_j(i)$, that correspond to the probability of $i$ coming from the $j$ gaussian. Finally, with this we classify the particles as $P_{red}$ and $P_{white} = 1 - P_{red}$. Note that, we assign a posteriori the label $red$ to the family correlated with more mobile particles.

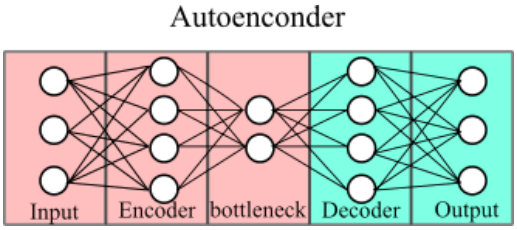


Figure 7.2: Schematic diagram of the autoencoder.

### 7.4.1 Results

We apply the previous methodology to the Kob-Andersen and Wahnström mixture systems previously explained. We calculate the input vector $\bar{Q}(i)_l$ for each particle and then, from the UML we obtain the probability of each particle to belong to the red cluster $P_{red}$. In order to assess the ability of the ML to capture the particles associated with slow and fast regions, we calculate the Spearman's correlation between the propensity and the probability $P_{red}$ for each of the systems. However, in order to follow a similar procedure as in Chapter 6 and improve the correlation we obtain a locally averaged order parameter $\bar{P}_{red}$ by averaging the value of $P_{red}$ over a spherical region with a cut-off radius of $r_c = 2\sigma_L$.

In Fig 7.3 we show the Spearman's correlation of the small and the big parti-

cles of the Wahnström mixture at the lowest temperature investigated $T^* = 0.7$. By comparing Fig. 7.1 a) we can observe that the correlation of the averaged $\bar{P}_{red}$ outperforms the correlation with tetrahedrality. This shows that the structural variations captured by the UML method are inherently linked to different dynamical behavior.

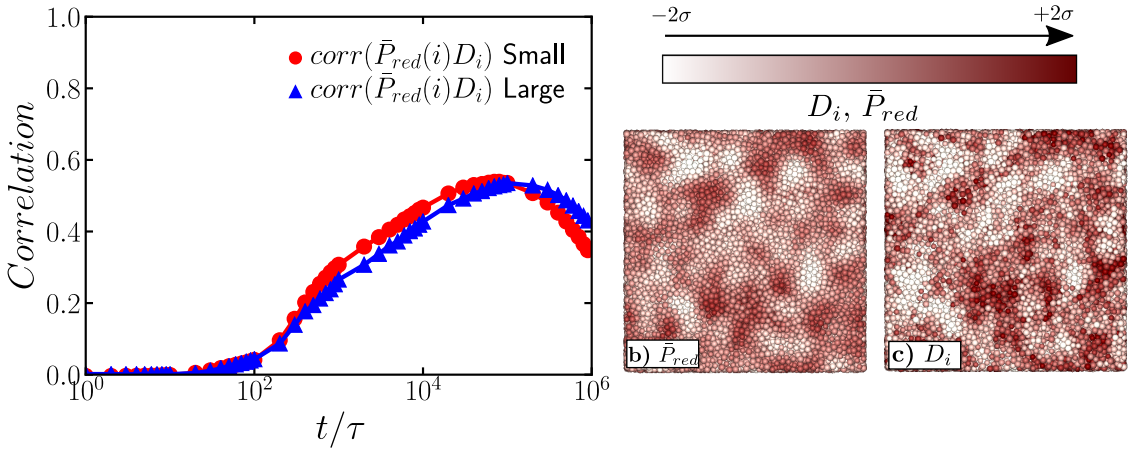


Figure 7.3: a) Spearman's correlation between the averaged probability $\bar{P}_{red}$ and dynamic propensity $D_i$ for the Wahnström mixture at $T^* = 0.7$ with particles colored accordingly to b) its propensity and c) its $\bar{P}_{red}$.

In the case of the Kob-Andersen mixture the picture is more complicated. In Fig. 7.4 we show the same correlation for the Kob-Andersen mixture at the lowest temperature. In this case, the correlation also outperforms the correlation with tetrahedrality, however it is still lower than the correlation found for the Wahnström mixture. This in one side might be related to the fact that this Kob-Andersen mixture is near to the gas-liquid phase coexistence [210, 211] that can induce heterogeneities at larger length scales and this information is lost as our input is highly local.

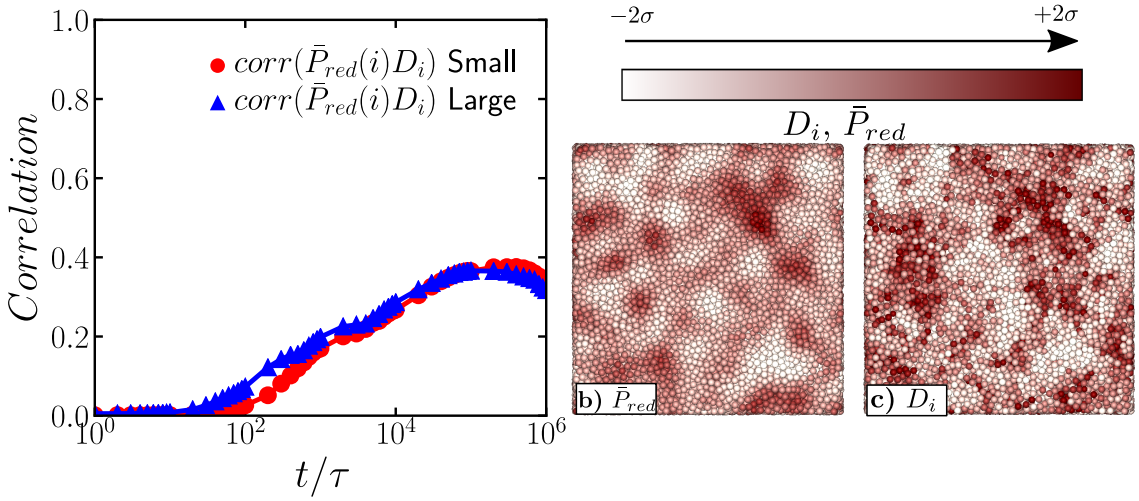


Figure 7.4: a) Spearman's correlation between the averaged probability $\bar{P}_{red}$ and dynamic propensity $D_i$ for the Kob-Andersen mixture at $T^* = 0.5$ with particles colored accordingly to b) its propensity and c) its $\bar{P}_{red}$.

Now we turn our attention to different degrees of undercooling. When pre-

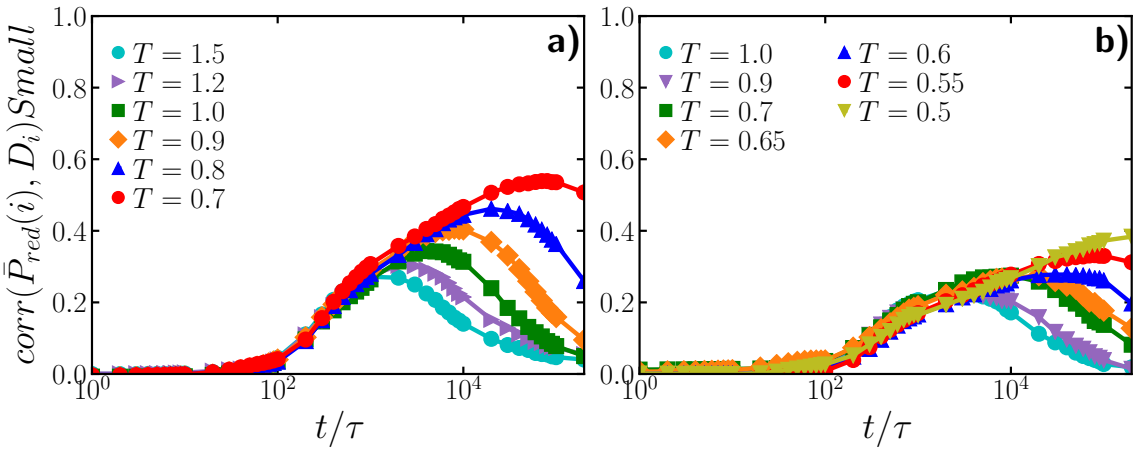


Figure 7.5: Spearman's correlation between the averaged probability $\bar{P}_{red}$ and dynamic propensity $D_i$ for a) Wahnström and b) Kob-Andersen mixtures. Different colors represent different temperatures. The large particles show similar behavior.

dicting dynamics using TLS in the Wahnström mixture, the correlation gets stronger as the system gets deeper in the glassy regime. To check whether this is also captured by the UML, we train the autoencoder for each studied temperature for both mixtures, and we calculate the $\bar{P}_{red}$ for each temperature. Once more, we correlate this quantity with the propensity. In Fig. 7.5 we show the correlation between $\bar{P}_{red}$ and dynamic propensity $D_i$ for both systems at all temperatures. As we can note, in the Wahnström mixture the correlation grows in a similar way as in the correlation between the TLS and propensity (Fig. 7.1 a)) having its maximum value at the lowest temperature. Interestingly, in the Kob-Andersen mixture a similar trend is shown differently from the TLS and propensity shown in Fig. 7.1 b). This is a good indicator that the UML is capturing the structural information that changes as the system is supercooled.

## 7.5 Conclusions

The results of this Chapter provide strong indications that in glassy systems the regions with different dynamics, slow or fast, are related with regions with slightly different local environments. Here, we began by applying the ideas of the tetrahedrality of the local structure (TLS) studied in Chapter 6 to other models. We found that the TLS correlates strongly with the different local dynamics. In particular, as in the case of hard-sphere mixtures, regions with slower dynamics are correlated with regions of high values of tetrahedrality. In this model the temperature is one of the parameters that controls the glassiness of the system, and by going deeper into the glassy regime the correlations between the TLS and the local dynamics get stronger. Note that the local favored structure of hard-sphere mixtures and Wahnström mixture are similar, as in both the icosahedral and the defective icosahedral cluster are highly present. These structures can be easily deconstructed in tetrahedral clusters.

In the case of Kob-Andersen mixture, the TLS do not perform as well as in the

Wahnström mixture. Note that, in this mixture the local favored structures are more complex and they are related with bicapped square antiprisms and capped trigonal prismatic structures [7,74]. Moreover the TLS is not capable of capturing better correlations as the system was undercooled.

In order to deal with this type of mixtures, we turned our attention to an elegant method that allows us to distinguish between particles with different structural environments: unsupervised machine learning (UML).

From applying the UML to Kob-Andersen and Wahnström we found that for both systems, the UML captures structures that are well correlated to local dynamics. Moreover, the correlations outperform the ones obtained from the TLS. Note that, UML does not have any a priori information of the type of cluster, and so it is able to capture non-trivial structures that can be correlated with the local dynamics.

The main advantage of the UML, is that it is capable of predicting dynamical information from only structural information of one snapshot. Moreover, it is a simple and computationally non-expensive technique that can be applied to any glass-former. These results open the door to predict the dynamics in various other glassy systems, with different degrees of undercooling in a simple way. Moreover, the flexibility of UML allows to improve the correlations by adding to the input other structural descriptors depending on the general characteristics of the systems.

## 7.6 Acknowledgments

The section of machine learning was done in collaboration with the research group of Laura Filion from Utrecht University. I would like to thank Emanuele Boattini and Laura Filion for the calculations on machine learning and for fruitful discussions about machine learning and the prediction of structure. I would also like to thank also Saheli Mitra for providing the equilibrated configurations of Kob-Andersen and Wahnström mixtures.

Some of the figures from ML are reproduced from E. Boattini, S. Marín-Aguilar, S. Mitra, G. Foffi, F. Smallenburg and L. Filion, "Autonomously revealing hidden local structures in supercooled liquids". arXiv:2003.00586 (2020) [17].

Moreover, some of the text and images from the section tetrahedrality and other models were reproduced from S. Marín-Aguilar, H. H. Wensink, G. Foffi, and F. Smallenburg, "Tetrahedrality dictates dynamics in hard sphere mixtures", *Phys. Rev. Lett.*, vol. 124, no. 24, pp. 208005, 2020. Copyright ©2020 American Physical Society

Chapter 8

# Conclusions

*Life is an unfoldment, and the further we travel*
*the more truth we can comprehend.*
*To understand the things that are at our door*
*is the best preparation*
*for understanding those that lie beyond.*
***Hypatia of Alexandria***

Finally, we close this thesis by summarizing the main conclusions of each Chapter.

In recent years there have been studies that give compelling evidence that the changes in dynamics in the glassy regime are accompanied by slight changes in the local structure [6–8, 77]. In this thesis we perform an in-depth study of the interplay between structure and dynamics of glassy colloidal systems. To do so, we used computational techniques, from molecular dynamics to machine learning techniques. In general, we draw on the relation between structure and dynamics to explore the idea of controlling dynamics by controlling the structure. Additionally, one of the big unknowns is whether we can extract information of the dynamical behavior from only structural information. In this sense, we explored the ability of predicting dynamical behavior from counting specific types of clusters in hard-sphere systems. Finally, we used machine learning techniques to distinguish between regions which are prone to have faster dynamics by only structural information.

We will divide the conclusions into two sections, one related to controlling dynamics by using patchy particles and one focusing on how to extract dynamical information from the structure.

## Controlling dynamics of glassy colloidal systems: Patchy Particles

We show that the use of patchy particles as glass formers allows us to control the dynamics. Here, we summarize the main conclusions of Chapters 3, 4 and 5.

- **Reentrance and patchy particles.** One of the advantages of the use of patchy particles is that we can interpolate between two extreme interactions: hard spheres and square wells. This allows us to explore the reentrant behavior of the glassy dynamics found in systems with short-ranged isotropic interactions. In Chapter 3 we explored binary systems of patchy particles with two geometries: $12$-patches and $6$-patches and we varied the size of the patches. In both cases the reentrance is conserved. However, the maximum in diffusivity is shifted to lower temperatures as the size of the patches was reduced. This can be understood from the fact that lower temperatures are needed for the systems with smaller patches form the same number of bonds as the systems with larger patches. Moreover, in general the values of the diffusivity increase with the size of the patches.

- **The importance of the location of the patches.** In order to characterize the importance of the location of the patches on dynamics, we compared patchy particle systems from 3 to 20 patches with the same amount of surface covered by them ($40\%$). We located the patches such that the minimum distance between them is maximized. We found that essentially the dynamical behavior of the systems is independent of the number of patches when they are compared with the same coverage, i.e. the diffusivity was the same. The exception to this rule are the geometries with icosahedral ordering, i.e. $10_{ico}$, $11$ and $12$-patch cases. In those cases, at high temperatures the behavior is the same as in the other geometries as the systems behave essentially as hard spheres. However, as the temperature is decreased the dynamical behavior of these cases stands out as the diffusivity becomes dramatically smaller than for the other geometries. In particular, for the $12$-patch case the diffusion decreases almost two orders of magnitude compared to the others at the lowest equilibrated temperature.

- **Controlling dynamics through icosahedrality.** Since Frank's ideas [5] about the high probability of finding icosahedral clusters in the glassy regime, it has been found that the locally favored structures for certain glass formers are icosahedral clusters [7,8,104]. While going deeper into the glassy regime the number of these structures increases. In our patchy particle systems, we found that for the $10_{ico}$, $11$ and $12$ patch cases the number of icosahedral clusters increases sharply as the temperature decreases. This increase is accompanied by an extreme dynamical slowdown. We conclude that patchy particles are able to disrupt the local structure and that one route for controlling the arrest and dynamical slowdown of glassy colloidal systems is through the use of patchy particles that reinforce icosahedral clusters.

- **Rotational dynamics of glassy patchy particles.** The use of patchy particles as glass formers also allows us to explore the rotational dynamics of

the system as the interaction potential between the particles is inherently directional and anisotropic. We dedicated Chapter 4 to explore the rotational dynamics of two cases of patchy particle systems, one with $12$ patches and the second with $6$ patches. For both systems, we varied the size of the patches to explore its effect on rotational dynamics. We found that the rotational relaxation time is faster than the translational one. Additionally, rotational dynamics are highly dependent on the size and location of the patches, in particular when the size of the patches is small or the temperature is high, many of the particles can spin freely in their cages. In contrast, predominantly in the $12$-patch case, when the patches are relatively large, the rotations get arrested as a consequence of the high number of bonds each particle has.

- **Rotational dynamics in patchy particles is driven by local rearrangements.** In the glassy regime, translational relaxation needs collective rearrangements to decorrelate from the initial configuration. Contrary in the rotational relaxation in glassy patchy particles where we found that the particles orientation can relax by adjusting their orientation within its local environment without the need of larger rearrangements. This was corroborated through the results of local dynamical Monte Carlo where we rotate a particle within a fixed cage made by their neighbours and we recovered the rotational behaviour of both patchy particles obtained from the full molecular dynamics. Moreover, we found that for the $12$-patch case the number of icosahedral clusters is reinforced with an optimal patch size ($\theta \simeq 15^{\circ}$) related with slower rotational dynamics. Hence, the local structure has also a direct impact on the way rotational dynamics decorrelate.

- **Monodisperse patchy particles.** Finally, based on the ability of patchy particles to disrupt the local structure, in Chapter 5 we proposed the use of patchy particles as monodisperse glass formers. In particular we explored two cases: $12$ and $8$ patches. We found that both of them are capable of avoid crystallization at low temperatures, making them good candidates to explore glassy dynamics in a monodisperse system. However, as the $12$ patches induce a high concentration of icosahedral clusters, both the local and the global dynamics deviate from the one expected for a 'simple liquid'. In contrast, the $8$-patch case preserves the 'liquid'-like structure, but still avoids crystallization and displays the typical features of glassy systems: two-step relaxation and slower dynamics with the decrease of temperature. This makes it an interesting candidate for a monodisperse glass former. Interestingly, neither the Stokes-Einstein relation nor the Stokes-Einstein-Debye relation seem to break down in the monodisperse patchy glass former.

## How does the structure help us in predicting dynamics?

Despite the growing control over experimental patchy particles [90, 119, 120], glassy systems formed by spherical patchy particles have not been yet reported.

Hence, we turned our attention to a system where there is the possibility of comparing with experimental data: hard spheres. Moreover, we would like to know if we can infer dynamical features through only structural information. Here, we will summarize the main conclusions of Chapters 6 and 7.

- **The structure and dynamics of hard-sphere mixtures is highly dependent on the size ratio and composition.** As simple as hard-sphere systems appear, in the glassy regime we demonstrated that the dynamical behavior (through the calculation of diffusion time) drastically changes with the size ratio and composition of the binary mixture. These variations do not follow any trivial relation with composition. Moreover, the structure of the mixture is also highly dependent on the properties of it. In particular, we quantified the fraction of particles involved in icosahedral clusters (icosahedrality). This last property is not capable of satisfactorily capture all the changes on dynamics.

- **Tetrahedrality of the local structure can predict global dynamics of hard-sphere mixtures.** Together with the icosahedra, there are several other clusters that appear while the systems goes deeper into the glassy regime. However, none of them by themselves are capable of capturing all the changes on dynamics. Instead, we proposed a new order parameter, the Tetrahedrality of the Local Structure (TLS) which consist on counting the number of tetrahedra each particle is involved in. We showed that the TLS captures well all the changes on dynamics through different size ratios and compositions. Moreover, it performs well at a wide variety of packing fractions. In general, the TLS is capable of predicting the global dynamics as all the data from different mixtures (binary and polydisperse) per packing fraction collapse onto an exponential curve. Moreover, all the data can be collapsed onto a single exponential curve with only two fitting parameters, providing a simple expression to infer dynamical behaviour by only counting the number of tetrahedra per particle.

- **TLS correlates well with the changes on local dynamics.** Regarding the local dynamics, the TLS shows strong correlations between local tetrahedrality and propensity. In particular, the regions with slower dynamics are related with higher values of tetrahedrality and vice versa. The TLS works well on predicting both the global and the local dynamics, and it is in line with other order parameters previously proposed [25, 185].

- **TLS performs well with Wahnström mixture.** In Chapter 7 we explored the idea of extending the TLS to other glass formers: Wahnström and Kob-Andersen mixtures. In particular, we found that the TLS presents strong correlations with the local propensity in the Wahnström mixture. Moreover, as the system is cooled down the correlations are stronger. Note that, the Wahnström mixture is essentially repulsive and the locally favored structures are similar to the ones of hard-sphere mixtures. This is in contrast to the Kob-Andersen mixture, where we found poor correlations between tetrahedrality and propensity. Note that Kob-Andersen mixture has non-additive interactions that can disrupt the local structure in a non-trivial

way [7, 185].

- **Unsupervised machine leaning techniques distinguish between regions correlated with local dynamics.** Finally, we turned our attention to an alternative technique that can help on capturing the non-trivial structural changes related with dynamics. We showed that by using a simple unsupervised machine learning with only structural input taken from the bond order parameters, we can classify the particle into two families with similar structural characteristics. One of these families correlates well with the local propensity. We applied this methodology to Wahnström and Kob-Andersen mixtures. And, for both the correlations outperform the ones from the TLS as now there is no biasing on picking any particular structure. These results provide evidence that UML techniques are a powerful and direct new approaches to detect structural variations in glassy systems.

As in all research, once an answer is given more questions appear. Moreover there are always places to improve or extend our work. Here, interesting questions and possible future work arose from the TLS and its extensions. First of all, the study of the TLS in hard-sphere mixtures can now be compared with experimental data through the use of colloidal particles with hard-sphere like interactions and with the help of confocal microscopy. This will open the door to understand better the role of the tetrahedrality in dynamical arrest and to corroborate that the TLS is capable of predicting both local and global dynamics.

Moreover, interesting behaviors happen when glassy systems are subjected to deformations. In particular, depending on the shear amplitude the dynamical behavior of deeply supercooled glasses shows a yielding transition [212]. It would be interesting to explore the relation of this changes on dynamics with TLS on deformed hard-sphere or Wahnström mixtures. One of the relevant dynamical behaviors above yielding is the appearance of a shear band (a region with faster dynamics). Examining the role of tetrahedrality in the formation and structure of the shear band would be an interesting avenue for future research.

Finally, regarding the machine learning techniques, there is a vast amount of room for new research. First, it would be interesting to see if the correlations can get stronger if other structural parameters are used as input, in particular in the case of Kob-Andersen mixture. The UML can be also applied to other glass formers to assess its performance. Moreover, it would be interesting to explore how well unsupervised machine learning techniques are capable of predicting regions that are prone to rearrange when the systems are subjected to deformations.

Appendix A

# Relation between viscosity and relaxation time

One of the fingerprints of the glassy regime is the anomalous relaxation behavior reflected in the two step relaxation and moreover the behavior of the relaxation time with temperature which leads to distinguish between strong and fragile glass formers. The latter distinction was made first through the behavior of the viscosity with time (reflected in the Angell plot as shown in Fig. 1.2), however it is common to assume that the viscosity is proportional to the relaxation time. Here, we show the derivation of this assumption starting from the Maxwell model.

In the Maxwell model in order to analyze coupled elastic and viscous behaviours, a stress is applied to a coupled spring and dashpot as shown in Fig. A.1.

The elastic contribution from the spring can be described as: $\sigma = G\epsilon_1$, where $\sigma$ is the shear-stress, $\epsilon_1$ the strain and $G$ the shear modulus. The viscous contribution of the dashpot is $\sigma = \eta\dot{\epsilon_2}$, where $\eta$ is the viscosity and $\dot{\epsilon_2}$ the strain rate. If the total strain is conserved: $\epsilon = \epsilon_1 + \epsilon_2$, the viscoelastic response can be written as [2, 213–215]:

$$\dot{\epsilon} = \frac{\sigma}{\eta} + \frac{\dot{\sigma}}{G} \tag{A.1}$$

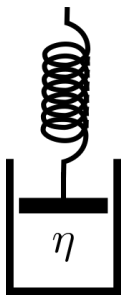


Figure A.1: Scheme of Maxwell model.

The fact that this equation combines the viscous and elastic contributions makes it relevant to a wide variety of fluids [216], specifically, for liquids with steady-state flow with $\dot{\sigma} = 0$ and solids where the viscosity goes to infinite [213].

If a sudden shear displacement of the form $\dot{\epsilon} = \epsilon_0\delta(t)$ is imposed to the system, the shear-stress goes like $\sigma = G\epsilon_0$ at time $t = 0$. In particular, in solid-like systems

the shear modulus approaches to a limiting value $G_\infty$ [217], thus $\sigma = \epsilon_0 G_\infty$. For larger times, $\dot{\epsilon} = 0$ and the shear-stress decays exponentially:

$$\sigma(t) = \exp\left(-\frac{G_\infty}{\eta}t\right), \tag{A.2}$$

where we identify the relaxation time $\tau = \eta/G_\infty$. In the supercooled liquid regime $G_\infty$ does not vary considerably and the validity of this relation holds.

Appendix B

# Dynamical Heterogeneity and Lengthscales of Hard-Sphere mixtures

As we have mentioned in Chapter 1 one of the fingerprints of the glassy regime is the arise of dynamical heterogeneity. The hard-sphere mixtures studied in Chapter 6 present as well dynamical heterogeneity as it was shown through the calculation of dynamical propensity. However, from the calculation of dynamical propensity it is not possible to extract a dynamical correlation length.

As the system goes deeper into the glassy regime the dynamical correlation length grows. Whether it is accompanied by a growing structural correlation length is still subject of debate [98, 101, 218–220].

In this Appendix, we will show how to calculate and characterize dynamical heterogeneity and some results about correlation lengths from the hard-sphere mixtures from Chapter 6.

## Dynamical heterogeneity: Methods

The heterogeneities are time dependent, and in particular there is a time interval $t^*$ where the system presents the maximal heterogeneities. One way of obtaining the time interval $t^*$ is by defining a time-dependent order parameter $Q$ that quantifies the similarities of the overall structure with time. This is done by calculating an overlapping function which counts the number of particles that stay in a local vicinity after a time interval. The order parameter $Q$ is as follows [221]:

$$Q(t) = \int d\mathbf{r}'_{\mathbf{1}} d\mathbf{r}'_{\mathbf{2}} \rho(\mathbf{r}'_{\mathbf{1}}, 0)\rho(\mathbf{r}'_{\mathbf{2}}, t) w(|\mathbf{r}'_{\mathbf{1}} - \mathbf{r}'_{\mathbf{2}}|)) \tag{B.1}$$

$$= \sum_{i=1}^{N} \sum_{j=1}^{N} w(|\mathbf{r_i}(0) - \mathbf{r_j}(t)|), \tag{B.2}$$

where $\rho(\mathbf{r},t) = \sum_{i=1}^{N} \delta(\mathbf{r} - \mathbf{r_i})$ is the local density at position $\mathbf{r}$ and time $t$, and $w(|\mathbf{r_i}(0) - \mathbf{r_j}(t)|)$ is the overlapping function which takes values of 1 or 0 depending on the distance between the particle $i$ and $j$. The overlapping function is:

$$w(|\mathbf{r_i}(0) - \mathbf{r_j}(t)|) = \begin{cases} 1 & |\mathbf{r_i}(0) - \mathbf{r_j}(t)| < a \\ 0 & \text{otherwise,} \end{cases} \tag{B.3}$$

where $a$ is a fraction of the diameter of the particle $\sigma$. In particular, we take $a = 0.3\sigma_L$, which has been proven to give the most accurate results [221]. The overlapping function measures the number of particles that follow any of these two cases in a time interval: in the first case a particle has not moved more than $a$ from its initial position and in the second case, the particle moves more than $a$ but it is replaced by another particle that moves to the initial position of the first particle. The former are known as localized particles and the latter as delocalized.

At long times, $Q$ decays to $\rho\frac{4}{3}\pi a^3$ that corresponds to the fraction of the volume occupied by the particles [221].

At time $t^*$ the system presents the largest heterogeneities which correspond to large fluctuations of $Q$. In order to obtain $t^*$ we characterize the fluctuations of $Q$ [221–223]:

$$\chi_4 = \frac{V}{k_B T N^2} \left[ \left\langle Q^2(t) \right\rangle - \left\langle Q(t) \right\rangle^2 \right]. \tag{B.4}$$

As we pointed out in Chapter 1, there is evidence that as the system gets closer to the glass transition a dynamical correlation length grows. Unlike two-point correlation functions that do not capture this grow [219, 224], four-point correlation functions have been successful on capturing the changes on dynamical heterogeneity [218, 221, 222]. They can be measured from the real space as an analogy of the radial distribution function or in the reciprocal space analogue to the structure factor. Here we focus on a four point correlation function in real-space defined as [221]:

$$g_4(\mathbf{r},t) = \left\langle \frac{1}{N\rho} \sum_{ijkl} \delta(\mathbf{r} - \mathbf{r_k}(0) + \mathbf{r_i}(0)) w(|\mathbf{r_i}(0) - \mathbf{r_j}(t)|) w(|\mathbf{r_k}(0) - \mathbf{r_l}(t)|) \right\rangle - \left\langle \frac{Q(t)}{N} \right\rangle^2, \tag{B.5}$$

where $w$ is the overlap function. From Eq. B.5 we can define a general correlation function $g_4^*(r,t)$ that decays to $0$ at long distances by factorizing the contribution of $\left\langle \frac{Q(t)}{N} \right\rangle^2$ [222]:

$$g_4(r,t) = \left\langle \frac{Q(t)}{N} \right\rangle^2 g_4^*(r,t). \tag{B.6}$$

Finally, we can extract a dynamical correlation length from the four point correlation $g_4^*$ evaluated at time $t^*$. To do so, the decay of the maximum values of

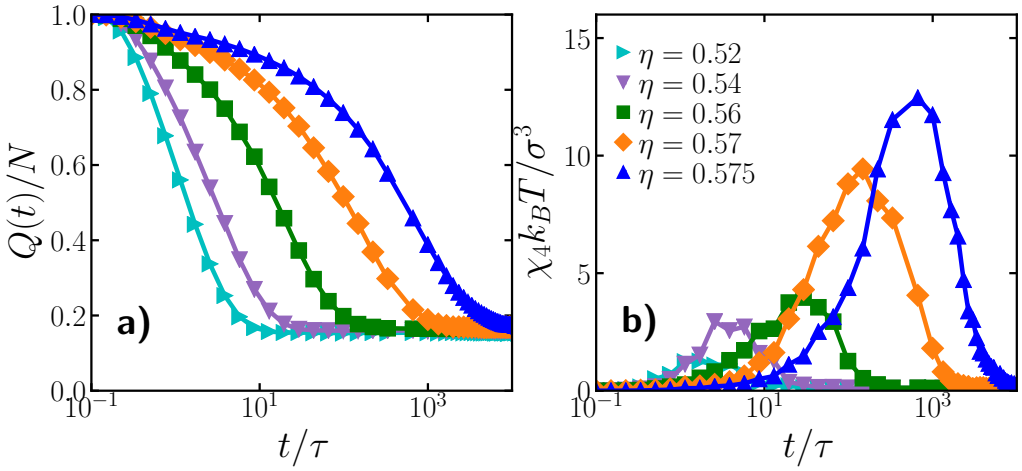


Figure B.1: a) Order parameter $Q(t)$ of a hard-sphere system with size ratio $q = 0.85$ and composition $x_L = 0.300$, each line corresponds to a different packing fraction $\eta$. b) Dynamical susceptibility $\chi_4$ of the same system.

$g_4^*$ are fitted with an exponential function: $A \exp -r/\xi_4$, where $A$ and $\xi_4$ are fitting parameters, and $\xi_4$ corresponds to the dynamic correlation length. This type of fitting is called 'envelope fitting'.

# Results

We begin this section by calculating the dynamical correlation length of one of the slowest binary systems from Chapter 6. To better characterize it we perform bigger simulations with $N = 10000$ particles of the binary mixture with size ratio $q = 0.85$ and composition $x_L = 0.300$ for all the studied packing fraction ($\eta = 0.52$ to $0.58$).

First, we calculate the order parameter $Q$ that quantifies the number of particles that in a time $t$ stay within a vicinity characterized by the parameter $a$ from their original position. We take the parameter $a = 0.3\sigma_L$ as it captures well the changes in heterogeneity [225]. In Fig. B.1 a) we show $Q(t)$ for all the packing fractions investigated. At low packing fractions, the system is just entering into the glassy regime and there is no large heterogeneity as the particles have sufficient space to move and break the cage, leading to a fast decay of $Q(t)$. Contrary to the largest packing fractions, where the particles need longer times to move far from their original positions. Note that the decay of $Q(t)/N$ at infinite times goes to a value corresponding to $4/3\pi\rho a^3$.

Once we have the order parameter $Q(t)$ we calculate its fluctuations $\chi_4$ and we calculate the time where the heterogeneities are the largest. In Fig. B.1 b) we show $\chi_4$ for all the packing fractions investigated. Note that, in all our $\eta$ we find a maximum in $\chi_4$ which suggests that all the systems present heterogeneities though at higher packing fractions the fluctuations are larger as the system becomes more

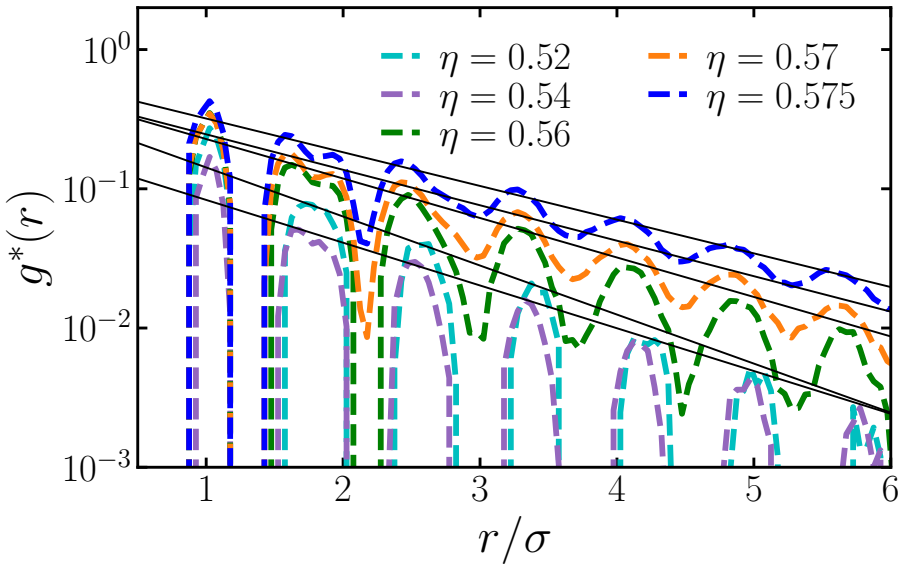


Figure B.2: Four point correlation function $g_4$ of a hard-sphere system with size ratio $q = 0.85$ and composition $x_L = 0.300$, each dashed-line corresponds to a different packing fraction $\eta$. The continuous lines correspond to the exponential envelope fitting.

arrested and as consequence more heterogeneous. From $\chi_4$, we extract the time $t^*$ corresponding to the the time where we find the maximal fluctuations. Interestingly, the time $t^*$ is always on the order of the $\alpha$-relaxation time.

Finally, to extract the dynamic correlation length we calculate the four-point correlation $g_4^*$ at time $t^*$ and we do an 'envelope fitting' with an exponential function $A \exp -x/\xi_4$, where $A$ and $\xi_4$ are fitting parameters and $\xi_4$ corresponds to the dynamic correlation length.

We show in Fig. B.2 the four point correlation $g_4^*$ with their corresponding fitting. Clearly, we see that at high packing fractions the correlation is longer than at lower packing fractions indicating an increase in the correlation length. Note that, the dynamic correlation length can be also extracted from the limit of small wave vectors $k$ of a reciprocal 4-point-structure factor $S_4(k,t)$ [225], however in order to have sufficiently data at small $k$ the size of the system has to be considerable larger. However, the calculation from $g_4^*$ give us a good estimate of the dynamical correlation length and more important the increasing behavior of $\xi_4$ to larger packing fractions is well captured.

Before showing the results of the dynamic correlation length, we calculate a rough estimation of the static correlation length to compare the two length scales.

Following a similar approach as for the dynamical one, we calculate the decay of a two point correlation function. We define a spatial tetrahedral two-point correlation function as:

$$g_{tet}(r) = \frac{\sum_{i \neq j} q_i q_j \delta(r + r_i(0) - r_j(0))}{\sum_{i \neq j} \delta(r + r_i(0) - r_j(0))}, \tag{B.7}$$

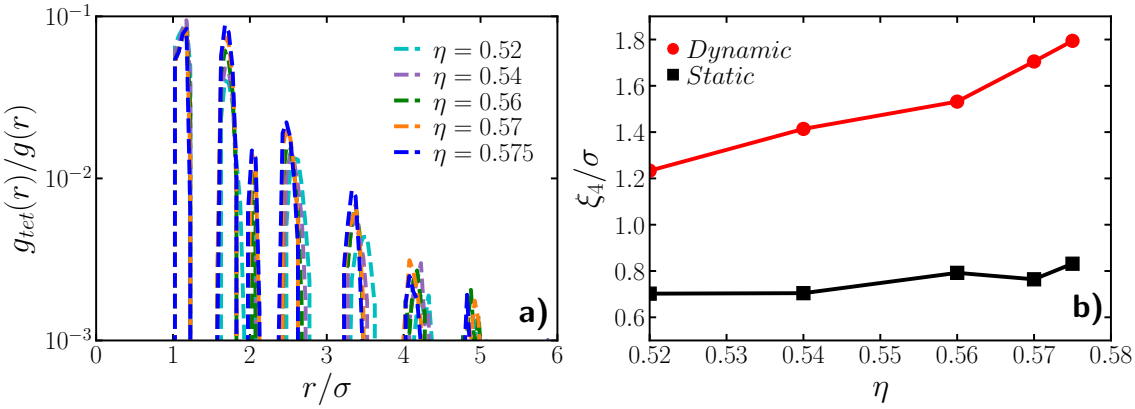


Figure B.3: a)Two point tetrahedra correlation function of a binary mixture with $q = 0.85$ and composition $x_L = 0.3$. b) Dynamic and static correlation lengths of the same system.

where $q_i$ is:

$$q_i = \frac{n_{tet}(i) - \langle n_{\text{tet}} \rangle}{\sqrt{\langle n_{\text{tet}}^2 \rangle - \langle n_{\text{tet}} \rangle^2}}. \tag{B.8}$$

In Fig. B.3 a) we show the decay of $g_{tet}$ for the same systems as above. Differently from the decay of $g_4$, $g_{tet}$ presents almost identical behaviors for all the packing fractions studied. This static correlation do not capture large changes on the structural heterogeneity. Still, we can extract a correlation length using the same methodology as in $g_4$ to compare between those two length scales. We do an exponential envelope fit to the decay of $g_{tet}$. In Fig. B.3 b) we show the comparison between the two length scales. Although the decay of $g_{tet}$ looks almost identical for all $\eta$, the correlation length shows a modest increase with packing fraction.

# Bibliography


[1] L. Berthier and G. Biroli, "Theoretical perspective on the glass transition and amorphous materials," *Reviews of Modern Physics*, vol. 83, no. 2, p. 587, 2011.

[2] D. Uhlman and N. Kreidl, "Glass science and technology,(volume 1), glass-forming systems," *ed. DR Uhlmmann and NJ Kreidl, Academic Press inc*, p. 8, 1983.

[3] D. Kivelson, S. A. Kivelson, X. Zhao, Z. Nussinov, and G. Tarjus, *A thermodynamic theory of supercooled liquids*. Taylor, 1995.

[4] G. Tarjus, S. A. Kivelson, Z. Nussinov, and P. Viot, "The frustration-based approach of supercooled liquids and the glass transition: a review and critical assessment," *J. Phys.: Condens. Matter*, vol. 17, no. 50, p. R1143, 2005.

[5] F. C. Frank, "Supercooling of liquids," *Proc. Royal Soc. A*, vol. 215, no. 1120, pp. 43–46, 1952.

[6] C. P. Royall and S. R. Williams, "The role of local structure in dynamical arrest," *Phys. Rep.*, vol. 560, pp. 1–75, 2015.

[7] D. Coslovich and G. Pastore, "Understanding fragility in supercooled lennard-jones mixtures. i. locally preferred structures," *The Journal of chemical physics*, vol. 127, no. 12, p. 124504, 2007.

[8] M. Leocmach and H. Tanaka, "Roles of icosahedral and crystal-like order in the hard spheres glass transition," *Nature communications*, vol. 3, no. 1, pp. 1–8, 2012.

[9] H. Tong and H. Tanaka, "Structural order as a genuine control parameter of dynamics in simple glass formers," *Nature communications*, vol. 10, no. 1, pp. 1–10, 2019.

[10] N. Kern and D. Frenkel, "Fluid-fluid coexistence in colloidal systems with short-ranged strongly directional attraction," *J. Chem. Phys.*, vol. 118, no. 21, pp. 9882 – 9889, 2003.

[11] A. Malins, S. R. Williams, J. Eggers, and C. P. Royall, "Identification of structure in condensed matter with the topological cluster classification," *J. Chem. Phys.*, vol. 139, no. 23, p. 234506, 2013.

[12] C. De Michele and D. Leporini, "Viscous flow and jump dynamics in molecular supercooled liquids. ii. rotations," *Phys. Rev. E*, vol. 63, no. 3, p. 036702, 2001.

[13] T. Kawasaki and K. Kim, "Spurious violation of the stokes–einstein–debye relation in supercooled water," *Scientific reports*, vol. 9, no. 1, pp. 1–9, 2019.

[14] S. Marín-Aguilar, H. H. Wensink, G. Foffi, and F. Smallenburg, "Slowing down supercooled liquids by manipulating their local structure," *Soft Matter*, vol. 15, no. 48, pp. 9886–9893, 2019.

[15] S. Marín-Aguilar, H. H. Wensink, G. Foffi, and F. Smallenburg, "Rotational and translational dynamics in dense fluids of patchy particles," *The Journal of Chemical Physics*, vol. 152, no. 8, p. 084501, 2020.

[16] S. Marín-Aguilar, H. H. Wensink, G. Foffi, and F. Smallenburg, "Tetrahedrality dictates dynamics in hard sphere mixtures," *Physical Review Letters*, vol. 124, no. 20, p. 208005, 2020.

[17] E. Boattini, S. Marín-Aguilar, S. Mitra, G. Foffi, F. Smallenburg, and L. Filion, "Autonomously revealing hidden local structures in supercooled liquids," *Nature communications*, vol. 11, no. 5479, 2020.

[18] H. G. Pfaender, "The history of glass," in *Schott Guide to Glass*, pp. 1–15, Springer, 1996.

[19] J. D. Musgraves, J. Hu, and L. Calvez, *Springer Handbook of Glass*. Springer Nature, 2019.

[20] C. Vichery and J.-M. Nedelec, "Bioactive glass nanoparticles: from synthesis to materials design for biomedical applications," *Materials*, vol. 9, no. 4, p. 288, 2016.

[21] D. Moura, M. Souza, L. Liverani, G. Rella, G. Luz, J. Mano, and A. Boccaccini, "Development of a bioactive glass-polymer composite for wound healing applications," *Materials Science and Engineering: C*, vol. 76, pp. 224–232, 2017.

[22] M. B. Maas, G. H. Maybery, W. J. Perold, D. P. Neveling, and L. M. Dicks, "Borosilicate glass fiber-optic biosensor for the detection of escherichia coli," *Current microbiology*, vol. 75, no. 2, pp. 150–155, 2018.

[23] J. M. Ward, Y. Yang, and S. N. Chormaic, "Glass-on-glass fabrication of bottle-shaped tunable microlasers and their applications," *Scientific reports*, vol. 6, p. 25152, 2016.

[24] A. Malins, J. Eggers, C. P. Royall, S. R. Williams, and H. Tanaka, "Identification of long-lived clusters and their link to slow dynamics in a model glass former," *J. Chem. Phys.*, vol. 138, no. 12, p. 12A535, 2013.

[25] H. Tanaka, H. Tong, R. Shi, and J. Russo, "Revealing key structural features hidden in liquids and glasses," *Nature Reviews Physics*, vol. 1, no. 5, pp. 333–348, 2019.

[26] F. Arceri, F. P. Landes, L. Berthier, and G. Biroli, "Glasses and aging: A statistical mechanics perspective," *arXiv preprint arXiv:2006.09725*, 2020.

[27] F. Sausset, G. Biroli, and J. Kurchan, "Do solids flow?," *Journal of Statistical Physics*, vol. 140, no. 4, pp. 718–727, 2010.

[28] M. Holmes, N. Parker, and M. Povey, "Temperature dependence of bulk viscosity in water using acoustic spectroscopy," in *Journal of Physics: Conference Series*, vol. 269, p. 012011, IOP Publishing, 2011.

[29] K. J. Buschow, R. W. Cahn, M. C. Flemings, B. Ilschner, E. J. Kramer, and S. Mahajan, "Encyclopedia of materials," *Science and technology*, vol. 1, p. 11, 2001.

[30] G. Biroli and J. P. Garrahan, "Perspective: The glass transition," *The Journal of chemical physics*, vol. 138, no. 12, p. 12A301, 2013.

[31] P. G. Debenedetti and F. H. Stillinger, "Supercooled liquids and the glass transition," *Nature*, vol. 410, no. 6825, pp. 259–267, 2001.

[32] M. Tarzia, A. de Candia, A. Fierro, M. Nicodemi, and A. Coniglio, "Glass transition in granular media," *EPL (Europhysics Letters)*, vol. 66, no. 4, p. 531, 2004.

[33] A. J. Liu and S. R. Nagel, "Jamming is not just cool any more," *Nature*, vol. 396, no. 6706, pp. 21–22, 1998.

[34] M. Cates, J. Wittmer, J.-P. Bouchaud, and P. Claudin, "Jamming, force chains, and fragile matter," *Physical review letters*, vol. 81, no. 9, p. 1841, 1998.

[35] F. Stillinger, "Relaxation behavior in atomic and molecular glasses," *Physical Review B*, vol. 41, no. 4, p. 2409, 1990.

[36] T. Hecksher, N. B. Olsen, K. Niss, and J. C. Dyre, "Physical aging of molecular glasses studied by a device allowing for rapid thermal equilibration," *The Journal of chemical physics*, vol. 133, no. 17, p. 174514, 2010.

[37] G. Monaco, D. Fioretto, L. Comez, and G. Ruocco, "Glass transition and density fluctuations in the fragile glass former orthoterphenyl," *Physical Review E*, vol. 63, no. 6, p. 061502, 2001.

[38] P. N. Pusey and W. van Megen, "Observation of a glass transition in suspensions of spherical colloidal particles," *Physical review letters*, vol. 59, no. 18, p. 2083, 1987.

[39] G. L. Hunter and E. R. Weeks, "The physics of the colloidal glass transition," *Reports on progress in physics*, vol. 75, no. 6, p. 066501, 2012.

[40] J.-P. Hansen and I. R. McDonald, *Theory of simple liquids*. Elsevier, 1990.

[41] C. A. Angell, K. L. Ngai, G. B. McKenna, P. F. McMillan, and S. W. Martin, "Relaxation in glassforming liquids and amorphous solids," *Journal of applied physics*, vol. 88, no. 6, pp. 3113–3157, 2000.

[42] K. Ngai, *Relaxation and diffusion in complex systems*. Springer Science & Business Media, 2011.

[43] I. Campbell, J.-M. Flesselles, R. Jullien, and R. Botet, "Nonexponential relaxation in spin glasses and glassy systems," *Physical Review B*, vol. 37, no. 7, p. 3825, 1988.

[44] P. Luo, P. Wen, H. Bai, B. Ruta, and W. Wang, "Relaxation decoupling in metallic glasses at low temperatures," *Physical review letters*, vol. 118, no. 22, p. 225901, 2017.

[45] J. Phillips, "Stretched exponential relaxation in molecular and electronic glasses," *Reports on Progress in Physics*, vol. 59, no. 9, p. 1133, 1996.

[46] P. Pusey, "Colloidal glasses," *Journal of Physics: Condensed Matter*, vol. 20, no. 49, p. 494202, 2008.

[47] C. A. Angell, "Formation of glasses from liquids and biopolymers," *Science*, vol. 267, no. 5206, pp. 1924–1935, 1995.

[48] M. D. Ediger, C. A. Angell, and S. R. Nagel, "Supercooled liquids and glasses," *The journal of physical chemistry*, vol. 100, no. 31, pp. 13200–13212, 1996.

[49] W. Kob, M. Nauroth, and F. Sciortino, "Quantitative tests of mode-coupling theory for fragile and strong glass formers," *Journal of non-crystalline solids*, vol. 307, pp. 181–187, 2002.

[50] C. Angell, "Strong and fragile liquids," *Relaxations in complex systems*, vol. 3, no. 11, 1985.

[51] L. García-Colín, L. Del Castillo, and P. Goldstein, "Theoretical basis for the vogel-fulcher-tammann equation," *Physical Review B*, vol. 40, no. 10, p. 7040, 1989.

[52] M. D. Ediger, "Spatially heterogeneous dynamics in supercooled liquids," *Annual review of physical chemistry*, vol. 51, no. 1, pp. 99–128, 2000.

[53] H. Tanaka, T. Kawasaki, H. Shintani, and K. Watanabe, "Critical-like behaviour of glass-forming liquids," *Nature materials*, vol. 9, no. 4, pp. 324–331, 2010.

[54] V. Trappe, E. Pitard, L. Ramos, A. Robert, H. Bissig, and L. Cipelletti, "Investigation of q-dependent dynamical heterogeneity in a colloidal gel by x-ray photon correlation spectroscopy," *Physical Review E*, vol. 76, no. 5, p. 051404, 2007.

[55] R. Böhmer, R. Chamberlin, G. Diezemann, B. Geil, A. Heuer, G. Hinze, S. Kuebler, R. Richert, B. Schiener, H. Sillescu, *et al.*, "Nature of the non-exponential primary relaxation in structural glass-formers probed by dynamically selective experiments," *Journal of non-crystalline solids*, vol. 235, pp. 1–9, 1998.

[56] L. Cipelletti and E. R. Weeks, "Glassy dynamics and dynamical heterogeneity in colloids," *Dynamical heterogeneities in glasses, colloids, and granular media*, vol. 150, p. 110, 2011.

[57] C. Donati, S. C. Glotzer, P. H. Poole, W. Kob, and S. J. Plimpton, "Spatial correlations of mobility and immobility in a glass-forming lennard-jones liquid," *Physical Review E*, vol. 60, no. 3, p. 3107, 1999.

[58] E. Flenner, H. Staley, and G. Szamel, "Universal features of dynamic heterogeneity in supercooled liquids," *Physical review letters*, vol. 112, no. 9, p. 097801, 2014.

[59] J. Sethna *et al.*, *Statistical mechanics: entropy, order parameters, and complexity*, vol. 14. Oxford University Press, 2006.

[60] H. M. Jaeger, S. R. Nagel, and R. P. Behringer, "Granular solids, liquids, and gases," *Reviews of modern physics*, vol. 68, no. 4, p. 1259, 1996.

[61] A. D. McNaught, A. Wilkinson, *et al.*, *Compendium of chemical terminology*, vol. 1669. Blackwell Science Oxford, 1997.

[62] G. Adam and J. H. Gibbs, "On the temperature dependence of cooperative relaxation properties in glass-forming liquids," *J. Chem. Phys.*, vol. 43, no. 1, pp. 139–146, 1965.

[63] J. C. Dyre, T. Hechsher, and K. Niss, "A brief critique of the adam–gibbs entropy model," *Journal of Non-Crystalline Solids*, vol. 355, no. 10-12, pp. 624–627, 2009.

[64] F. W. Starr, J. F. Douglas, and S. Sastry, "The relationship of dynamical heterogeneity to the adam-gibbs and random first-order transition theories of glass formation," *The Journal of chemical physics*, vol. 138, no. 12, p. 12A541, 2013.

[65] L. Janssen, "Mode-coupling theory of the glass transition: A primer," *Frontiers in Physics*, vol. 6, p. 97, 2018.

[66] D. R. Reichman and P. Charbonneau, "Mode-coupling theory," *Journal of Statistical Mechanics: Theory and Experiment*, vol. 2005, no. 05, p. P05013, 2005.

[67] W. Götze, *Complex dynamics of glass-forming liquids: A mode-coupling theory*, vol. 143. OUP Oxford, 2008.

[68] W. Kob, "The mode-coupling theory of the glass transition," ACS Publications, 1997.

[69] T. R. Kirkpatrick, D. Thirumalai, and P. G. Wolynes, "Scaling concepts for the dynamics of viscous liquids near an ideal glassy state," *Phys. Rev. A*, vol. 40, no. 2, p. 1045, 1989.

[70] D. Chandler and J. P. Garrahan, "Dynamics on the way to forming glass: Bubbles in space-time," *Annual review of physical chemistry*, vol. 61, pp. 191–217, 2010.

[71] C. Kittel and P. McEuen, *Introduction to solid state physics*, vol. 8. Wiley New York, 1976.

[72] J.-F. Sadoc and R. Mosseri, *Geometrical frustration*. Cambridge University Press, 2006.

[73] A. J. Liu and S. R. Nagel, *Jamming and rheology: constrained dynamics on microscopic and macroscopic scales*. CRC Press, 2001.

[74] C. P. Royall, A. Malins, A. J. Dunleavy, and R. Pinney, "Strong geometric frustration in model glassformers," *J. Non-Cryst. Solids*, vol. 407, pp. 34–43, 2015.

[75] A. Cavagna, "Supercooled liquids for pedestrians," *Physics Reports*, vol. 476, no. 4-6, pp. 51–124, 2009.

[76] J. P. Doye, D. J. Wales, and R. S. Berry, "The effect of the range of the potential on the structures of clusters," *The Journal of chemical physics*, vol. 103, no. 10, pp. 4234–4249, 1995.

[77] A. Malins, J. Eggers, H. Tanaka, and C. P. Royall, "Lifetimes and lengthscales of structural motifs in a model glassformer," *Faraday discussions*, vol. 167, pp. 405–423, 2013.

[78] H. N. Lekkerkerker and R. Tuinier, "Depletion interaction," in *Colloids and the depletion interaction*, pp. 57–108, Springer, 2011.

[79] S. C. Glotzer and M. J. Solomon, "Anisotropy of building blocks and their assembly into complex structures," *Nat. Mater.*, vol. 6, no. 8, p. 557, 2007.

[80] S. Sacanna and D. J. Pine, "Shape-anisotropic colloids: Building blocks for complex assemblies," *Current opinion in colloid & interface science*, vol. 16, no. 2, pp. 96–105, 2011.

[81] B. J. Alder and T. E. Wainwright, "Phase transition for a hard sphere system," *The Journal of chemical physics*, vol. 27, no. 5, pp. 1208–1209, 1957.

[82] P. N. Pusey and W. Van Megen, "Phase behaviour of concentrated suspensions of nearly hard colloidal spheres," *Nature*, vol. 320, no. 6060, pp. 340–342, 1986.

[83] W. Kranendonk and D. Frenkel, "Computer simulation of solid-liquid coexistence in binary hard-sphere mixtures," *Journal of Physics: Condensed Matter*, vol. 1, no. 41, p. 7735, 1989.

[84] F. Sciortino and P. Tartaglia, "Glassy colloidal systems," *Advances in Physics*, vol. 54, no. 6-7, pp. 471–524, 2005.

[85] F. Sciortino, "One liquid, two glasses," *Nat. Mater.*, vol. 1, pp. 145 – 146, 2002.

[86] E. Zaccarelli, G. Foffi, K. A. Dawson, S. V. Buldyrev, F. Sciortino, and P. Tartaglia, "Confirmation of anomalous dynamical arrest in attractive colloids: A molecular dynamics study," *Phys. Rev. E*, vol. 66, p. 041402, 2002.

[87] J. Bergenholtz and M. Fuchs, "Nonergodicity transitions in colloidal suspensions with attractive interactions," *Physical Review E*, vol. 59, no. 5, p. 5706, 1999.

[88] L. Cipelletti and L. Ramos, "Slow dynamics in glassy soft matter," *Journal of Physics: Condensed Matter*, vol. 17, no. 6, p. R253, 2005.

[89] E. Bianchi, R. Blaak, and C. N. Likos, "Patchy colloids: state of the art and perspectives," *Phys. Chem. Chem. Phys.*, vol. 13, no. 14, p. 6397, 2011.

[90] J. S. Oh, G.-R. Yi, D. J. Pine, *et al.*, "Photo-printing of faceted dna patchy particles," *Proceedings of the National Academy of Sciences*, vol. 117, no. 20, pp. 10645–10653, 2020.

[91] F. Smallenburg and F. Sciortino, "Liquids more stable than crystals in particles with limited valence and flexible bonds," *Nat. Phys.*, vol. 9, no. 9, p. 554, 2013.

[92] E. Bianchi, J. Largo, P. Tartaglia, E. Zaccarelli, and F. Sciortino, "Phase diagram of patchy colloids: Towards empty liquids," *Physical review letters*, vol. 97, no. 16, p. 168301, 2006.

[93] D. Frenkel and B. Smit, *Understanding molecular simulation: from algorithms to applications*, vol. 1. Elsevier, 2001.

[94] D. C. Rapaport and D. C. R. Rapaport, *The art of molecular dynamics simulation*. Cambridge university press, 2004.

[95] L. Hernández de la Peña, R. van Zon, J. Schofield, and S. B. Opps, "Discontinuous molecular dynamics for semiflexible and rigid bodies," *J. Chem. Phys.*, vol. 126, no. 7, p. 074105, 2007.

[96] W. Brostow, J.-P. Dussault, and B. L. Fox, "Construction of voronoi polyhedra," *Journal of Computational Physics*, vol. 29, no. 1, pp. 81–92, 1978.

[97] M. Dzugutov and U. Dahlborg, "Molecular dynamics study of the coherent density correlation function in a supercooled simple one-component liquid," *Journal of non-crystalline solids*, vol. 131, pp. 62–65, 1991.

[98] J. E. Hallett, F. Turci, and C. P. Royall, "Local structure in deeply supercooled liquids exhibits growing lengthscales and dynamical correlations," *Nature communications*, vol. 9, no. 1, pp. 1–10, 2018.

[99] H. Tong and H. Tanaka, "Revealing hidden structural order controlling both fast and slow glassy dynamics in supercooled liquids," *Phys. Rev. X*, vol. 8, no. 1, p. 011041, 2018.

[100] J. A. van Meel, L. Filion, C. Valeriani, and D. Frenkel, "A parameter-free, solid-angle based, nearest-neighbor algorithm," *The Journal of chemical physics*, vol. 136, no. 23, p. 234107, 2012.

[101] J. E. Hallet, F. Turci, and P. Royall, "Local structure in deeply supercooled liquids exhibits growing lengthscales and dynamical correlations.," *Nat. Commun.*, vol. 9, p. 3272, 2018.

[102] C. P. Royall and W. Kob, "Locally favoured structures and dynamic length scales in a simple glass-former.," *J. Stat. Mech.: Theo. Exp.*, vol. 2017, p. 024001, 2017.

[103] H. Shintani and H. Tanaka, "Frustration on the way to crystallization in glass," *Nat. Phys.*, vol. 2, no. 3, p. 200, 2006.

[104] H. Tanaka, "Roles of local icosahedral chemical ordering in glass and quasicrystal formation in metallic glass formers," *J. Phys. Condens. Matter*, vol. 15, no. 31, p. L491, 2003.

[105] D. B. Miracle, T. Egami, K. M. Flores, and K. F. Kelton, "Structural aspects of metallic glasses," *MRS Bull.*, vol. 32, no. 8, pp. 629–634, 2007.

[106] J. P. Doye, D. J. Wales, F. H. Zetterling, and M. Dzugutov, "The favored cluster structures of model glass formers," *J. Chem. Phys.*, vol. 118, no. 6, pp. 2792–2799, 2003.

[107] J. Taffs and C. P. Royall, "The role of fivefold symmetry in suppressing crystallization," *Nat. Commun.*, vol. 7, p. 13225, 2016.

[108] Q. Chen, S. C. Bae, and S. Granick, "Directed self-assembly of a colloidal kagome lattice," *Nature*, vol. 469, no. 7330, pp. 381–384, 2011.

[109] P. F. Damasceno, M. Engel, and S. C. Glotzer, "Predictive self-assembly of polyhedra into complex structures," *Science*, vol. 337, no. 6093, pp. 453–457, 2012.

[110] O. Marin, M. Alesker, S. Guttman, G. Gershinsky, E. Edri, H. Shpaisman, R. E. Guerra, D. Zitoun, M. Deutsch, and E. Sloutskin, "Self-faceting of emulsion droplets as a route to solid icosahedra and other polyhedra," *Journal of colloid and interface science*, vol. 538, pp. 541–545, 2019.

[111] R. M. Choueiri, E. Galati, H. Thérien-Aubin, A. Klinkova, E. M. Larin, A. Querejeta-Fernández, L. Han, H. L. Xin, O. Gang, E. B. Zhulina, *et al.*, "Surface patterning of nanoparticles with polymer patches," *Nature*, vol. 538, no. 7623, p. 79, 2016.

[112] G.-R. Yi, D. J. Pine, and S. Sacanna, "Recent progress on patchy colloids and their self-assembly," *J. Phys.: Condens. Matter*, vol. 25, no. 19, p. 193101, 2013.

[113] V. Meester, R. W. Verweij, C. van der Wel, and D. J. Kraft, "Colloidal recycling: Reconfiguration of random aggregates into patchy particles," *ACS Nano*, vol. 10, no. 4, pp. 4322–4329, 2016.

[114] S. Biffi, R. Cerbino, G. Nava, F. Bomboi, F. Sciortino, and T. Bellini, "Equilibrium gels of low-valence dna nanostars: a colloidal model for strong glass formers," *Soft Matter*, vol. 11, no. 16, pp. 3132–3138, 2015.

[115] I. I. Smalyukh, "Liquid crystal colloids," *Annu. Rev. Condens. Matter Phys.*, vol. 9, pp. 207–226, 2018.

[116] W. Liu, M. Tagawa, H. L. Xin, T. Wang, H. Emamy, H. Li, K. G. Yager, F. W. Starr, A. V. Tkachenko, and O. Gang, "Diamond family of nanoparticle superlattices," *Science*, vol. 351, no. 6273, pp. 582–586, 2016.

[117] C. De Michele, S. Gabrielli, P. Tartaglia, and F. Sciortino, "Dynamics in the presence of attractive patchy interactions," *J. Phys. Chem. B*, vol. 110, no. 15, pp. 8064–8079, 2006.

[118] N. J. A. Sloane, R. H. Hardin, W. D. Smith, *et al.*, "Spherical codes," *Available at http://neilsloane.com/packings/*, 2000.

[119] Z. Gong, T. Hueckel, G.-R. Yi, and S. Sacanna, "Patchy particles made by colloidal fusion," *Nature*, vol. 550, no. 7675, pp. 234–238, 2017.

[120] É. Duguet, C. Hubert, C. Chomette, A. Perro, and S. Ravaine, "Patchy colloidal particles for programmed self-assembly," *Comptes Rendus Chimie*, vol. 19, no. 1-2, pp. 173–182, 2016.

[121] D. Landau and E. M. Lifshitz, *Quantum Mechanics Non-rekativistic Theory*, vol. 3. Pergamon, 1965.

[122] Y. Wang, S. Teitel, and C. Dellago, "Melting of icosahedral gold nanoclusters from molecular dynamics simulations," *J. Chem. Phys.*, vol. 122, p. 214722, June 2005.

[123] C. P. Royall, S. R. Williams, and H. Tanaka, "Vitrification and gelation in sticky spheres," *The Journal of chemical physics*, vol. 148, no. 4, p. 044501, 2018.

[124] H. Yoshino, "Translational and orientational glass transitions in the large-dimensional limit: a generalized replicated liquid theory and an application to patchy colloids," *arXiv preprint arXiv:1807.04095*, 2018.

[125] G. Foffi and F. Sciortino, "On the possibility of extending the noro- frenkel generalized law of correspondent states to nonisotropic patchy interactions," *The Journal of Physical Chemistry B*, vol. 111, no. 33, pp. 9702–9705, 2007.

[126] G. Tarjus and D. Kivelson, "Breakdown of the stokes–einstein relation in supercooled liquids," *The Journal of chemical physics*, vol. 103, no. 8, pp. 3071–3073, 1995.

[127] A.-P. Hynninen, L. Filion, and M. Dijkstra, "Stability of LS and $LS_2$ crystal structures in binary mixtures of hard and charged spheres," *J. Chem. Phys.*, vol. 131, no. 6, p. 064902, 2009.

[128] P. Ronceray and P. Harrowell, "From liquid structure to configurational entropy: Introducing structural covariance," *Journal of Statistical Mechanics: Theory and Experiment*, vol. 2016, no. 8, p. 084002, 2016.

[129] P. Ronceray and P. Harrowell, "Suppression of crystalline fluctuations by competing structures in a supercooled liquid," *Physical Review E*, vol. 96, no. 4, p. 042602, 2017.

[130] B. M. Carter, F. Turci, P. Ronceray, and C. P. Royall, "Structural covariance in the hard sphere fluid," *The Journal of chemical physics*, vol. 148, no. 20, p. 204511, 2018.

[131] M. Celino, V. Rosato, A. Di Cicco, A. Trapananti, and C. Massobrio, "Role of defective icosahedra in undercooled copper," *Phys. Rev. B*, vol. 75, no. 17, p. 174210, 2007.

[132] Y. Cheng, H. Sheng, and E. Ma, "Relationship between structure, dynamics, and mechanical properties in metallic glass-forming alloys," *Phys. Rev. B*, vol. 78, no. 1, p. 014207, 2008.

[133] P. J. W. Debye, *Polar molecules*. Chemical Catalog Company, Incorporated, 1929.

[134] M. Dzugutov, S. I. Simdyankin, and F. H. M. Zetterling, "Decoupling of diffusion from structural relaxation and spatial heterogeneity in a supercooled simple liquid," *Phys. Rev. Lett.*, vol. 89, no. 19, p. 195701, 2002.

[135] K. V. Edmond, M. T. Elsesser, G. L. Hunter, D. J. Pine, and E. R. Weeks, "Decoupling of rotational and translational diffusion in supercooled colloidal fluids," *Proc. Natl. Acad. Sci. USA*, vol. 109, no. 44, pp. 17891–17896, 2012.

[136] M. G. Mazza, N. Giovambattista, H. E. Stanley, and F. W. Starr, "Connection of translational and rotational dynamical heterogeneities with the breakdown of the stokes-einstein and stokes-einstein-debye relations in water," *Phys. Rev. E*, vol. 76, no. 3, p. 031203, 2007.

[137] S.-H. Chong and W. Götze, "Structural relaxation in a system of dumbbell molecules," *Phys. Rev. E*, vol. 65, no. 5, p. 051201, 2002.

[138] S.-H. Chong, A. J. Moreno, F. Sciortino, and W. Kob, "Evidence for the weak steric hindrance scenario in the supercooled-state reorientational dynamics," *Phys. Rev. Lett.*, vol. 94, no. 21, p. 215701, 2005.

[139] C. K. Mishra and R. Ganapathy, "Shape of dynamical heterogeneities and fractional stokes-einstein and stokes-einstein-debye relations in quasi-two-dimensional suspensions of colloidal ellipsoids," *Phys. Rev. Lett.*, vol. 114, no. 19, p. 198302, 2015.

[140] M. Roos, M. Ott, M. Hofmann, S. Link, E. Rössler, J. Balbach, A. Krushelnitsky, and K. Saalwächter, "Coupling and decoupling of rotational and translational diffusion of proteins under crowding conditions," *J. Am. Chem. Soc.*, vol. 138, no. 32, pp. 10365–10372, 2016.

[141] S.-H. Chong and W. Kob, "Coupling and decoupling between translational and rotational dynamics in a supercooled molecular liquid," *Phys. Rev. Lett.*, vol. 102, no. 2, p. 025702, 2009.

[142] T. G. Lombardo, P. G. Debenedetti, and F. H. Stillinger, "Computational probes of molecular motion in the lewis-wahnström model for ortho-terphenyl," *J. Chem. Phys.*, vol. 125, no. 17, p. 174507, 2006.

[143] L. Rovigatti and F. Sciortino, "Self and collective correlation functions in a gel of tetrahedral patchy particles," *Mol. Phys.*, vol. 109, no. 23-24, pp. 2889–2896, 2011.

[144] J. Tavares, C. Dias, N. Araújo, and M. Telo da Gama, "Dynamics of patchy particles in and out of equilibrium," *J. Phys. Chem B*, vol. 122, no. 13, pp. 3514–3518, 2017.

[145] I. Bitsanis, H. Davis, and M. Tirrell, "Brownian dynamics of nondilute solutions of rodlike polymers. 2. high concentrations," *Macromolecules*, vol. 23, no. 4, pp. 1157–1165, 1990.

[146] T. Kirchhoff, H. Löwen, and R. Klein, "Dynamical correlations in suspensions of charged rodlike macromolecules," *Physical Review E*, vol. 53, no. 5, p. 5011, 1996.

[147] G. Hinze, G. Diezemann, and T. Basche, "Rotational correlation functions of single molecules," *Physical review letters*, vol. 93, no. 20, p. 203001, 2004.

[148] E. Sanz and D. Marenduzzo, "Dynamic monte carlo versus brownian dynamics: A comparison for self-diffusion and crystallization in colloidal fluids," *J. Chem. Phys.*, vol. 132, no. 19, p. 194102, 2010.

[149] T. Palberg, E. Bartsch, R. Beyer, M. Hofmann, N. Lorenz, J. Marquis, R. Niu, and T. Okubo, "To make a glass—avoid the crystal," *Journal of Statistical Mechanics: Theory and Experiment*, vol. 2016, no. 7, p. 074007, 2016.

[150] W. F. Smith, J. Hashemi, and F. Presuel-Moreno, *Foundations of materials science and engineering*. Mcgraw-Hill Publishing, 2006.

[151] J. Russo, F. Romano, and H. Tanaka, "Glass forming ability in systems with competing orderings," *Physical Review X*, vol. 8, no. 2, p. 021040, 2018.

[152] C. A. Angell, "Glass formation and glass transition in supercooled liquids, with insights from study of related phenomena in crystals," *Journal of Non-Crystalline Solids*, vol. 354, no. 42-44, pp. 4703–4712, 2008.

[153] V. Molinero, S. Sastry, and C. A. Angell, "Tuning of tetrahedrality in a silicon potential yields a series of monatomic (metal-like) glass formers of very high fragility," *Physical review letters*, vol. 97, no. 7, p. 075701, 2006.

[154] R. Di Leonardo, L. Angelani, G. Parisi, and G. Ruocco, "Off-equilibrium effective temperature in monatomic lennard-jones glass," *Physical review letters*, vol. 84, no. 26, p. 6054, 2000.

[155] M. Bhat, V. Molinero, E. Soignard, V. Solomon, S. Sastry, J. Yarger, and C. Angell, "Vitrification of a monatomic metallic liquid," *Nature*, vol. 448, no. 7155, pp. 787–790, 2007.

[156] T. Mizuguchi and T. Odagaki, "Glass formation and crystallization of a simple monatomic liquid," *Physical Review E*, vol. 79, no. 5, p. 051501, 2009.

[157] V. Van Hoang and T. Odagaki, "Glasses of simple liquids with double-well interaction potential," *Physica B: Condensed Matter*, vol. 403, no. 21-22, pp. 3910–3915, 2008.

[158] M. Engel and H.-R. Trebin, "Self-assembly of monatomic complex crystals and quasicrystals with a double-well interaction potential," *Physical review letters*, vol. 98, no. 22, p. 225505, 2007.

[159] M. Elenius, T. Oppelstrup, and M. Dzugutov, "Evidence for a simple monatomic ideal glass former: The thermodynamic glass transition from a stable liquid phase," *The Journal of chemical physics*, vol. 133, no. 17, p. 174502, 2010.

[160] A. Ikeda and K. Miyazaki, "Glass transition of the monodisperse gaussian core model," *Physical review letters*, vol. 106, no. 1, p. 015701, 2011.

[161] M. Dzugutov, "Glass formation in a simple monatomic liquid with icosahedral inherent local order," *Physical Review A*, vol. 46, no. 6, p. R2984, 1992.

[162] P. J. Steinhardt, D. R. Nelson, and M. Ronchetti, "Bond orientational order in liquids and glasses," *Phys. Rev. B*, vol. 28, p. 784, 1983.

[163] T. S. Ingebrigtsen, T. B. Schrøder, and J. C. Dyre, "What is a simple liquid?," *Physical Review X*, vol. 2, no. 1, p. 011011, 2012.

[164] S. Buzzaccaro, R. Rusconi, and R. Piazza, "Sticky hard spheres: equation of state, phase diagram, and metastable gels," *Physical review letters*, vol. 99, no. 9, p. 098301, 2007.

[165] G. Foffi, G. D. McCullagh, A. Lawlor, E. Zaccarelli, K. A. Dawson, F. Sciortino, P. Tartaglia, D. Pini, and G. Stell, "Phase equilibria and glass transition in colloidal systems with short-ranged attractive interactions: application to protein crystallization," *Physical Review E*, vol. 65, no. 3, p. 031407, 2002.

[166] E. Zaccarelli, F. Sciortino, and P. Tartaglia, "Numerical study of the glass–glass transition in short-ranged attractive colloids," *Journal of Physics: Condensed Matter*, vol. 16, no. 42, p. S4849, 2004.

[167] G. Foffi, F. Sciortino, E. Zaccarelli, and P. Tartaglia, "Dynamical arrest in dense short-ranged attractive colloids," *Journal of Physics: Condensed Matter*, vol. 16, no. 38, p. S3791, 2004.

[168] P. Charbonneau, A. Ikeda, J. Van Meel, and K. Miyazaki, "Numerical and theoretical study of a monodisperse hard-sphere glass former," *Physical review E*, vol. 81, no. 4, p. 040501, 2010.

[169] W. van Megen and S. M. Underwood, "Glass transition in colloidal hard spheres: Mode-coupling theory analysis," *Phys. Rev. Lett.*, vol. 70, no. 18, p. 2766, 1993.

[170] E. R. Weeks, J. C. Crocker, A. C. Levitt, A. Schofield, and D. A. Weitz, "Three-dimensional direct imaging of structural relaxation near the colloidal glass transition," *Science*, vol. 287, no. 5453, pp. 627–631, 2000.

[171] L. Berthier, G. Biroli, J.-P. Bouchaud, L. Cipelletti, D. El Masri, D. L'Hôte, F. Ladieu, and M. Pierno, "Direct experimental evidence of a growing length scale accompanying the glass transition," *Science*, vol. 310, no. 5755, pp. 1797–1800, 2005.

[172] G. Brambilla, D. El Masri, M. Pierno, L. Berthier, L. Cipelletti, G. Petekidis, and A. B. Schofield, "Probing the equilibrium dynamics of colloidal hard spheres above the mode-coupling glass transition," *Phys. Rev. Lett.*, vol. 102, no. 8, p. 085703, 2009.

[173] W. K. Kegel and A. van Blaaderen, "Direct observation of dynamical heterogeneities in colloidal hard-sphere suspensions," *Science*, vol. 287, no. 5451, pp. 290–293, 2000.

[174] G. Parisi and F. Zamponi, "Mean-field theory of hard sphere glasses and jamming," *Rev. Mod. Phys.*, vol. 82, no. 1, p. 789, 2010.

[175] J. Barrat, W. Gotze, and A. Latz, "The liquid-glass transition of the hard-sphere system," *J. Phys. Condens. Matter*, vol. 1, no. 39, p. 7163, 1989.

[176] W. Götze and T. Voigtmann, "Effect of composition changes on the structural relaxation of a binary mixture," *Phys. Rev. E*, vol. 67, no. 2, p. 021502, 2003.

[177] G. Foffi, W. Götze, F. Sciortino, P. Tartaglia, and T. Voigtmann, "Mixing effects for the structural relaxation in binary hard-sphere liquids," *Phys. Rev. Lett.*, vol. 91, no. 8, p. 085701, 2003.

[178] E. Lázaro-Lázaro, J. A. Perera-Burgos, P. Laermann, T. Sentjabrskaja, G. Pérez-Ángel, M. Laurati, S. U. Egelhaaf, M. Medina-Noyola, T. Voigtmann, R. Castañeda-Priego, and L. F. Elizondo-Aguilera, "Glassy dynamics in asymmetric binary mixtures of hard spheres," *Phys. Rev. E*, vol. 99, no. 4, p. 042603, 2019.

[179] A. Anikeenko, N. Medvedev, and T. Aste, "Structural and entropic insights into the nature of the random-close-packing limit," *Physical review E*, vol. 77, no. 3, p. 031101, 2008.

[180] A. Anikeenko and N. Medvedev, "Polytetrahedral nature of the dense disordered packings of hard spheres," *Physical review letters*, vol. 98, no. 23, p. 235504, 2007.

[181] L. Berthier and R. L. Jack, "Structure and dynamics of glass formers: Predictability at large length scales," *Physical Review E*, vol. 76, no. 4, p. 041509, 2007.

[182] A. Widmer-Cooper and P. Harrowell, "On the study of collective dynamics in supercooled liquids through the statistics of the isoconfigurational ensemble," *The Journal of chemical physics*, vol. 126, no. 15, p. 154503, 2007.

[183] T. Dasgupta, G. M. Coli, and M. Dijkstra, "Softness suppresses fivefold symmetry and enhances crystallization of binary laves phases in nearly hard spheres," *arXiv preprint arXiv:1906.10680*, 2019.

[184] E. Boattini, M. Ram, F. Smallenburg, and L. Filion, "Neural-network-based order parameters for classification of binary hard-sphere crystal structures," *Molecular Physics*, vol. 116, no. 21-22, pp. 3066–3075, 2018.

[185] G. M. Hocky, D. Coslovich, A. Ikeda, and D. R. Reichman, "Correlation of local order with particle mobility in supercooled liquids is highly system dependent," *Physical review letters*, vol. 113, no. 15, p. 157801, 2014.

[186] V. J. Anderson and H. N. Lekkerkerker, "Insights into phase transition kinetics from colloid science," *Nature*, vol. 416, no. 6883, pp. 811–815, 2002.

[187] S. Sengupta, S. Karmakar, C. Dasgupta, and S. Sastry, "Breakdown of the stokes-einstein relation in two, three, and four dimensions," *The Journal of chemical physics*, vol. 138, no. 12, p. 12A548, 2013.

[188] S. Wei, Z. Evenson, M. Stolpe, P. Lucas, and C. A. Angell, "Breakdown of the stokes-einstein relation above the melting temperature in a liquid phase-change material," *Science advances*, vol. 4, no. 11, p. eaat8632, 2018.

[189] P. Sprent and N. C. Smeeton, *Applied nonparametric statistical methods*. CRC press, 2016.

[190] A. Widmer-Cooper, P. Harrowell, and H. Fynewever, "How reproducible are dynamic heterogeneities in a supercooled liquid?," *Phys. Rev. Lett.*, vol. 93, no. 13, p. 135701, 2004.

[191] E. Martinez-Sotelo, M. Escobedo-Sánchez, and M. Laurati, "Effect of size disparity on the structure and dynamics of the small component in concentrated binary colloidal mixtures," *J. Chem. Phys.*, vol. 151, no. 16, p. 164504, 2019.

[192] M. Laurati, P. Maßhoff, K. J. Mutch, S. U. Egelhaaf, and A. Zaccone, "Long-lived neighbors determine the rheological response of glasses," *Phys. Rev. Lett.*, vol. 118, no. 1, p. 018002, 2017.

[193] J. Baumgartl, R. P. A. Dullens, M. Dijkstra, R. Roth, and C. Bechinger, "Experimental observation of structural crossover in binary mixtures of colloidal hard spheres," *Phys. Rev. Lett.*, vol. 98, no. 19, p. 198303, 2007.

[194] J. M. Lynch, G. C. Cianci, and E. R. Weeks, "Dynamics and structure of an aging binary colloidal glass," *Phys. Rev. E*, vol. 78, no. 3, p. 031410, 2008.

[195] T. Narumi, S. V. Franklin, K. W. Desmond, M. Tokuyama, and E. R. Weeks, "Spatial and temporal dynamical heterogeneities approaching the binary colloidal glass transition," *Soft Matter*, vol. 7, no. 4, pp. 1472–1482, 2011.

[196] S. Vivek, C. P. Kelleher, P. M. Chaikin, and E. R. Weeks, "Long-wavelength fluctuations and the glass transition in two dimensions and three dimensions," *Proc. Natl. Acad. Sci. U.S.A.*, vol. 114, no. 8, pp. 1850–1855, 2017.

[197] D. Wang, T. Dasgupta, E. B. van der Wee, D. Zanaga, T. Altantzis, Y. Wu, G. M. Coli, C. B. Murray, S. Bals, M. Dijkstra, and A. van Blaaderen, "Binary icosahedral quasicrystals of hard spheres in spherical confinement," *arXiv preprint arXiv:1906.10088*, 2019.

[198] J.-P. Bouchaud and G. Biroli, "On the adam-gibbs-kirkpatrick-thirumalai-wolynes scenario for the viscosity increase in glasses," *J. Chem. Phys.*, vol. 121, no. 15, pp. 7347–7354, 2004.

[199] R. L. Jack, A. J. Dunleavy, and C. P. Royall, "Information-theoretic measurements of coupling between structure and dynamics in glass formers," *Physical review letters*, vol. 113, no. 9, p. 095703, 2014.

[200] G. Wahnström, "Molecular-dynamics study of a supercooled two-component lennard-jones system," *Physical Review A*, vol. 44, no. 6, p. 3752, 1991.

[201] W. Kob and H. C. Andersen, "Testing mode-coupling theory for a supercooled binary lennard-jones mixture i: The van hove correlation function," *Physical Review E*, vol. 51, no. 5, p. 4626, 1995.

[202] J. Paret, R. L. Jack, and D. Coslovich, "Assessing the structural heterogeneity of supercooled liquids through community inference," *The Journal of Chemical Physics*, vol. 152, no. 14, p. 144502, 2020.

[203] V. Bapst, T. Keck, A. Grabska-Barwińska, C. Donner, E. D. Cubuk, S. Schoenholz, A. Obika, A. Nelson, T. Back, D. Hassabis, *et al.*, "Unveiling the predictive power of static structure in glassy systems," *Nature Physics*, vol. 16, no. 4, pp. 448–454, 2020.

[204] E. Alpaydin, *Introduction to machine learning*. MIT press, 2020.

[205] S. B. Kotsiantis, I. Zaharakis, and P. Pintelas, "Supervised machine learning: A review of classification techniques," *Emerging artificial intelligence applications in computer engineering*, vol. 160, no. 1, pp. 3–24, 2007.

[206] E. D. Cubuk, S. S. Schoenholz, J. M. Rieser, B. D. Malone, J. Rottler, D. J. Durian, E. Kaxiras, and A. J. Liu, "Identifying structural flow defects in disordered solids using machine-learning methods," *Physical review letters*, vol. 114, no. 10, p. 108001, 2015.

[207] S. S. Schoenholz, E. D. Cubuk, E. Kaxiras, and A. J. Liu, "Relationship between local structure and relaxation in out-of-equilibrium glassy systems," *Proceedings of the National Academy of Sciences*, vol. 114, no. 2, pp. 263–267, 2017.

[208] E. Boattini, M. Dijkstra, and L. Filion, "Unsupervised learning for local structure detection in colloidal systems," *The Journal of chemical physics*, vol. 151, no. 15, p. 154901, 2019.

[209] S. Plimpton, "Fast parallel algorithms for short-range molecular dynamics. 1995," 1995.

[210] S. Sastry, "Liquid limits: Glass transition and liquid-gas spinodal boundaries of metastable liquids," *Physical Review Letters*, vol. 85, no. 3, p. 590, 2000.

[211] L. Berthier and G. Tarjus, "Nonperturbative effect of attractive forces in viscous liquids," *Physical review letters*, vol. 103, no. 17, p. 170601, 2009.

[212] P. Leishangthem, A. D. Parmar, and S. Sastry, "The yielding transition in amorphous solids under oscillatory shear deformation," *Nature communications*, vol. 8, no. 1, pp. 1–8, 2017.

[213] J. C. Dyre, "Colloquium: The glass transition and elastic models of glass-forming liquids," *Reviews of modern physics*, vol. 78, no. 3, p. 953, 2006.

[214] J. W. Goodwin and R. W. Hughes, *Rheology for chemists: an introduction*. Royal Society of Chemistry, 2008.

[215] V. Fombuena, T. Boronat, L. Sánchez-Nácher, D. García-Sanoguera, and R. Balart, "Utilidad de los modelos de viscoelasticidad en el aprendizaje de la ingeniería de materiales poliméricos," *Modelling in Science Education and Learning*, vol. 10, no. 1, pp. 137–148, 2017.

[216] S. Karra, V. t. Pra u ša, and K. Rajagopal, "On maxwell fluids with relaxation time and viscosity depending on the pressure," *International Journal of Non-Linear Mechanics*, vol. 46, no. 6, pp. 819–827, 2011.

[217] J. C. Dyre, N. B. Olsen, and T. Christensen, "Local elastic expansion model for viscous-flow activation energies of glass-forming molecular liquids," *Physical Review B*, vol. 53, no. 5, p. 2171, 1996.

[218] C. Dasgupta, A. Indrani, S. Ramaswamy, and M. Phani, "Is there a growing correlation length near the glass transition?," *EPL (Europhysics Letters)*, vol. 15, no. 3, p. 307, 1991.

[219] P. H. Poole, C. Donati, and S. C. Glotzer, "Spatial correlations of particle displacements in a glass-forming liquid," *Physica A: Statistical Mechanics and its Applications*, vol. 261, no. 1-2, pp. 51–59, 1998.

[220] B. Charbonneau, P. Charbonneau, and G. Tarjus, "Geometrical frustration and static correlations in a simple glass former," *Physical review letters*, vol. 108, no. 3, p. 035701, 2012.

[221] N. Lačević, F. W. Starr, T. Schrøder, and S. Glotzer, "Spatially heterogeneous dynamics investigated via a time-dependent four-point density correlation function," *The Journal of chemical physics*, vol. 119, no. 14, pp. 7372–7387, 2003.

[222] N. Lačević, F. W. Starr, T. Schrøder, V. Novikov, and S. Glotzer, "Growing correlation length on cooling below the onset of caging in a simulated glass-forming liquid," *Physical Review E*, vol. 66, no. 3, p. 030101, 2002.

[223] S. C. Glotzer, V. N. Novikov, and T. B. Schrøder, "Time-dependent, four-point density correlation function description of dynamical heterogeneity

and decoupling in supercooled liquids," *The Journal of Chemical Physics*, vol. 112, no. 2, pp. 509–512, 2000.

[224] A. van Blaaderen and P. Wiltzius, "Real-space structure of colloidal hard-sphere glasses," *Science*, vol. 270, no. 5239, pp. 1177–1179, 1995.

[225] N. Lacevic, *Dynamical heterogeneity in simulated glass-forming liquids studied via a four-point spatiotemporal density correlation function*. Citeseer, 2003.

université PARIS-SACLAY

ÉCOLE DOCTORALE
Physique en l'Île-de-France (PIF)

**Titre:** Structure locale et dynamique des systèmes colloïdaux à densité élevée

**Mots clés:** Dynamique vitreuse, Particules à patchs, Simulations moléculaires, Colloïdes.

**Résumé:** Le rôle de la structure dans la dynamique colloïdale vitreuse est encore un sujet de débat. Cependant, il existe des preuves d'un lien direct entre les changements de la dynamique et les propriétés structurelles du système. Nous explorons l'interaction de la structure et de la dynamique locales en utilisant des particules à patchs. Pour ce faire, nous utilisons des simulations de dynamique moléculaire. Nous montrons qu'en renforçant la géométrie icosaédrique, le dynamique du système présente un ralentissement extrême. Grâce à ces résultats, nous fournissons une voie pour contrôler la dynamique vitreuse par l'utilisation de particules à patchs.

De plus, il est intéressant de savoir si nous pouvons extraire des informations sur la dynamique en utilisant uniquement des informations structurelles. Afin d'explorer ce point, nous simulons une grande variété de mélanges de sphères dures. Nous montrons que la dynamique globale de ces systèmes peut être prédite avec précision en introduisant un nouveau paramètre d'ordre appelé tétraédralité de la structure locale qui compte le nombre de tétraèdres auxquels chaque particule participe. Les prédictions de ce paramètre d'ordre restent valables pour dans une grande variété de densités, ce qui prouve son universalité dans cette famille de précurseurs de verre. De plus, il est également capable de saisir les changements sur la dynamique locale, car les régions à forte tétraédralité sont fortement corrélées avec les régions à dynamique lente. Enfin, nous explorons l'utilisation de techniques d'apprentissage machine non supervisé pour classer les particules ayant des environnements structurels différents.

**Title:** Local structure and dynamics of dense colloidal systems: from patchy particles to hard spheres

**Keywords:** Glassy dynamics, Patchy particles, Molecular simulations, Colloids.

**Abstract:** The role played by the structure in determining the dynamics of glassy colloidal systems is still a subject of debate. However, there is compelling evidence of a direct link between changes in the local structure and the dynamical slowdown in glassy systems. Here, we explore the interplay between local structure and dynamics by using patchy particles as glass formers. This is done by making use of molecular dynamics simulations. We show that reinforcing icosahedral geometry causes, the system to exhibit an extreme slowdown in its dynamics. With these results, we provide a route for controlling glassy dynamics through the use of patchy particles.

Additionally, an interesting point is whether we can extract information about dynamics from only structural information. In order to explore this point, we simulate a wide variety of hard-sphere mixtures. We show that global dynamics of these systems can be precisely predicted by quantifying the tetrahedrality of the local structure: an order parameter that consists of counting the number of tetrahedra each particle participates in. The predictions of this order parameter maintain their accuracy over a wide variety of densities proving its universality in this family of glass formers. Moreover, it is also capable of capturing the changes in the local dynamics, as regions with high tetrahedrality are strongly correlated with regions with slow dynamics. Finally, we demonstrate that unsupervised machine learning techniques can be used to classify particles with different structural environments, which are strongly correlated to local dynamics.

Université Paris-Saclay
Espace Technologique / Immeuble Discovery
Route de l'Orme aux Merisiers RD 128 / 91190 Saint-Aubin, France